UNIVERSITY OF MICHIGAN
APR 13 1959
ENGINEERING LIBRARY

The Canadian Journal of Chemical Engineering

formerly

CANADIAN JOURNAL OF TECHNOLOGY

CONTENTS

Tray Drying of Fine Powder	*J. A. Wheat* *D. A. MacLeod*	47
Use of Lead in Chemical and Metallurgical Plant Construction	*A. Turner* *J. R. Wellington* *L. Williams*	55
The Pyrolysis of a Heavy Crude Oil in a Fluidized Bed	*G. G. Madgwick* *C. H. Amberg* *W. S. Peterson*	65
Empirical Correlation of Azeotrope Data: An Extension of the Meissner-Greenfield Correlation	*A. I. Johnson* *J. A. Madonis*	71
Solar Energy: Economics and Engineering Research at the University of Wisconsin	*J. A. Duffie* *G. O. G. Löf*	77
The Effects of Shape and Reynolds Number on Drag in the Motion of a Freely Oriented Body in an Infinite Fluid	*H. A. Becker*	85

Published by
THE CHEMICAL INSTITUTE OF CANADA
OTTAWA

Opportunity for
ENQUIRING MINDS

Each year C-I-L provides fellowships to promising young Canadian scientists for advanced post-graduate studies. Through this program, now in its eighteenth year, nearly 200 men and women have had the opportunity to carry out original work and so add to their own — and Canada's — store of scientific knowledge. Grants to universities to expand facilities and to endow chairs of science further support the development of trained, enquiring minds.

C-I-L's own activities, so dependent on constant development and research, provide scope and a congenial atmosphere for many trained talents, working together in the ever-new world of chemistry.

SOME OF THE RESEARCH PROJECTS CARRIED ON BY HOLDERS OF C-I-L FELLOWSHIPS:

isotopes produced in nuclear fission • chemistry of wood carbohydrates • wood pulping with liquid ammonia • soil fertility • electrically activated oxygen • gas engineering • nitrogen derivatives of steroids • the use of gaseous ammonia as a plant nutrient • mechanisms of organic reactions using radioactive carbon • spectral analysis of molecules • reactions of active nitrogen • waterfowl habits.

CANADIAN INDUSTRIES LIMITED

Serving Canadians Through Chemistry

C-I-L

Agricultural Chemicals • Ammunition • Coated Fabrics • Industrial Chemicals • Commercial Explosives • Paints • Plastics • Textile Fibres

The Canadian Journal of Chemical Engineering

formerly

Canadian Journal of Technology

VOLUME 37 APRIL, 1959 NUMBER 2

Managing Editor
T. H. G. Michael

Publishing Editor
D. W. Emmerson

Assistant Publishing Editors
R. G. Watson
R. N. Callaghan

Circulation Manager
M. M. Lockey

EDITORIAL BOARD

Chairman
W. M. CAMPBELL, Atomic Energy of Canada Limited, Chalk River, Ont.

A. CHOLETTE, Laval University, Quebec, Que.

L. D. DOUGAN, Polymer Corp. Limited, Sarnia, Ont.

W. H. GAUVIN, McGill University, Montreal, Que.

GLEN GAY, Defence Research Board, Ottawa, Ont.

G. W. GOVIER, University of Alberta, Edmonton, Alta.

A. I. JOHNSON, University of Toronto, Toronto, Ont.

E. B. LUSBY, Imperial Oil Limited, Toronto, Ont.

LEO MARION, National Research Council, Ottawa, Ont.

R. R. McLAUGHLIN, University of Toronto, Toronto, Ont.

G. L. OSBERG, National Research Council, Ottawa, Ont.

H. R. L. STREIGHT, Du Pont of Canada Limited, Montreal, Que.

EX-OFFICIO

C. E. CARSON, President, The Chemical Institute of Canada

H. S. SUTHERLAND, Chairman of the Board of Directors

H. BORDEN MARSHALL, Director of Publicity and Publications

W. G. DICKS, Associate Director of Publicity and Publications

Authorized as second class mail, Post Office Department, Ottawa. Printed in Canada

Manuscripts for publication should be submitted to the Publishing Editor: D. W. Emmerson, *The Canadian Journal of Chemical Engineering*, 18 Rideau Street, Ottawa 2, Ont. (Instructions to authors are on the last page).

Editorial, Production and Circulation Offices: 18 Rideau Street, Ottawa 2, Ont.

Advertising Office: C. N. McCuaig, manager of advertising sales, *The Canadian Journal of Chemical Engineering*, Room 601, 217 Bay Street, Toronto, Ont. Telephone—EMpire 3-3871.

Plates and Advertising Copy: Send to *The Canadian Journal of Chemical Engineering*, 18 Rideau Street, Ottawa 2, Ont.

Subscription Rates: In Canada—$3.00 per year and 75c per single copy; U.S. and U.K.—$4.00; Foreign—$4.50.

Change of Address: Advise Circulation Department in advance of change of address, providing old as well as new address. Enclose address label if possible.

The Canadian Journal of Chemical Engineering is published by The Chemical Institute of Canada every two months.

Unless it is specifically stated to the contrary, the Institute assumes no responsibility for the statements and opinions expressed in *The Canadian Journal of Chemical Engineering*. Views expressed in the editorials do not necessarily represent the official position of the Institute.

Tray Drying of Fine Powders[1]

J. A. WHEAT[2] and D. A. MacLEOD[2]

Drying rates of finely powdered aluminum soaps and diatomaceous silicas were determined in a tray dryer. The weight of solid on the tray was automatically recorded. As expected for fine powders, plots of drying rate against moisture content were concave downward. The data were correlated by equations of the form $N = aX_G^{0.625}$ where N is the drying rate in lb./(hr.)(sq.ft.) and X_G is the free moisture content in lb. of water per lb. of dry solid. A straight line was obtained by plotting log a for aluminum stearate against the reciprocal of absolute temperature and a similar relationship was assumed to hold for the other materials which were dried at two temperatures only. Intercepts of the temperature plots seemed to depend upon bulk density or average particle size but no general correlation was possible.

THE term drying usually refers to the removal of a liquid from a solid by applying heat and carrying away the vapor in a gas by either natural or forced convection. In tray drying, heated air is passed over the wet solid which is placed in shallow trays supported on fixed or removable racks. A large proportion of the air, about 80-90%, is recirculated to reduce the amount of heat required. Tray drying is a batch process as far as the solid is concerned but the air flow is continuous.

In the investigation reported in this paper, mixtures of water and fine powders were dried in a tray suspended from a balance on the top of the dryer. The weight of the tray was automatically recorded and the drying rate correlated with moisture content.

THEORETICAL

The theoretical and fundamental concepts of solids drying have been summarized by Marshall and Friedman[1] and Treybal[2]. There are a number of important papers on tray drying[3-15], some of which [5, 8, 12, 13] refer more particularly to the drying of granular solids.

In general, liquid moves by diffusion through homogeneous solids such as sodium soaps and by capillary action in granular solids[1, 15]. In fibrous materials and some fine powders such as pigments and clay, the mechanism depends upon the moisture content.

Water is held in the spaces between the particles of a granular solid in three different states[9, 10, 12, 14] depending upon the amount of water present. In the capillary state, all the pore spaces are completely filled with water. In the funicular state, the particles are covered by a continuous film of water but there is some air in the interstitial spaces. In the pendular state, the small amount of water present is held at the points of contact of the particles. Evaporation from granular solids during the capillary state causes the liquid surface to recede between the particles on the surface and the resulting curvature produces a suction. As evaporation proceeds, the suction increases. When it exceeds a certain value (the entry suction [8, 12]), air enters the solid through the larger capillaries to replace the water carried to the surface through the smaller capillaries and the water changes to the funicular state. Evaporation at the surface and transfer of water by capillary action continue until the reserves of liquid within the solid dry up. When the water at the surface is in the pendular state, evaporation occurs in a zone that gradually recedes from the surface. Water moves to the evaporation zone and the vapor must diffuse through the solid to the surface and then to the air stream.

When experimentally determined drying rates are plotted against moisture contents, lines resembling curve N-1 of Figure 1 result. Section BC represents the constant rate period, CD the first falling rate period and DE the second falling rate period. Point C is defined as the critical moisture content and point E is the equilibrium moisture content.

During the constant rate period, evaporation is from a surface film of water that is replenished by diffusion or capillary action as rapidly as it is depleted. At some

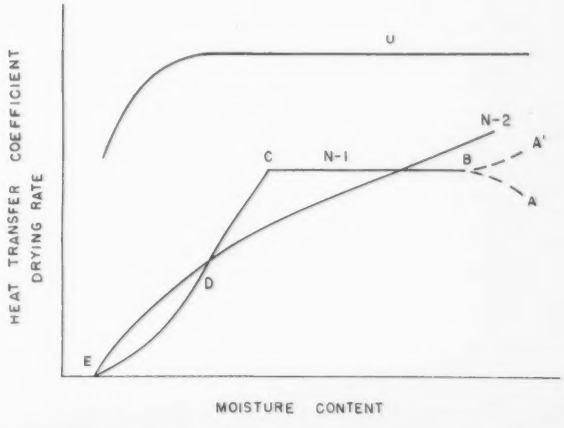

Figure 1—Changes in drying rate and heat transfer coefficient with moisture content.

[1]*Manuscript received August 22, 1958.*
[2]*Defence Research Chemical Laboratories, Ottawa, Ont.*
Contribution from Defence Research Chemical Laboratories, Ottawa, Ont. Issued as D.R.C.L. Report No. 277.

point it will no longer be possible for water to reach the surface as rapidly as it can be evaporated and the drying rate will decrease. This critical moisture content depends upon the solid, the particle size, and the bed thickness as well as on the properties of the air stream. The first falling rate period is called the period of unsaturated surface drying because drying occurs at the surface but on a diminishing fraction of it. The rate of drying is frequently linear with moisture content during this period and depends upon the air stream properties, the critical moisture content, and the rate during the constant rate period. The period of unsaturated surface drying may not occur at all or it may occupy the entire falling rate period. The second falling rate period begins when the pendular state exists at the surface. The rate of drying now depends on the movement of water within the solid and is independent of the velocity and humidity of the air but, of course, is still affected by the air temperature. Although it is often assumed to be a straight line[1, 2, 8] for making rough calculations of the drying time, it had generally been accepted that the DE portion of the drying rate curve was concave upward for both granular and continuous solids. Newitt and co-workers[12, 13] obtained concave upward curves for some granular solids but with fine particles (5 microns) the curves resembled N-2 of Figure 1. Oliver and Newitt concluded that in beds of fine particles, the suction pressures were so great that the continuous threads of liquid were broken by the release of air and by vaporization of liquid. Liquid water, therefore, could not be carried to the surface by capillary action but, instead, was evaporated below the surface.

Several authors have shown[3, 10] that the overall heat transfer coefficient between the air and the solid is constant as long as evaporation occurs at the surface even though the drying rate is decreasing but that it decreases as the plane of vaporization recedes into the solid (curve U of Figure 1).

Quantitative relationships

Heat is transferred to the solid by convection from the air, q_C; conduction from the sides and bottom of the tray, q_B; and radiation from the tray above, q_R.

In the constant rate period, the total heat transferred is related to the drying rate by

$$q = q_C + q_B + q_R = NA\lambda \quad \ldots\ldots(1)$$

The coefficient for the transfer of heat to a flat plate such as the bottom of the tray is given [2, 16] by

$$j_H = \frac{h}{c_p V \rho}\left(\frac{c_p \mu}{k}\right)^{2/3} = 0.036\ Re^{-0.2} \quad \ldots\ldots(2)$$

for Reynold's number above 15,000. In this case, the Reynolds number is expressed by

$$Re = \frac{ZV\rho}{\mu} \quad \ldots\ldots(3)$$

However, higher coefficients are obtained in tray drying, probably because of the rougher surfaces and, for the air-water system, Treybal [2] recommended

$$h_C = 0.01\ G^{0.8} \quad \ldots\ldots(4)$$

for G between 500 and 6000 lb./(hr.)(sq. ft.). The radiation heat transfer coefficient may be estimated from

$$h_R = \frac{0.173\epsilon}{T_R - T_s}\left[\left(\frac{T_R}{100}\right)^4 - \left(\frac{T_s}{100}\right)^4\right] \quad \ldots\ldots(5)$$

The temperature of the solid surface is not ordinarily known but during the constant rate period the mass transfer equation

$$N = k_H (H_s - H) \quad \ldots\ldots(6)$$

may be combined with

$$\frac{h_C}{k_H} = c_s = 0.24 + 0.446H \quad \ldots\ldots(7)$$

to arrive at the equation

$$\frac{(H_s - H)\lambda}{c_s} = (t_a - t_s) + \frac{h_B A_B}{h_C A}(t_a - t_B) + \frac{h_R}{h_C}(t_R - t_s) \quad \ldots\ldots(8)$$

This may be solved simultaneously with the saturated humidity curve to give t_S and H_S. The drying rate can then be calculated. These equations are applied later to evaporation from a free water surface.

Many authors have presented equations for the falling rate period based on either diffusion [1, 3, 4, 11] or on an assumed linear relationship between drying rate and free moisture content [1, 2, 3, 11]. If a uniform moisture distribution is assumed at the start of the falling rate period, equation (9) is an approximate form of the diffusion equation.

$$N = \frac{W_S D \pi^2}{4AL^2}(X - X^*) \quad \ldots\ldots(9)$$

In this equation, D is the diffusivity of water in the solid and it changes with moisture content [11, 15]. The empirical linear equation is expressed by

$$N = K(X - X^*) \quad \ldots\ldots(10)$$

where

$$K = \frac{N_C}{X_C - X^*} \quad \ldots\ldots(11)$$

According to Friedman and Marshall [1], equations (10) and (11) apply to coarse granular solids and to certain materials at high moisture contents while equation (9) applies to single phase solid systems and to materials such as wood, paper, and clay at low moisture contents. Frequently, the diffusion equation satisfies drying rate data even though diffusion is not taking place [8]. In the absence of more detailed data, equations (10) and (11) are sometimes applied to the second falling rate period [2]. However, neither type of equation can be used for a drying rate curve like N-2 of Figure 1.

EXPERIMENTAL

Tray dryer

The tray dryer was constructed some years previously for routine drying of various materials and throughout these experiments it was being used to dry small experimental lots of aluminum soaps. Air was circulated with an 18 in. vaneaxial fan directly connected to a motor mounted outside the dryer (Figure 2). In one series of measurements, air velocities between the trays were determined with an Alnor Thermoanemometer and, over the height of the dryer, were found to vary in no particular pattern from 4.8 to 6.5 ft./sec. with an average of 5.5 ft./sec. Air was exhausted from the dryer with a small blower and make-up air allowed to enter, as shown

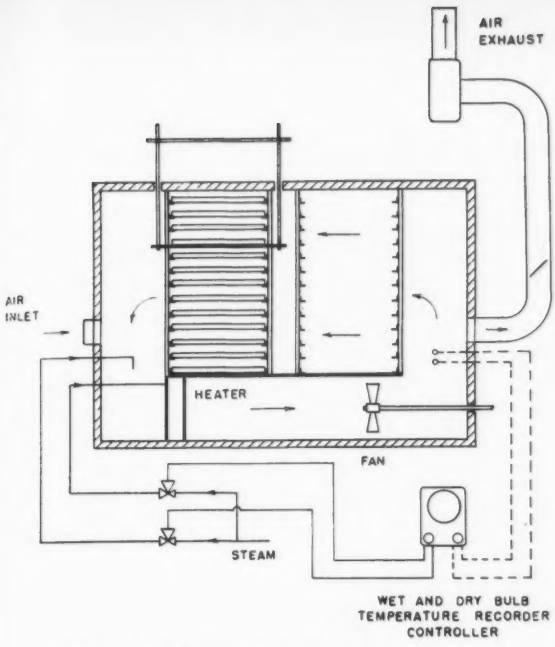

Figure 2—Drawing of the tray dryer used.

in Figure 2. The dry bulb temperature of the air was automatically controlled by regulating the flow of steam to a heater and the wet bulb temperature by regulating a steam spray.

Inside the dryer, the two tiers each had 13 shelves spaced 4 in. apart and each shelf held two 18 in. by 28 in. trays. The upstream tier and the back half of the down stream tier were not used but were filled with loaded trays so that the air flow would resemble more closely the flow in an actual dryer. For the same reason, only alternate trays of the remaining portion were used. Four trays of aluminum soap were usually being dried and the tenth position from the bottom was used for the test tray. The regular drying trays had wire mesh bottoms but the test tray and the dummy tray above it had solid bottoms. The test tray was made of stainless steel and was $1\frac{1}{4}$ in. deep. It was fitted with twelve thermocouples placed in a line down the middle of the tray parallel to the air flow. Two couples were soldered to the bottom of the tray and two placed $\frac{1}{4}$, $\frac{1}{2}$, $\frac{3}{4}$, 1, and $1\frac{1}{4}$ in. above the bottom. Wires for these couples were brought from below the tray up through two rows of small tubes 2 in. apart and stretched across the intervening space. The tops of the tubes were sealed with de Khotinsky cement. The couples were connected to two 12 point Jones connectors, the other halves of which were attached to the framework supporting the tray. Loops of flexible copper wire connected the plugs to thermocouple extension wires. The plugs and the soldered connections were at the same level and only a few inches apart so that they would be at the same temperature. Temperatures were recorded with a 12 point potentiometer recorder.

Two vertical rods extended from the tray supporting framework through the roof of the dryer and the floor above it. A single horizontal bar attached to the beam of a balance was clamped to these vertical rods.

Automatic weight recorder

The balance was modified considerably and pneumatic

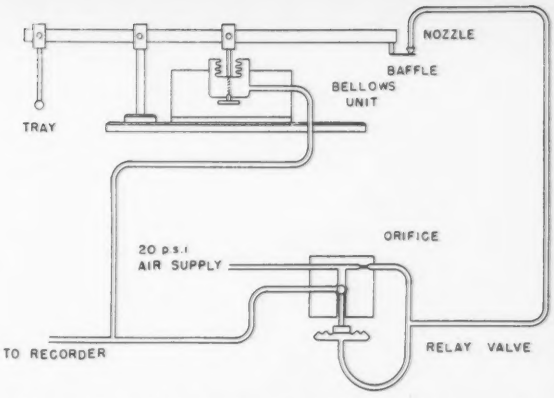

Figure 3—Schematic drawing of the weight recorder.

components attached to it so that the weight on the tray could be automatically recorded. The system used was essentially the same as a pneumatic controller. Referring to Figure 3, a decrease in weight on the tray moved the baffle away from the nozzle, causing the nozzle back-pressure to decrease. This increased the relay valve output pressure which restored the beam to its original position. The relay valve output pressure was also connected to a 3 to 18 p.s.i. pressure recorder whose action was reversed so that scale reading varied directly with weight. The range of the instrument could be changed by moving the bellows unit along the beam and the zero set by (1) changing the tension on the bellows spring, (2) altering counterweights on either end of the beam, (3) adjusting the nozzle or baffle position, or (4) for slight adjustments, changing the position of the recording pen. The instrument was set so that a zero reading was obtained with the empty tray in position and it was calibrated by placing known weights on the tray. During calibration, readings gave a standard deviation of 0.035 lb. (for an instrument range of about 11 lb.) but in actual use, recorder weights at the end of a run were in error by about 0.25 lb. The recorder weights were always high, possibly because of a frictional resistance.

Materials

The materials dried were of two types: aluminum soaps prepared here and commercial diatomaceous silica. One type of aluminum distearate and three different aluminum dilaurates were prepared by combining the respective sodium soaps with aluminum sulfate and sodium hydroxide. Freshly prepared material was used for each run. Physical properties of the diatomaceous silicas are given in Table 1. Particle size data were taken from a bulletin published by Canadian Johns-Manville Company from whom the materials were purchased while the bulk density and moisture content were determined here. These solids were mixed with water in a double conical solids blender and used several times before discarding.

Procedure

The test tray was placed in the dryer, the thermocouples plugged in, and the weight recorder set to read zero. A known weight of wet solid was then placed in the tray and spread as evenly as possible. The following morning, or later in the day if necessary, the tray was removed and the contents weighed. Samples of the dry solid were taken for determination of moisture content with an infrared moisture balance using a 125 watt infrared lamp mounted about 1.5 in. from the sample.

TABLE 1
PROPERTIES OF DIATOMACEOUS SILICAS

Particle size, microns	Filter-Cel	Hyflo Super-Cel	Celite 545
>40	2.5	6.0	24.0
40–20	8.0	15.5	52.0
20–10	14.0	33.5	18.5
10–6	19.0	22.0	4.5
6–2	37.5	21.5	1.0
<2	19.0	1.5	
Mositure content, %	3.1	0.1	0.0
Bulk density, g./ml.	0.22	0.28	0.33

Aluminum stearate was dried at three different temperatures and the other materials at two. Two runs were made with distilled water in the tray instead of wet solid.

RESULTS

Data processing

Hourly values of the average temperature of the two top thermocouples, which were always well above the surface, were averaged to give the air temperature for each run. The difference between these two couples was usually of the order of 2°F. Readings during a typical run are plotted against moisture content in Figure 4. The weight of dry solid, W_S, was determined from the weight and moisture content at the end of each run. The initial moisture content was computed from this and the original weight. Tray weights at various intervals were read from the chart and the initial and final readings compared with actual weighings; any error was assumed to have been a linear function of drying time. Corrected weights were then used to calculate incremental drying rates which were plotted against time. Smoothed values were read off and plotted against moisture content as shown in Figure 4 for one run. Values of the rate at fixed moisture contents were taken from this plot and tabulated. These rates for a number of runs with the same solid at the same temperature were average and correlated with moisture content as described later.

Early runs

Before a correlating method had been derived, a number of additional measurements and calculations were made. The diffusivity, D, was calculated from equation (9) and plotted against X as shown in Figure 4 for one run. For this plot, L was assumed to be constant at the final value. Assuming it to be a linear function of the free water content gave different, but just as variable, values of D. It is known [1] that D varies with moisture content but plots for several other runs gave variously shaped curves so no correlation between D and X was possible. Thus, the simplified diffusion equation could not be applied to the data.

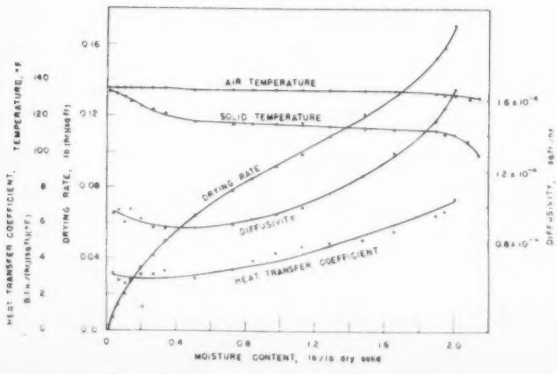

Figure 4—Results for a typical run with aluminum stearate.

The mean temperature of the bed, which is also shown in Figure 4, was arrived at by averaging the readings of the thermocouples covered by the bed. For this particular run, the bed depth was 0.68 in. at the start and 0.30 in. at the end. By assuming L to be a linear function of the free water content, it was estimated that the thermocouples half an inch above the bottom became uncovered at a moisture content of about 120%. Thus, six readings were averaged at moisture contents above this value and four below it. A plot of the temperature at any one point in the bed would resemble the mean temperature plot in shape. As expected, the temperatures at the bottom were generally higher than at points near the middle of the bed.

The overall heat transfer coefficient was calculated from

$$U = \frac{q}{A\,(t_a - t_m)} \qquad (12)$$

$$q = N\lambda A + (W + 0.25W_S)\frac{dt_m}{d\tau} \qquad (13)$$

where 0.25 is the estimated heat capacity of the dry solid. The rate of temperature change, $dt_m/d\tau$, was obtained from a smoothed plot of $\Delta t_m/\Delta d\tau$ against τ. In all runs for which it was calculated, U showed a steady decrease.

Evaporation of water

Data for the two runs in which water was evaporated were as follows:

	Run 1	Run 2
Air velocity, ft./sec.	5.25	5.42
Air temperature, t_a	131.9	132.1
Air humidity, H	0.021	0.021
Specific heat, c_s	0.249	0.249
Constant rate, N_C	0.252	0.252
Bottom temperature, t_B	97.5	96.6
Water temperature, t_m	97.5	96.6
Area of bottom and sides, A_B	4.70	4.70
Area of evaporating surface, A	3.50	3.50

The temperature of the bottom of the tray above the test tray was taken to be the same as the air temperaure and the radiant heat transfer coefficients were calculated from equation (5) using an emissivity of 0.96 [17] and an assumed surface temperature of 96°F. The convection heat transfer coefficients to the bottom of the test tray were calculated from equation (2).

	Run 1	Run 2
Radiant heat transfer, h_R	1.26	1.26
q_R	167.2	167.8
Bottom heat transfer, h_B	1.52	1.52
q_B	246.0	254.0
Total heat transfer, q	916.8	916.8

These data were substituted into equations (1) and (8), which were solved simultaneously with the saturated humidity curve to obtain the following:

	Run 1	Run 2
Convection heat transfer, h_C	3.95	3.91
q_C	503.6	495.0
Mass transfer coefficient, k_H	15.8	15.7
Surface temperature, t_s	95.1	94.0

The convection heat transfer coefficient is higher than the 3.0 predicted by equation (4). Perhaps there was additional air turbulence because the water level was below the top of the tray.

Aluminum stearate

Average drying rates of aluminum stearate at selected moisture contents are given in Table 2 for one temperature. The air temperature ranged from 131.5 to 135.3°F. with an average of 133.7°F. and a standard deviation of 0.9. There was a total of 24 runs but they did not all extend to the higher moisture contents so fewer points were available at moistures above 50%. Drying rate is plotted against moisture content for this and two other temperatures in the lower portion of Figure 5. The straight lines in the upper portion were obtained by subtracting a constant from the moisture content. This constant, which was found by trial and error to be 0.01, represents the equilibrium moisture content. The straight lines, therefore, are plots of drying rate against free moisture content, X - X* or X_G and the equations are of the form

$$N = a\,X_G{}^b \qquad (14)$$

TABLE 2
DRYING RATE OF ALUMINUM STEARATE
(133.7°F.)

Moisture, lb./lb. dry solid	Number of runs	Rate, lb./(hr.)(sq. ft.)	Standard Deviation	Calculated rate, lb./(hr.)(sq. ft.)	Error, %
0.025	24	0.0077	0.0031	0.0081	5.2
0.05	24	0.0144	0.0040	0.0149	4.0
0.10	24	0.0246	0.0055	0.0248	0.9
0.25	24	0.0452	0.0092	0.0458	1.3
0.50	24	0.0717	0.0120	0.0715	0.3
1.00	17	0.1161	0.0136	0.1111	4.3
1.50	9	0.1466	0.0146	0.1434	2.2
2.00	4	0.1780	0.0087	0.1718	3.5

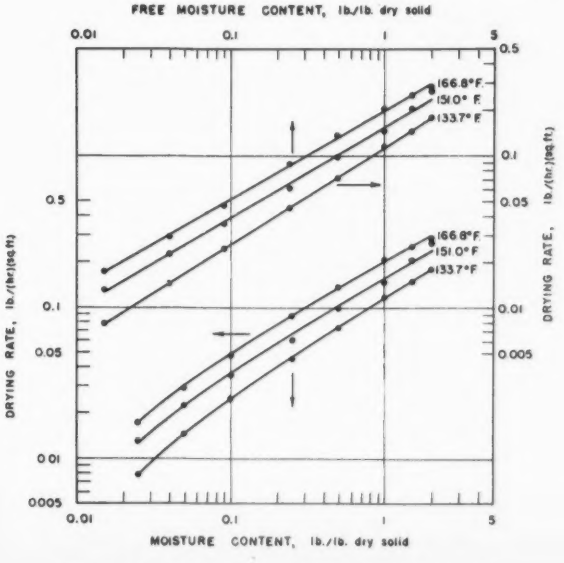

Figure 5—Drying rate of aluminum stearate.

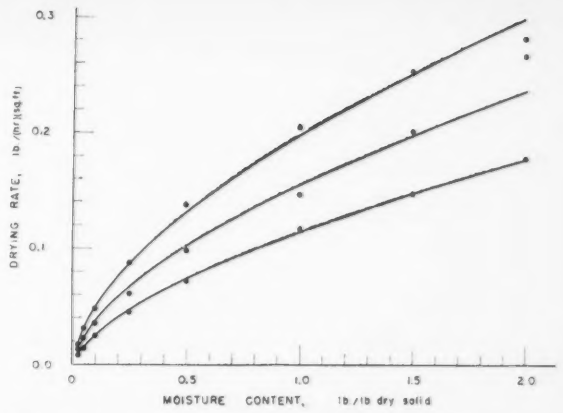

Figure 6—Linear plot of drying rate of aluminum stearate.

Figure 6 is an arithmetic plot of the same data and equations showing that the lines are concave downward. Values of the constants a and b determined by the method of least squares are given in Table 3. As can be seen by Figures 5 and 6, the equations fit the data very well. Correlation coefficients were above 0.998 and the standard errors of estimate were 0.8, 7.6 and 3.7% respectively. These errors indicate the accuracy with which the regression equations fit the average rate data while the standard deviations of Table 2 indicate the uniformity of the rates from run to run. The calculated rates and percentage errors in Table 2 will be explained later.

TABLE 3
RATE EQUATION CONSTANTS FOR
THE DRYING OF ALUMINUM STEARATE

Air temp., °F.	Number of runs	Equilibrium moisture, lb./lb. dry solid	a	b
133.7	24	0.01	0.1144	0.6432
151.0	13	0.01	0.1556	0.6036
166.8	10	0.01	0.1989	0.5865

As expected, a straight line was obtained by plotting log a against the reciprocal of absolute temperature but although b decreased with temperature no simple straight line relationship was apparent.

Other materials

Rate equation constants for six additional materials each at two temperatures are given in Table 4. The effect of temperature on a was reasonably consistent but b increased with temperature for two materials and decreased for the remainder.

General correlation

Since all values of b were between 0.54 and 0.72 it was thought that a constant value could be used. This would make the equations less accurate for any particular solid but they would be more generally applicable and only one constant would be required for each combination of material and temperature. As an additional advantage to using a constant b, it was found that the resulting values of a gave more consistent slopes when log a was plotted against the reciprocal of absolute temperature. The aver-

TABLE 4

RATE EQUATION CONSTANTS

Material	Air temp., °F.	Number of runs	a	b
Aluminum laurate A	133.9	4	0.1442	0.6737
	171.0	4	0.1838	0.5893
Aluminum laurate B	134.6	3	0.1325	0.7168
	169.2	4	0.1745	0.5959
Aluminum laurate C	135.0	4	0.1622	0.5774
	168.8	4	0.2566	0.5459
Filter-Cel	134.8	8	0.1481	0.6347
	166.8	7	0.2330	0.6667
Hyflo Super-Cel	133.7	11	0.1763	0.6253
	165.9	8	0.2774	0.6691
Celite 545	133.7	8	0.1995	0.6367
	163.8	8	0.3168	0.6022

TABLE 6

CONSTANTS FOR TEMPERATURE CORRELATING EQUATIONS

Material	Individual constants		Average slope
	C	D	C
Aluminum stearate	17,390	−7,095.3	1,037
Aluminum laurate A	119	−4,043.6	1,051
Aluminum laurate B	699	−5,180.5	964
Aluminum laurate C	2,330	−5,650.5	1,489
Filter-Cel	526	−4,879.5	1,190
Hyflo Super-Cel	231	−4,260.7	1,444
Celite 545	11,650	−6,526.6	1,760

age of the 15 values of b in Tables 3 and 4 is 0.625 and this was accepted as the exponent for all rate of drying equations. Thus, drying rates were given by

$$N = a\,X_G^{0.625} \quad \ldots\ldots (15)$$

For each solid and temperature, a was calculated at various moisture contents using experimentally determined rates like those given in Table 2 for aluminum stearate at 133.7°F. Calculated drying rates at each moisture content were then determined by substituting the average rate constant into equation (15) and these rates compared with the experimental rates. Average percentage errors and average values of a are given in Table 5, which is a summary of experimental conditions and results.

The average drying rates in Table 5 were calculated from an integrated form of equation (14) and are the average rates of drying from a free moisture content of 150% to the equilibrium moisture content. Drying rate, N, and moisture content are related by

$$N = \frac{-W_S}{A}\frac{dX}{d\tau} \quad \ldots\ldots (16)$$

and when this is substituted into equation (14) the resulting equation can be integrated to give

$$\tau = \frac{W_S}{Aa(1-b)}\left[X_{G1}^{1-b} - X_{G2}^{1-b}\right] \quad \ldots\ldots (17)$$

where τ is the time required to reduce the moisture from X_{G1} to X_{G2}. The amount of water evaporated during this time is

$$W_S\,(X_{G1} - X_{G2}) \quad \ldots\ldots (18)$$

so the average rate for $X_{G_1} = 1.50$ and $X_{G_2} = 0$ is

$$N_{av} = a\,(1-b)\,1.50^b \quad \ldots\ldots (19)$$

or for $b = 0.625$

$$N_{av} = 0.4831\,a \quad \ldots\ldots (20)$$

TABLE 5

SUMMARY OF EXPERIMENTAL RESULTS

Material	Air temp., °F.	Number of runs	Bed depth, in.		Tray loading, lb./sq. ft.	Equilibrium moisture, lb./lb. dry solid	a	Average error, %	Average rate $X_G = 1.50$ to $X_G = 0$, lb./(hr.) (sq. ft.)
			Initial	Final					
Aluminum stearate	133.7	24	0.61	0.36	0.69	0.01	0.1118	2.7	0.0540
	151.0	13	0.57	0.36	0.69	0.01	0.1603	6.2	0.0774
	166.8	10	0.51	0.28	0.60	0.01	0.2102	5.5	0.1015
Aluminum laurate A	133.9	4	0.59	0.44	0.64	0.01	0.1309	4.5	0.0632
	171.0	4	0.60	0.52	0.72	0.01	0.1954	6.8	0.0944
Aluminum laurate B	134.6	3	0.62	0.40	0.66	0.01	0.1147	12.4	0.0554
	169.6	4	0.64	0.43	0.74	0.01	0.1853	4.3	0.0895
Aluminum laurate C	135.0	4	0.66	0.50	0.47	0.015	0.1745	8.4	0.0843
	168.8	4	0.64	0.50	0.54	0.015	0.2908	12.2	0.1405
Filter-Cel	134.8	8	0.42	0.38	0.60	0.015	0.1435	3.0	0.0693
	166.8	7	0.42	0.39	0.62	0.009	0.2182	5.7	0.1054
Hyflo Super-Cel	133.7	11	0.41	0.33	0.63	0.002	0.1764	1.1	0.0852
	165.9	8	0.58	0.42	0.81	0.002	0.2552	7.1	0.1233
Celite 545	133.7	8	0.40	0.28	0.62	0.004	0.1953	2.4	0.0943
	163.8	8	0.55	0.36	0.82	0.004	0.3320	3.6	0.1604

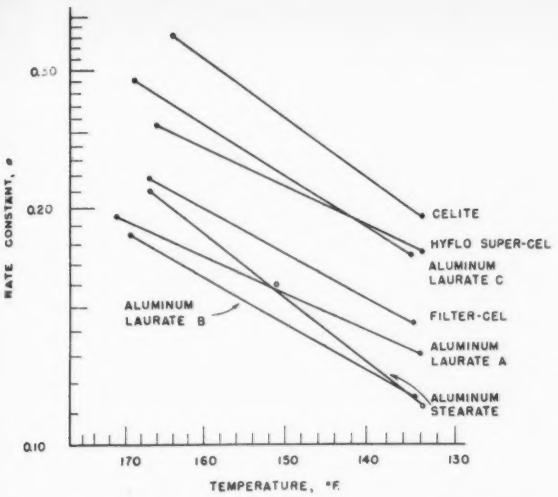

Figure 7—Variation of rate constant with temperature.

Effect of temperature

The rate constants of Table 5 are plotted against temperature in Figure 7. The straight line relationship obtained with aluminum stearate was assumed to hold for the other materials that were dried at two temperatures only. The equations of the lines are

$$a = C\,e^{D/T} \quad \ldots\ldots\ldots\ldots\ldots\ldots\ldots\ldots (21)$$

and the constants C and D for each material are given in Table 6. The average slope corresponds to an activation energy of 10,680 B.t.u./lb. mole or 5932 cal./g. mole of water. This average slope and averages of the respective pairs of a and T_a were substituted into

$$a = Ce^{-5552.1/T_a} \quad \ldots\ldots\ldots\ldots\ldots\ldots\ldots\ldots (22)$$

to obtain a more uniform set of values of C (Table 6). Plots of this equation for each material are given in Figure 8. Graphically, these lines have a slope equal to the

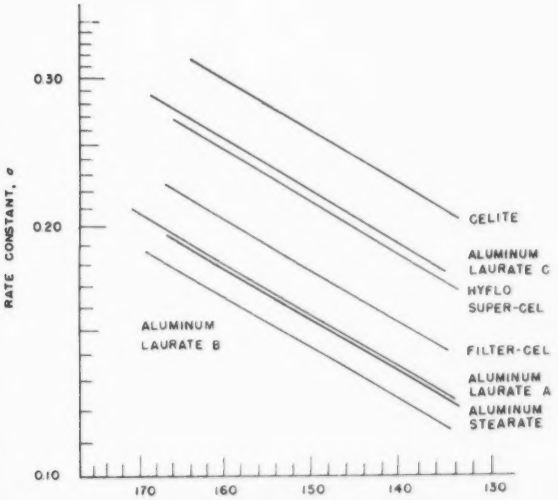

Figure 8—Variation of rate constant with temperature using average slope of the lines in Figure 7.

average slope and pass through the mid points of the respective lines of Figure 7.

For the three diatomaceous silica materials, log C gave almost a straight line when plotted against bulk density but aluminum soap results were some distance from this line and not as consistent although the general trend was the same. Log C for the diatomaceous silicas gave a smooth curve when plotted against average particle size, but, unfortunately, particle sizes of the aluminum soaps were not available.

Effect of tray loading

To investigate the effect of tray loading, rate constants were calculated for each aluminum stearate run and plotted against tray loading, final bed depth, and bulk density. At the highest temperature, there appeared to be a significant correlation but at the two lower temperatures it was obvious that there was none. The same was true when both slope and intercept were calculated for each run. In general, b correlated considerably better than a giving a significant correlation at two temperatures but not the third. At the lowest temperature, there was no correlation between W_s/A and drying rates at $X = 0.05$ but there was at $X = 0.50$; at the highest temperature the reverse was true. Thus it appears that tray loading had no significant effect over the range used, which was from 0.35 to 1.15 lb./sq.ft. The drying rates of the diatomaceous silicas substantiated this conclusion as there was no difference between rates at tray loadings of 0.4 and 0.8 lb./sq.ft.

CONCLUSIONS

All experimentally determined drying rates were in the falling rate zone as no constant rate period was observed. Moreover, since the overall heat transfer coefficient decreased throughout each run, they were all in the second falling rate zone, which is characterized by evaporation below the surface. Plots of drying rate against moisture content were concave downward agreeing with the conclusion of Pearse, Oliver and Newitt [13] that such curves are obtained with fine powders. In a number of runs, there was a tendency for the curve to change to concave upward at the higher moisture contents. According to Oliver and Newitt this probably happened because some water was being transferred by capillary forces.

The experimentally determined drying rates were satisfied by an empirically derived equation that is similar to the commonly used linear equation (10) except that the moisture content exponent was 0.625 instead of unity.

Nomenclature

A = Area of evaporating surface, sq. ft.
A_B = Area of bottom and sides of the tray, sq. ft.
a = Constant (equation 14)
b = Constant (equation 14)
C = Constant (equation 21)
c_s = Heat capacity of humid air, B.t.u./(lb. dry air) (°F.)
c_p = Heat capacity at constant pressure, B.t.u./(lb.) (°F.)
D = Diffusivity of water in the solid, sq. ft./hr.
D = Constant (equation 21)
e = 2.7183
G = Mass velocity, lb./(hr.) (sq. ft.)
H = Humidity of the air, lb./lb. dry air
H_s = Saturation humidity at the temperature of the surface, lb./lb. dry air
h = Heat transfer coefficient, B.t.u./(hr.) (sq. ft.) (°F.)
h_C = Convection heat transfer coefficient from air to the surface, B.t.u./(hr.) (sq. ft.) (°F.)
h_B = Convection heat transfer coefficient from air to bottom and sides of the tray, B.t.u./(hr.) (sq. ft.) (°F.)
h_R = Radiation heat transfer coefficient from surface above the solid to the solid, B.t.u./(hr.) (sq. ft.) (°F.)
j_H = Heat transfer factor defined by equation 2.

K = Constant (equations 10 and 11)
k = Thermal conductivity of the air, B.t.u./(hr.) (sq. ft.) (°F./ft.)
k_H = Mass transfer coefficient, lb./(hr.) (sq. ft.) (unit H)
L = Thickness of solid, ft.
N = Drying rate, lb./(hr.) (sq. ft.), $-dW/Ad\theta$
N_C = Drying rate during the constant rate period, lb/(hr.) (sq. ft.)
q = Total heat transferred to the tray, B.t.u./hr.
q_C = Heat transferred to the solid, by convection, B.t.u./hr.
q_B = Heat transferred through the bottom and sides, B.t.u./hr.
q_R = Heat transferred by radiation, B.t.u./hr.
Re = Reynolds number, $ZV\rho/\mu$, dimensionless
T_a = Temperature of the air, °R.
T_R = Temperature of the radiating surface, °R.
T_s = Temperature of the solid surface, °R.
t_a = Temperature of the air, °F.
t_B = Temperature of the bottom of the tray, °F.
t_m = Mean temperature of the solid, °F
t_R = Temperature of the radiating surface, °F.
t_s = Temperature of the solid surface, °F.
U = Overall heat transfer coefficient between the air and the solid, B.t.u./(hr.) (sq. ft.) (°F.)
V = Air velocity, ft./hr.
W = Weight of water on the tray, lb.
W_S = Weight of dry solid on the tray, lb.
X = Moisture content, lb/lb. dry solid
X_C = Critical moisture content, lb./lb. dry solid
X_G = Free moisture content, $X - X^*$, lb./lb. dry solid
X^* = Equilibrium moisture content, lb./lb. dry solid
Z = Length of tray, ft.
ϵ = Emissivity of the drying surface, dimensionless
λ = Latent heat of vaporization, B.t.u./lb.
μ = Air viscosity, lb./(hr.) (ft.)
π = 3.14159
ρ = Air density, lb./cu. ft.
τ = Time, hr.

References

(1) Perry, J. H., editor, "Chemical Engineers' Handbook", 3rd ed. McGraw-Hill Book Co., Inc., New York (1950).

(2) Treybal, R. E., "Mass-Transfer Operations", McGraw-Hill Book Co., Inc., New York (1955).

(3) Sherwood, T. K., Ind. Eng. Chem., 21, 12 (1929); 21, 976 (1929); 24, 307 (1932).

(4) Gilliland, E. R., and Sherwood, T. K., Ind. Eng. Chem., 25, 1134 (1933).

(5) Comings, E. W., and Sherwood, T. K., Ind. Eng. Chem., 26, 1096 (1934).

(6) Sherwood, T. K., and Comings, E. W., Trans. Am. Inst. Chem. Engrs., 28, 118 (1932).

(7) Sherwood, T. K., Trans. Am. Inst. Chem. Engrs., 32, 150 (1936).

(8) Ceaglske,, N. H., and Hougen, O. A., Ind. Eng. Chem., 29, 805 (1937).

(9) Ceaglske, N. H., and Hougen, O. A., Trans. Am. Inst. Chem. Engrs., 33, 283 (1937).

(10) Gilliland, E. R., Ind. Eng. Chem., 30, 506 (1938).

(11) Van Arsdel, W. B., Chem. Eng. Prog., 43, 13 (1947).

(12) Pearse, J. F., Oliver, T. R., and Newitt, D. M., Trans Inst. Chem. Engrs., (London), 27, 1 (1949).

(13) Oliver, T. R., and Newitt, D. M., Trans. Inst. Chem. Engrs., (London), 27, 9 (1949).

(14) Ludt, R. W., A.I.Ch.E. Journal, 3, 343 (1947).

(15) Hougen, O. A., McCauley, H. J., and Marshall, W. R., Jr., Trans. Am. Inst. Chem. Engrs., 36, 183 (1940).

(16) Maisel, D. S., and Sherwood, T. K., Chem. Eng. Prog., 46, 131 (1950).

(17) McAdams, W. H., "Heat Transmission", 3rd ed. McGraw-Hill Book Co., Inc., New York (1954).

★ ★ ★

Use of Lead in Chemical and Metallurgical Plant Construction[1]

A. TURNER[2], *J. R. WELLINGTON*[2] *and L. WILLIAMS*[3]

The use of lead in the chemical and metallurgical operations at Trail, B.C. is described.

A wide variety of corrosive environments are encountered, including phosphoric and sulphuric acids, sulphur dioxide, fluorides, and ammonium sulphate. It is found that except in the presence of fluorine compounds, 6% antimonial lead is more resistant to corrosion than is soft lead.

The mechanical properties of lead are reviewed with particular reference to its high specific gravity, low mechanical strength, creep and fatigue properties. Principles of plant design to give adequate support, to provide for thermal expansion and contraction, and to minimize the effects of creep and fatigue are enunciated, and illustrated by proven designs that have given long periods of satisfactory service.

LEAD has a history of usefulness dating back to antiquity. In our present industrial economy, flooded with new custom-built products, each designed for its specific application, lead has survived because its unique properties make it still the first choice, and often the only rational choice, for many services. Its use in chemical plant construction dates back to the very foundations of chemical industry, and it is reported to have been used in England as early as 1746 in the construction of sulphuric acid chambers.

In the subsequent development of the Chamber Process for sulphuric acid manufacture, it has remained the only material of construction with the necessary resistance to corrosion which can be easily fabricated into such large units.

These merits have gained general recognition, and experience in the use of lead chambers and their auxiliary equipment has provided a foundation for a much wider application of lead in the chemical industry.

Outstanding, but probably less obvious advantages of lead construction are its versatility and its ease of manipulation. It can be obtained in a variety of forms including large sheets, large or small pipes and a variety of cast shapes. It is easily cast by the simplest foundry techniques. Pipe and sheet are easily shaped and welded, and they require no expensive plant to do a workmanlike job. Piping and linings can be cut, patched or altered by the use of simple tools and with little difficulty to adapt plant to changing requirements. Salvaged plant can be transplanted to new locations, where it is as good as new construction. Shop scrap can be easily remelted and cast into slabs, pipe hangers or fittings in simple chill moulds.

In addition to these merits, lead equipment requires no upkeep painting because the bare metal remains neat and smart. When it is finally scrapped, the scrap value of the lead is equal to a substantial proportion of the first cost.

It would seem inevitable that any material of construction with so many useful attributes would suffer some handicap. In the case of lead, the softness and ductility which makes it so easily fabricated is but an aspect of its inherent mechanical weakness, which has been a factor in discouraging its wider use. After reviewing the corrosion-resisting and the mechanical properties of lead, this paper describes successful design methods which have been developed to overcome this weakness.

Lead as a corrosion resisting structural material

Comparatively few types or alloys of lead are used for chemical plant construction. There are only two major ones. "Soft" lead may be a relatively pure lead, or commonly in the United States, an alloy of lead containing approximately 0.06% Cu, known as "Chemical Lead" (ASTM Specification B29-55). The second major type is "hard" lead, normally a lead-antimony alloy in the range 4-12%, 6% antimonial lead being the most common.

At Trail, the preferred material for the fabrication of process equipment is 6% antimonial lead. If a soft lead is required, pure lead (99.99+% Pb) is generally used. That Cominco is a large scale user and fabricator of lead equipment, and especially antimonial lead, for use within its own plants is shown by the statistical data in Table 1.

Six percent antimonial lead is used in preference to soft lead for two reasons: (1) because it has substantially

[1]*Manuscript received July 31, 1958.*
[2]*Research Engineers, Research and Development Division, The Consolidated Mining and Smelting Co. of Canada Limited, Trail, B.C.*
[3]*Superintendent of Development, Engineering Division, The Consolidated Mining and Smelting Co. of Canada Limited, Trail, B.C.*
Contribution from The Consolidated Mining and Smelting Co. of Canada Limited, Trail, B.C. and presented at the Joint A.I.Ch.E.-C.I.C. Chemical Engineering Conference, Montreal, April 20-23, 1958.

TABLE 1

QUANTITY OF LEAD EQUIPMENT FABRICATED ANNUALLY BY COMINCO*
(5-Year Average; in Tons)

Form	Lead**	6% Antimonial Lead
Sheet	70***	188
Pipe	2	160
Castings	Nil	110
Other	28	2
All forms	100	460

*Exclusive of silver-lead anodes and associated equipment for the electrolytic zinc process, equivalent to 725 tons/year.
**Refers to both pure lead (99.99+% Pb) and "Chemical Lead" (Pb + 0.06% Cu).
***Large proportion of soft lead sheet used for flashing.

better physical characteristics; and (2) because it has equally good or better corrosion resistance. The mechanical properties of lead and antimonial lead alloys will be described later. That the corrosion resistance of antimonial lead is generally equal to or better than lead is somewhat contrary to popular opinion. However, as will be shown by the following discussion, this is the general conclusion based on corrosion testing work and long practical experience in the field. This observation of course, is restricted to the corrosive media encountered at Trail, but the sulphur dioxide recovery system, sulphuric acid plants (over 40% of total Canadian production) wet phosphoric acid and fertilizer plants, and electrolytic zinc (zinc sulphate) process cover a wide range of conditions.

The generally good corrosion resistance of the 6% antimonial lead alloy may best be illustrated by considering specific plant corrosion tests. At Trail, Cominco operates a phosphate fertilizer plant based on the Dorr wet process for the production of phosphoric acid and subsequent manufacture of ammonium phosphate fertilizers. This plant and process have been described in the literature [1, 2].

With its various combinations of phosphoric, sulphuric and hydrofluoric acid solutions and slurries, all at relatively high (60 - 120°C.) operating temperatures, it

TABLE 2

CORROSION RATE OF VARIOUS METALS EXPOSED TO A GYPSUM/PHOSPHORIC-SULPHURIC ACID SLURRY
Sol'n.: 32% H_3PO_4, 0.4% H_2SO_4, 1% Fluorides, Temp.: 80-90°C.
Spool exposed for 15 days

Material	Corrosion Rate (ipy)
6% Sb-Lead	0.0019
Lead	0.0054
AISI 316L	0.0062
Nionel	0.0060

presents a most difficult corrosion problem. Fortunately, due to the omnipresence of the sulphate ion, lead is a useful material of construction for many parts of the plant. Six percent antimonial lead is used almost exclusively throughout this plant. For handling slurries, the 6% antimonial lead alloy is somewhat better than pure lead, as is shown by the data in Table 2. Of course, where abrasion is a serious problem, lead equipment must be brick-lined.

The results of field tests carried out in the various mixtures of phosphoric and sulphuric acid resulting from the countercurrent reaction and filtration process employed have shown that neither lead nor its alloys are corroded by these solutions. Test specimens of pure lead and 6% antimonial lead exposed to mixtures of phosphoric and sulphuric acid ranging in composition from 6 - 60% H_2PO_4, and in temperature from 60 - 75°C. show negligible weight losses after 30 days.

Comparative tests on lead, 6% antimonial lead and AISI Type 316 stainless steel (Table 3) carried out in various sections of the plant ventilating and fume recovery systems serve to illustrate the general conclusion that in dilute phosphoric-sulphuric acid and ammonium phosphate solutions the corrosion rate of 6% antimonial lead is of the same order, or lower than, pure lead. It should be noted here, however, that wherever fluorine compounds, (mainly SiF_4 and H_2SiF_6) tend to concentrate, the corrosion rate of lead, and for that matter most other metals, increases rapidly.

This concentration of fluorine compounds provides the only exception to the general conclusion that 6%

TABLE 3

CORROSION RATES OF LEAD AND STAINLESS STEEL EXPOSED IN VARIOUS VENTILATING DUCTS AND SCRUBBERS, PHOSPHATE FERTILIZER PLANT
(All corrosion rates in ipy)

Material	Fertilizer Section Reaction Agitator Ventilation System			Fertilizer Dust Recovery System[4]	Acid Section Reaction Agitators, Ventilation System[5]
	Gases from[1] Reaction Agitators	Scrubber Liquor[2]	Exit Gases[3] From Scrubber	Scrubber Liquor[4]	
6% Sb-Lead	0.002	0.003	<0.0001	Negligible	0.018
Lead	0.002	0.005	0.0010	0.003	0.013
AISI 316	0.0002	0.1	0.0001 (slight pitting)	Negligible	0.3

Note 1 — Air and steam plus phosphoric acid, mono-ammonium phosphate, trace SiF_4, 90°C. Spool exposed 14 days.
2 — Trace H_3PO_4, 3% H_2SO_4, 10 - 40% $(NH_4)_2SO_4$, 70°C.
3 — Air and steam plus sulphuric acid, ammonium sulphate, trace F, 70°C. Spool exposed 35 days.
4 — 8 - 16% H_3PO_4, Trace - 5% H_2SO_4, 3.3% NH_3/N, 80°C.
5 — Air and steam plus phosphoric acid, fluorine compounds, SiO_2, 50°C. Spool exposed 18 days.

TABLE 4

CORROSION RATE OF VARIOUS METALS EXPOSED IN FLUORINE REMOVAL EQUIPMENT

PHOSPHATE FERTILIZER PLANT

10 – 15% H_3PO_4, 25 – 40% H_2SO_4, ½% Fluorides. Solution highly aerated and agitated. 70 – 100°C. Spool exposed 12 days

Material	Corrosion Rate (ipy)
6% Sb-Lead	0.0007
Lead	0.0001
Durco D 10	0.060
Hasteloy C	0.066
Silver	0.066
Monel	0.12
Carpenter 20	0.28
Aluminum, 2S	Specimen Disappeared
Chromel A	Specimen Disappeared
Hasteloy B	Specimen Disappeared
AISI 316	Specimen Disappeared

antimonial lead has equal or better corrosion resistance than lead in this plant.

Fluorine is removed from the plant circuit by mixing a proportion of the phosphoric acid produced with concentrated sulphuric acid and agitating (stripping) the resultant hot solution with air. This operation, which is undoubtedly the most corrosive single operation within the Trail plants, is carried out in especially built units called "strippers". The strippers are made from cast 6% antimonial lead sheet, one inch thick, carbon brick lined. With some difficulty, a corrosion spool was exposed to the conditions inside a stripper with the results shown in Table 4.

It will be noted that lead is the only possible material of construction for this service. In actual fact, the corrosion rate of both lead and antimonial lead, while satisfactorily low, may vary from place to place inside the stripper, depending on fluorine concentration and degree of aeration and agitation. In practice, the strippers are fabricated from 6% antimonial lead in order to take advantage of the slightly better (at the operating temperature) mechanical properties of this alloy.

The well-known corrosion resistance of lead and its alloys to gases and solutions containing sulphur dioxide is utilized in many ways for handling the numerous gases and solutions of this type processed at Trail. Tables 5, 6 and 7 illustrate typical results. Again, the corrosion resistance of 6% antimonial lead to these solutions has been found to be equal to or superior to that of pure lead.

TABLE 5

CORROSION RATE OF VARIOUS METALS EXPOSED IN SO_2 (ZINC ROASTER) GAS COOLING (GLOVER) TOWER

SO_2 Saturated Water plus 2% H_2SO_4, at 45°C.
49 Days' Exposure

Material	Corrosion Rate (ipy)	Remarks
6% Sb-Lead	Negligible	No visible attack
Lead	Negligible	No visible attack
AISI 316	0.0006	Slight general attack
AISI 304	0.007	Slight pitting
AISI 310	0.06	Pitted
AISI 410	–	Specimen disappeared
AISI 446	–	Specimen disappeared
Mild Steel	–	Specimen disappeared
Aluminum, 2S	–	Specimen disappeared

TABLE 6

CORROSION RATE OF VARIOUS METALS EXPOSED IN JET CONDENSER, AMMONIUM SULPHATE PLANT

(0.1 gpl $(NH_4)_2SO_4$, 0.01 gpl SO_2, Turbulent Flow, Temperature 40°C.)
Spool Exposed for 25 days

Material	Corrosion Rate (ipy)	Remarks
6% Sb-Lead	0.003	Darkened
Lead	0.017	Darkened
AISI 316	0.001	Appearance unchanged
AISI 347	0.001	Appearance unchanged
Mild Steel	–	Specimen disappeared
Cast Steel	0.24	Severe pitting
Wrought Iron	0.55	Pitted
Aluminum, 2S	0.008	Some pitting
Copper	0.04	Pitted
Brass	0.05	Slight pitting

The data presented in Table 7 are of particular interest. The Doyle Scrubber [3] requires that the gas stream be impinged at high velocity into a liquid. Normally the incoming gas stream carrying some solid burden is directed by a nozzle into water. The outside of the nozzle is exposed to the water, saturated gas and splash. While lead is not normally thought of as an abrasion resistant material, in practice, 6% antimonial lead has proven to be admirably well suited for handling many gas-solid suspensions.

Although the corrosion rate for Type 316 stainless steel was negligible in the test results shown in Table 7, a pitting type of corrosion will occur in those areas where sludge build-up is experienced. Lead is preferred as a material of construction in this environment because it shows no tendency to corrode by pitting.

Historically, as noted above, the first important use of lead in the chemical industry was in the production of sulphuric acid by the chamber process. In this process, the sulphuric acid contains some oxides of nitrogen. In the search for improved lead alloys for chamber plant construction when the process first came into large scale use in the early 1900's, it was the practice of the day to test new alloys in the laboratory in hot strong acid. This technique culminated in the so-called "flash-test".

In the flash test, a specimen of lead or lead alloy of specific dimensions was immersed in concentrated sulphuric acid and the temperature of the acid was raised at a prescribed rate. At a certain temperature, a precipitate of lead sulphate rapidly formed in the acid. This temperature was defined as the flash point. Naturally, different impurities and alloys produced different results. The

TABLE 7

CORROSION RATE OF VARIOUS METALS EXPOSED TO VENTILATING GASES FROM THE LEAD SMELTER SINTER CRUSHING PLANT

Spool exposed for 140 days in the gas stream inside a Doyle Scrubber. Gases contain some solids, trace SO_2, are saturated with water vapour, and range in temperature from 40°F. (winter) to 140°F. (summer).

Material	Corrosion Rate (ipy)	Remarks
6% Sb-Lead	0.0001	No apparent change
Lead	0.0005	Some slight mechanical damage
AISI 316	Negligible	No apparent change
Mild Steel	0.07	Severe attack
Wood	–	Discoloured, otherwise no apparent change

TABLE 8

CORROSION RATE OF VARIOUS METALS EXPOSED TO 93% SULPHURIC ACID
Acid Aerated and Agitated — Temp. 25°C.
Spool Exposed for 33 days

Material	Corrosion Rate (ipy)
6% Sb-Lead	0.028
Lead	0.057
AISI 316	<0.001
Cast Iron	0.008

assumption was that the lead with the highest flash-point would give the best service. In the course of time, it was observed that the "order-of-merit" indicated by the flash test did not correlate with the results of actual corrosion tests carried out in the field or under accurately simulated service conditions, and the test was discarded. Today, the possible short-comings of the quick laboratory test and the merits of long term properly supervised corrosion tests under service conditions are widely recognized.

One of the alloying additions that gave a consistently low "flash-point" was antimony. Also, in short term tests in hot concentrated chamber acid, antimonial lead alloys gave somewhat higher weight losses than other leads and alloys. For this reason the antimonial lead alloys were at first erroneously regarded as unsuitable for other types of chemical plant construction. Fortunately, actual tests have shown that the higher strength lead-antimony alloys do have satisfactory corrosion resistance to many media, and these useful alloys have found increasingly wider use.

Another factor contributing to the increased use of antimonial lead alloys has been the increasing importance of the modern contact sulphuric acid plant, which brought about a fundamental change in the type of equipment and materials required for acid plant construction. In the five contact sulphuric acid plants at Trail, iron and steel are commonly used for handling concentrated sulphuric acid, and brick-lined steel for handling hot concentrated acid. Both pure lead and antimonial lead are used for handling the more dilute sulphuric acid solutions. While many soft lead structures have been in service for many years, modern practice is to use antimonial lead for most construction. That 6% antimonial lead may be used for handling even concentrated sulphuric acid (cold) is shown by the data in Table 8.

The mechanical properties of lead

Lead differs from the common structural metals inasmuch as its mechanical properties at ordinary temperatures tend toward those of a plastic solid rather than an elastic or rigid one. For this reason, laboratory results on the tensile strength, creep, and fatigue do not have the usual significance when interpreted for design purposes. Below is given a summary of the main results of laboratory studies of these properties, and it is shown later that with proper design, results can be obtained which are more satisfactory than would be anticipated from the results of laboratory tests.

Widely varying values have been obtained for the tensile strength, yield point and hardness of lead. These values are influenced not only by minor variations in composition, but also by the actual conditions of the test. Thus, it has been stated [4] that no figure recorded is of any value unless the rate of application of the load is also given. In illustration of this point, the following figures have been quoted for a particular sample of high purity lead at different rates of extension:

Time to fracture 1.5 minutes: ultimate tensile strength 2576 p.s.i.

Time to fracture 20 minutes: ultimate tensile strength 2195 p.s.i.

The tensile strength of lead under a short time test is evidently of little significance in the design of equipment for long life. More important are the strength under sustained loads for long periods of time, which is designated the creep strength, and the strength under repeated cycles of stress or strain, described as the fatigue strength.

Since the phenomena of creep and fatigue of any metal are more significant as one approaches its melting point, lead has been the subject of intensive research because it exhibits properties at ordinary temperatures which can only be studied in other structural metals at very high temperatures. For details of this work, reference should be made to papers published by Professor H. F. Moore and his associates at the University of Illinois, J. Neill Greenwood in Australia, G. L. Bailey and J. McKeown of the British Non-Ferrous Metals Research Association, and others.

Creep of lead and lead alloys

Moore, Betty and Dollins [5] have quoted experimental evidence to show that there is no limiting stress under either long-continued steady load, or with cycles of repeated stress, below which fracture of lead will not eventually occur. It has also been found that although alloying with 6% antimony increases the tensile strength of pure lead by about 5 times, the increase in creep strength is only about three times at ordinary temperatures. Greenwood [6] gives a comparison to illustrate this (Table 9).

These figures suggest that an alloy containing around 6% antimony has long-life properties better than either pure lead or the higher antimony alloys, both at ordinary or somewhat higher than ordinary temperatures. Since antimony additions above 6% make the lead difficult to work, these data give some support for the general practice of adopting the 6% alloy as a standard material for lead construction. As the temperature is raised, the improvement in creep strength due to the antimony decreases and eventually disappears at temperatures around 120°C. (250°F.) See Table 10 and Figure 1.

TABLE 9

COMPARISON OF TENSILE STRENGTH AND CALCULATED BREAKING STRESS FOR 30-YEAR LIFE

Alloys	20°C. (68°F.)		50°C. (120°F.)	
	Tensile Strength p.s.i.	Stress 30-Year Life p.s.i.	Tensile Strength p.s.i.	Stress 30-Year Life p.s.i.
Pure Lead	1,500	325	1,000	250
1%Sb	2,600	500	2,000	325
6%Sb	7,700	1,000	5,500	650
11%Sb	7,700	775	5,500	500

TABLE 10

MAXIMUM ALLOWABLE FIBRE STRESS IN EXTRUDED PIPE

Temperature		Equivalent Steam Gage Pressure p.s.i.	Maximum Allowable Fibre Stress p.s.i.	
°C.	°F.		Chemical Lead	6% Antimonial Lead
20	68		200	400
30	86		190	370
40	104		180	340
50	122		172	310
60	140		162	280
70	158		153	254
80	176		144	222
90	194		136	195
100	212	0	127	165
110	230	6	118	137
120	248	14	110	110
130	266	24	100	80
140	284	37	90	50
150	302	54	80	–
247	477	535	–	0
327	621	–	0	–

To calculate safe working pressure of lead pipe, use formula

$$P = \frac{2\,ST}{D} \text{ or } T = \frac{PD}{2S}$$

where P = safe working pressure in p.s.i.
S = maximum allowable fibre stress from above table
T = thickness of pipe wall in inches
D = inside diameter of pipe in inches

For mechanical or structural reasons, it is sometimes wise to allow additional wall thickness above that derived from this formula.

An attempt has been made [7] to develop a formula to express the stress required to produce failure in lead alloys after the elapse of any given period of time, but the extrapolations have been questioned because [8] the data did not fall in a straight line, and also because the creep of pure lead has been shown to be a discontinuous process of deformation with alternating periods of rapid and of extremely slow extension [9].

Fatigue of lead and lead alloys

Studies of fatigue of lead and lead alloys have been largely related to a distinctive type of intercrystalline cracking of cable sheathing in service. Similar failures have also been observed in lead piping which has been subjected to bending stresses immediately after fabrication. The same type of failure has been reproduced experimentally by use of a Haigh testing machine imposing repeated cycles of stress on a test specimen. Other types of test have also been devised which impose repeated bending stresses on the specimen, reproducing more closely the conditions encountered in service.

As in the case of creep, the endurance of lead to fatigue stresses is decreased as the temperature is raised. Thus Townsend [10] found that a sample which failed at 24 million reversals at 4°C. lasted only 4 million cycles at 32°C., while Beckinsale and Waterhouse [11] similarly found that lead which failed at 1.17 million reversals in a Haigh machine at ordinary temperatures, failed at 0.988 million at 100°C. and at 0.556 million at 150°C. all tests being made under repeated stresses of ±560 p.s.i.

The rate of reversal of cycles of stress has an important influence on the endurance under fatigue stresses, the number of cycles to failure decreasing as the frequency decreases, though the actual time to failure may increase [12, 13].

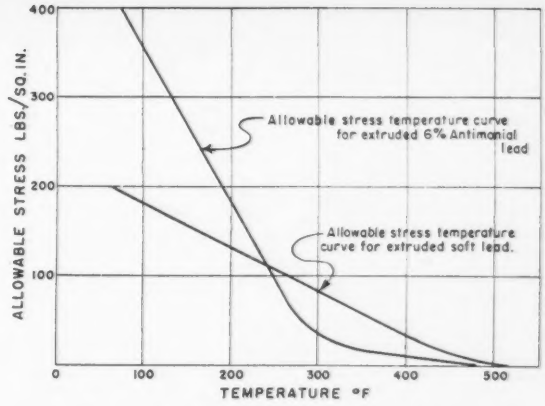

Figure 1—Allowable fibre stress in lead.

The effect of alloying elements is generally to cause grain refinement, which has the effect of increasing the fatigue resistance of lead, but even in alloys of comparable grain size, it has been found that the addition of antimony, tin, or other alloying elements increases the fatigue resistance. This improvement persists as the temperature is raised [14, 15].

From this brief review of the creep and fatigue properties of lead, it is evident that even at ordinary temperatures, the mechanical properties of metallic lead are difficult to define. For plant design purposes, therefore, guidance must be sought from empirical data based on actual experience.

A series of such figures developed for the design of extruded pipe systems was published by Roll [16], and are given in Table 10.

Although laboratory tests show that any continuous loading of lead, or any cyclic stress will eventually cause failure through creep or fatigue, practical experience has shown that with proper design and adequate support, lead construction will last indefinitely.

Lead tank and tower walls, for example, have been found to undergo a certain amount of distortion or bulging between their steel-frame support during their initial period of service, and then remain unchanged for long periods of time after arriving at their stable form.

Tanks are still in service at Trail which were installed 25 years ago having had very little repair or maintenance in the interval.

Design factors in lead installations

The successful use of lead construction is conditional on the recognition of the differences in the properties of lead which distinguish it from the more common structural materials. The most important of these are, of course, its mechanical weakness, its lack of elasticity which results in permanent deformation under stress, its tending to creep under any sustained load, and its low fatigue limit under repeated stresses. Its weight adds to the problems of design. The first requirement of any design is, therefore, to provide adequate support.

Even at moderately elevated temperatures, the problem of support is more exacting, as the strength of lead and its alloys falls off considerably with rising temperatures (see Figure 1).

A second requirement of design is the provision for expansion and contraction with changing temperatures. The ideal situation is one in which the installations are constructed in such a way that the lead is free to move without hindrance under the influence of changing temperatures. If free movement can be provided for, then there is no stress that could result in failure. In the traditional lead chambers [17], sheets were supported from their tops and hung free with lower edges over-lapping the up-turned edges of the floor of the chamber. These chambers were about 14' high, which is about the limit for free-hanging sheets of lead. If the requirements for support do not permit free contraction and expansion, then the fixed points of supports should not be too widely spaced, so that the amount of expansion to be taken up in each section remains small. Often, such design is satisfactory and there is no tendency towards failure through fatigue or creep. In large installations, properly designed expansion joints are provided so that excessive stresses cannot develop.

The adoption of 6% antimonial lead with its greater strength and fatigue resistance has made the problem of support somewhat easier to solve, but has also introduced new problems. Being less ductile, it is less able to adjust itself to local stresses and is somewhat more prone to cracking at points of concentrated stresses. Once this is recognized design can be adjusted to avoid such stress raisers and no trouble is encountered.

The application of these basic principles of design in lead construction, of adequate support, of proper provision for thermal changes, and of avoidance of stress raisers is illustrated by a number of installations in actual use in the Trail Plants. Since the practice of recent years has been toward the general use of 6% antimonial lead, the specific examples described have been constructed in that alloy. The principles involved, however, have an equal application to soft lead construction and the designs can be adapted to that material by recognition of the differences in its properties.

Lead piping

One of the great advantages of lead piping, in addition to its corrosion resistance, is its adaptability and the ease with which it can be installed. When pipe bends are required, straight pipe may be filled and packed with sand, and bent. During the operation, the outer wall becomes thinner and if the radius of the bend is less than four times the inside diameter of the pipe, this outer wall or "heel" is reinforced by "burning on" an added layer of lead. Shorter radius bends may be made by means of mitred joints between short sections of pipe. Alternatively, a variety of pipe fittings may be purchased as stock items, cast in chemical lead or 6% antimonial lead. These are supplied in four ways –

1) With solid lead flanges welded in place.
2) With cast iron or steel slip-on flanges.
3) With over-length for flanging in the field.
4) With plain ends for welding.

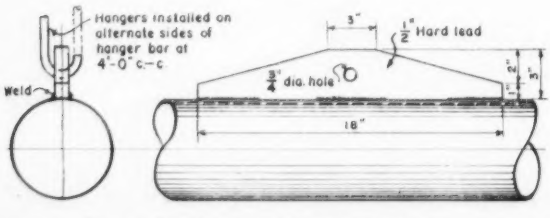

Figure 2—Method of hanging lead pipe.

When flanges are used, the diameter and drilling normally conforms to American Standards Association requirements for Class 125 cast iron flanges.

The traditional method of supporting pipe runs on continuous wooden supports or steel troughs has the disadvantage that any leakage causes damage to the supports, that free expansion and contraction are hindered, and that the location of any leak is not always evident, or easily accessible for repair.

The preferred method of hanging lead pipe in Cominco plants is illustrated (Figure 2). This method has the merit of infinite adaptability, neatness, and negligible up-keep cost since lead does not require any protective painting. It provides unhampered movement under stresses produced by expansion and contraction, and in this way is the ideal support for lead. Since the supports are all above the pipe, they are immune from damage from the contents of the pipe if leakage should occur, and the point of the leakage is easily located and accessible for repair.

The hanger bars are cast in simple chill moulds in the shop, using shop scrap.

Pipe runs up to 6" in diameter can be supported in this manner. Lengths up to 30 feet long have been prefabricated complete with hanger bars, hoisted in position, and the joints welded into position with butt welds in the field. Hanger bars are $\frac{1}{2}$" hard (6%) antimonial lead, 18" long, and are welded to the pipe at 4 to 8 foot centres on hard lead pipe.

Lead sheeting

Welded joints are standard construction in chemical engineering practice where lead linings or coverings must protect the supporting structure from infiltration of corrosive gases or solutions. In general, lap joints (Figure 3)

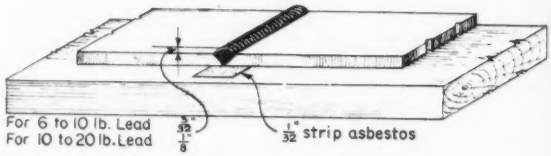

Figure 3—Typical welded butt joint.

are used for joints on vertical sheet lead. On horizontal surfaces, where the free movement of the lead may be restrained by the weight of the lead itself, or by the pressure of a liquid on the lead, there is a tendency for the bend of the lap joint to act as an expansion bend, localizing the stresses and strains and causing failure along the lap of the joint. For this reason, butt joints are used on horizontal surfaces (Figure 4).

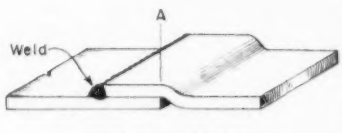

NOTE – When hydrostatic or other pressure (possibly the weight of Lead itself on a floor or roof) acts on a Lead surface with lap joints without allowance for expansion or contraction, any expansion or contraction of the Lead sheet will cause the bend at the lap joint to act as an expansion bend, localizing the stress and strain. Experience indicates that the Lead will eventually fail along Line "A". In this application, butt joints are recommended with full provision for expansion.

Figure 4—Typical lap joint.

Tanks

Unlined wood stave tanks are often used for holding liquids without ill effects except for the corrosion of the steel hoops. Lead pipe has been used to enclose the hoops, as indicated (Figure 5). This system is unsatisfactory because if any injury to the pipe allows entry of the solution, it will lie in the lower half, and may corrode the steel beyond repair before the damage is apparent. Effective protection is provided by draping lead strips over the pipe, leaving the hoop open for inspection, and allowing any leakage to drain away without causing damage to the hoop.

Since unlined wood stave tanks depend on the swelling of the staves for solution tightness there is a tendency for the staves to dry and shrink when the tanks are lead lined. The tightening of the hoops to maintain structural rigidity would have a most destructive effect on the lead lining. To avoid this condition, a reinforcing ring of wood is constructed around the inside top of the tank to maintain its original diameter and shape.

Details of the design of such a tank are shown (Figure 6). If the height of the wall does not exceed 12 feet, intermediate support of the vertical sheets is not necessary. It will also be noted that the side sheets are continued beyond the angle of the base and butt-jointed to the floor lining in a circle about 3 inches inside the circumference of the base. This provides some freedom for expansion and contraction of the wall lining without any concentration of stresses about fixed points, or along fixed lines.

In installations over 12 feet high, vertical seams are supported for their whole length. In making the lap joint, the vertical edge of the sheet is first secured to the wood with flat head nails about 8″ to 10″ apart, and clear of the edge of the sheet. The second sheet is lapped well over the nail heads and welded to give a lap of not more than 2″. The whole seam is then protected and supported by a burnt-on extruded lead supporting bar (Figure 7) $6\frac{1}{2}$″ x $\frac{1}{2}$″) which is secured by carriage bolts at intervals of 2 feet. The heads of the bolts are protected by a welded cover of lead sheet. Earlier methods of support depended on the use of a steel strap through which the supporting bolts were passed, the steel being protected by a welded-on cover of sheet lead. Such a method produced concentrations of stresses in the sheets in the vicinity of the supporting bolts. The adoption of the extruded supporting bar, with a continuous welded joint to the sheets on both sides, has eliminated this source of weakness.

Walls of all tanks, where possible, are lined with continuous sheets from top to bottom. This avoids concentrations of stresses where over-hand burning of lap joints crosses the vertical seam. If sheets of sufficient length are not obtainable from the supplier, two shorter sheets can be butt-welded end-to-end, before erection.

Flues

In the design of flues, the problems of support and expansion both become more difficult as the cross-section and the length of the flues increase.

Circular flues

Circular flues up to a diameter of 42″ have been constructed of lead and are operating satisfactorily. In the construction of these flues, antimonial sheet lead of about 12 pound weight is built around a cylindrical form and provided with welded-on circular $\frac{3}{8}$″ lead stiffener rings at 12″ intervals.

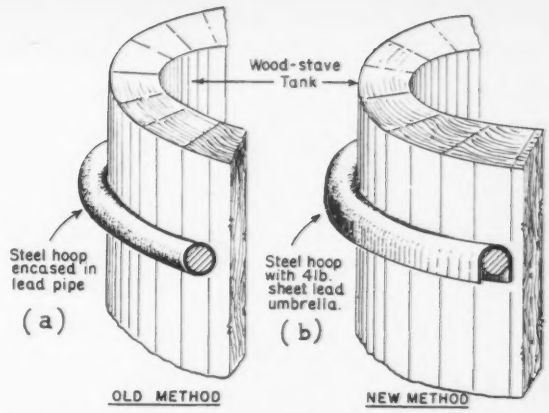

Figure 5—Methods of protecting steel hoops on wood stave tanks.

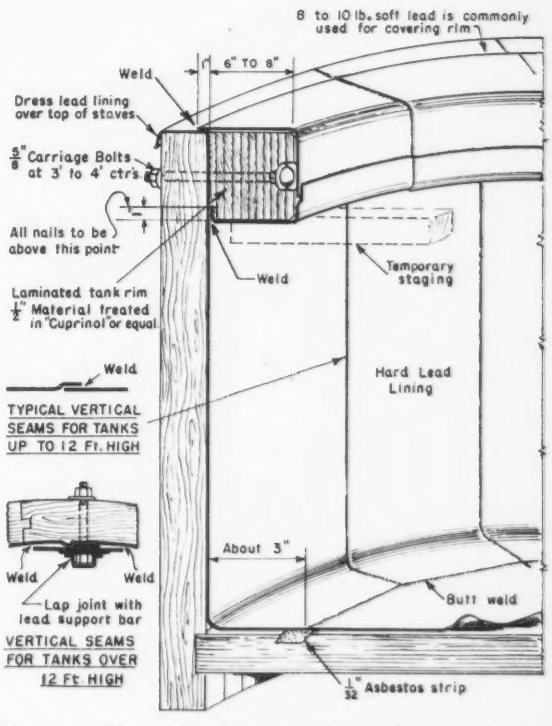
8 to 10 lb. soft lead is commonly used for covering rim
6" TO 8"
Weld
Dress lead lining over top of staves
⅜" Carriage Bolts at 3' to 4' ctrs.
All nails to be above this point
Laminated tank rim ½" Material treated in "Cuprinol" or equal
Weld
Temporary staging
Hard Lead Lining
TYPICAL VERTICAL SEAMS FOR TANKS UP TO 12 Ft. HIGH
About 3"
Weld
Weld
Lap joint with lead support bar
VERTICAL SEAMS FOR TANKS OVER 12 Ft. HIGH
Butt weld
1/32" Asbestos strip

Figure 6—Typical section through lead lined wood stave tank.

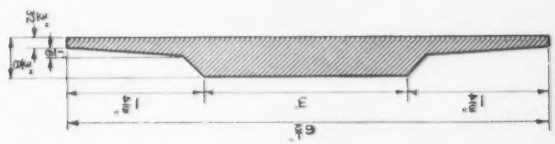

Figure 7—Lead supporting bar. For use in fabrication of lead vessels as stiffeners.

All joints in these flues are butt joints. In joining sections of larger flues, the lower half can be welded from the inside and the upper half from the outside.

The flue is supported by lugs on the stiffener rings, resting on longitudinal I beams on either side of the flue,

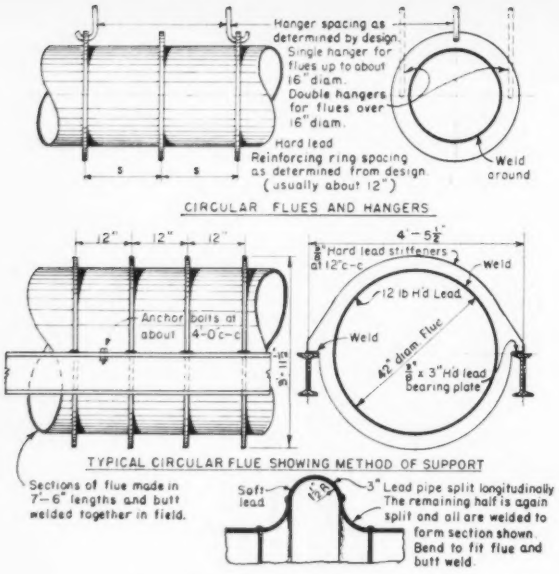
Hanger spacing as determined by design.
Single hanger for flues up to about 16" diam.
Double hangers for flues over 16" diam.
Hard lead
Reinforcing ring spacing as determined from design. (usually about 12")
Weld around
CIRCULAR FLUES AND HANGERS
12"
12"
12"
4'-5½"
Hard lead stiffeners at 12"c-c
Weld
12 lb Hd Lead
Weld
Anchor bolts at about 4'-0"c-c
42" diam Flue
⅜" x 3" Hd lead bearing plate
TYPICAL CIRCULAR FLUE SHOWING METHOD OF SUPPORT
Sections of flue made in 7'-6" lengths and butt welded together in field.
Soft lead
3" Lead pipe split longitudinally The remaining half is again split and all are welded to form section shown. Bend to fit flue and butt weld.

Figure 8—CIRCULAR FLUES:

(a) Circular flues and hangers.

(b) Typical circular flue showing method of support.

(c) Suggested method of allowing for longitudinal expansion.

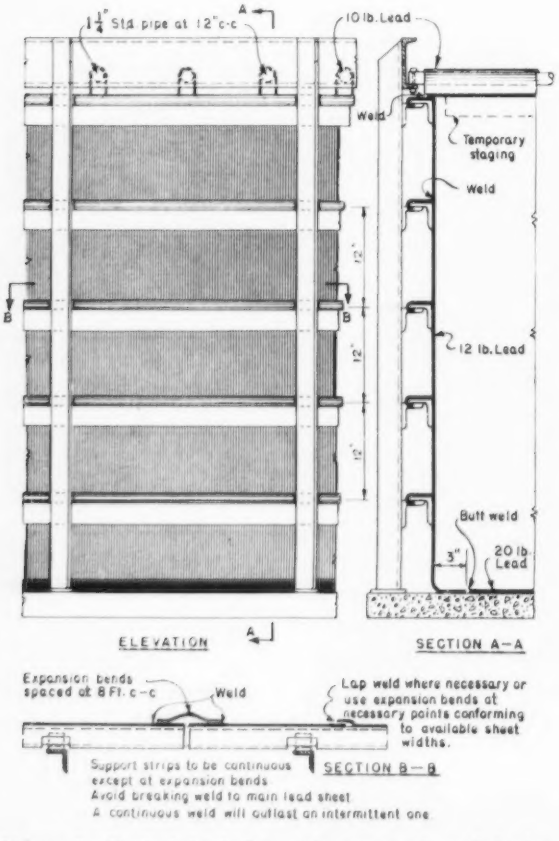

Figure 9—Typical lead flue with structural steel basket construction.

or by hangers hooked into holes drilled in the stiffeners. In the former case, the lugs are welded to a bearing plate of hard lead ⅜" x 3" resting on the surface of the I beam, and anchored to it with bolts at 4-foot intervals. This bearing plate absorbs some expansion stresses and so protects the flue from deformation. (See Figure 8).

When supported by hangers, a single row, hooked into holes at the top of the stiffeners, is adequate for flues up to 16" in diameter. For larger flues, double hangers hooked into holes drilled in the sides of the stiffener rings are required. Hangars are provided 3 feet apart to give adequate support. (See Figure 8).

In flues which are provided with bends, it is often not necessary to install expansion joints. But in long straight runs or where a flue joins another structure, expansion joints of soft lead, of the type illustrated, are necessary. (See Figure 8).

Towers and flues

In the past, it was Cominco practice to build towers and flues of laminated wood construction lined with lead. These had the disadvantage that the sheets were not accessible for inspection from the outside, and they have recently been superseded by a steel basket type of construction to support the lead sheet. These have the advantage that they can be easily inspected and repaired, sometimes while the vessel is still in service.

Structural details of steel basket construction are illustrated in Figure 9. Continuous 12 pound lead strips are welded to the sheet before it is erected, and these are anchored to the horizontal angle sections of the steel basket. It is most important that these strips be continuous, otherwise a point of weakness is developed at the gap.

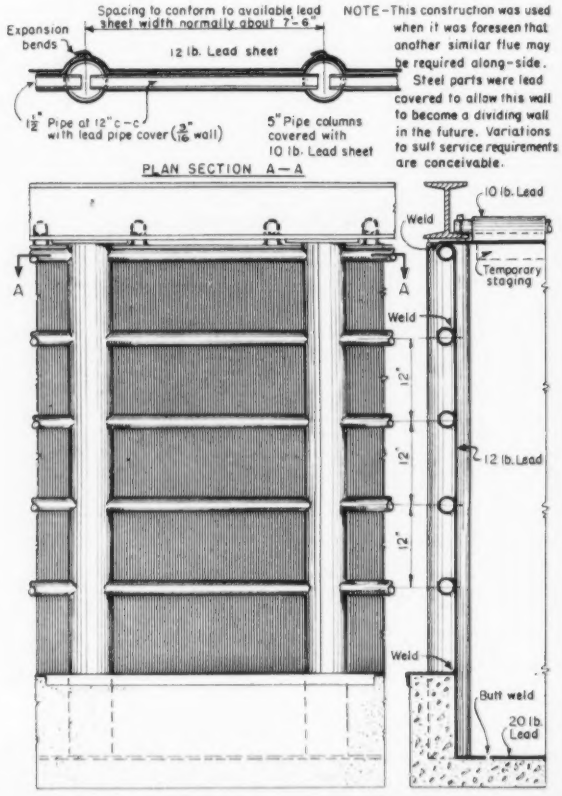
Spacing to conform to available lead sheet width normally about 7'-6"
Expansion bends
12 lb. Lead sheet
½" Pipe at 12"c-c with lead pipe cover (2/16" wall)
5" Pipe columns covered with 10 lb. Lead sheet
NOTE—This construction was used when it was foreseen that another similar flue may be required along-side. Steel parts were lead covered to allow this wall to become a dividing wall in the future. Variations to suit service requirements are conceivable.
PLAN SECTION A—A
10 lb. Lead
Weld
A
A
Temporary staging
Weld
12"
12"
12"
12 lb. Lead
Weld
Butt weld
20 lb. Lead

Figure 10—Typical lead flue with pipe basket construction.

The steel supports are continuous excepting where an expansion bend is inserted.

A later development in this type of flue construction is the pipe-basket construction illustrated in Figure 10. Expansion bends and vertical joints in this type of construction are combined in the design and located in the circumference of the vertical 5" pipe column.

Lead clad steel

Design requirements for lead construction in Cominco plants reach their extremes in a large flue exposed to pressure differentials, vibration, fluctuating temperatures, corrosive gases and intermittent condensation of moisture. All of these conditions are encountered in a gas-handling system conducting hot, dust-laden gases from the lead sinter plant to a Cottrell Plant and sulphur dioxide absorption units at Trail.

As part of a reconstruction program, a 300 x 9 ft. diameter flue was constructed to handle gases carrying a heavy dust burden and containing about 3% SO_2, entering at a temperature as high as 400°F. At the discharge end of the flue, a booster fan forces the gases down a cooling tower 50 ft. high and 30 ft. in diameter, concurrent with a fine spray of water which cools the gas and wets the dust particles to condition them for treatment in a Cottrell precipitator. Corrosive conditions are increased when there is condensation of moisture during shutdown periods when the flue cools down. Stainless steel could not be used because of pitting due to contact corrosion aggravated by the presence of fluorine compounds.

To meet these conditions, the whole of the flue was constructed of steel with a lead-clad interior lining, and the cooling tower was constructed of lead-clad steel, supported on a concrete sill and base. The steel casing of the booster fan, as received from the manufacturers, was lead sprayed at Trail, using a Metco wire gun, and the sprayed coating was further sealed with a coating of an epoxy-phenol resin. The steel fan runner was not coated, since it is easily replaced and is not subject to condensation of moisture.

The lead cladding was applied to cylindrical sections of the flue steel, in units of 9-ft. diameter and 8-ft. length. Internal surfaces of these cylinders were cleaned, fluxed, and then given a first coating of lead by rotating in a shallow bath, so that the surface of the steel dipped into the molten lead. No lead adhered to the unfluxed external steel surface. The main coating of lead, about 10 lb./sq. ft., (5/32 in.), was then applied using equipment and methods developed by Knapp Mills Incorporated of Long Island City, New York. The sections were then welded into units about 50 ft. in length, and the internal lead cladding applied over the welded joints by hand burning. These sections were provided with end flanges and were transported to the site and erected. The flanges were bolted up, and the cladding over the joints "burned" together in position.

The cooling tower was constructed of lead clad mild steel, clad by the Knapp Method, supported by a concrete sill and base. The mild steel plates were clad before construction, each plate being spot welded to form a cylinder, then cleaned, fluxed and clad in the same way as the sections of the flue. The plates were then re-rolled to the correct curvature and welded in position. The cladding at the welded joints was then sealed by cladding lead over them by hand methods. The vertical walls of the lower concrete part were protected by 12 lb. (3/16 in.) sheet lead welded to vertical supporting strips of lead inserted in the concrete. The floor was protected by sheet lead laid over the concrete, after the application of an intermediate dressing of asphalt. This lead was protected by a course of acid proof brick, against the possibility of mechanical damage if cleaning out of accumulated sludge should be necessary.

Finally, the external steel surfaces of the flue and the cooling tower were sandblasted and primed with a zinc-rich paint to provide cathodic protection, then given an outer coat of a silicone-base heat resistant paint.

Lead cladding or homogeneous bonded lead provides the ultimate in support of lead construction. Steel is the normal base material but others can be used. Operating temperatures can be carried close to the melting point of lead, thus extending lead's usefulness into a wide new field. Hand burning, pouring (casting) or the machine methods developed by Knapp Mills may be employed. Rotating elements such as fan runners, high temperature steam heating coils, and lined pipe for high pressures are easily constructed.

Due to the difference in the temperature coefficient of expansion between lead and steel, there is a long term tendency toward failure by intercrystalline cracking when extreme and frequent temperature fluctuations are encountered. In case of penetration of the lead at any one spot, there is no creep of the corrosive media behind the lining and repairs are easily effected. Good workmanship is essential, and the few reported early failures are ascribed to discontinuities in the lead and lack of complete bonding.

Economics

To illustrate cost of lead work, Table 11 gives construction estimates of a typical tank in several corrosion resistant materials. A tank 10 ft. in diameter and 20 ft. high for storage of an acid solution, has been used for the example. Labor was figured at an assumed shop rate of $4.00/hr, sheet lead and extruded lead at the current quoted price of 18.5¢/lb., and other materials at current prices.

TABLE 11

COMPARISON OF COST OF AN ACID TANK 10' DIAMETER, 20' HIGH WITH VARIOUS MATERIALS OF CONSTRUCTION

	Total Cost	Unit Cost Sq. Ft.
1/8" lead lining on 3" wood staves	$4800	$ 6.80
1/4" rubber lining on 1/4" mild steel	4700	6.67
3/16" lead cladding on 1/4" mild steel	5600	7.94
316 L stainless steel (average 1/8" plus)	9000	12.72

The design in each case is normal for the service, and the intention is merely to show the relative costs of construction in lead and in alternative materials.

These figures demonstrate that in first cost lead is competitive with other materials of construction. The scrap value of the lead in the example quoted, would represent an additional $600 (at current scrap quotations of 8.5¢/lb.) which would be recoverable at the end of the life of the installation. In more complex installations, the versatility of lead sheet construction would possibly result in rather lower costs in relation to other materials.

During the service life of the installation, the low maintenance costs, the excellent corrosion resistance, the ease and reliability with which modifications can be made in lead sheet equipment, and the excellent service at high temperatures given by lead-clad plant, contribute further to the overall economic advantages of lead construction.

References

(1) Atwell, J., Ind. Eng. Chem. 41, 1318 (July 1949).
(2) Anon, Can. Mining Journal, 75 (5) 297 (May 1954).
(3) Doyle, H., and Brooks, A. F., Ind. Eng. Chem. 49(12) 57A (Dec. 1957).
(4) Bailey, G. L., British Non-Ferrous Metals Research Association, Development Report D. 38 (1940).
(5) Moore, H. F., Betty, B. B., and Dollins, C. W., University of Illinois Bull. 272 (1935).
(6) Greenwood, J. N., Am. Soc. Testing Materials, Proc. 56, 858 (1956).
(7) Moore, H. F., and Dollins, C. W., University Illinois, Bulletin 347 (1943).
(8) Gohn, G. R., Arnold, S. M., and Bouton, G. M., American Society Testing Materials, Proc. 46, 990 (1946).
(9) Smith, A. A., Trans. Am. Inst. Mining Met. Eng., Inst. Metals Div., p. 165 (1941).
(10) Townsend, J. R., American Society Testing Materials, Proc. 27, 153 (1927).
(11) Beckinsale, S., and Waterhouse, H., Journal Inst. Metals, 39, 393 (1928).
(12) Dollins, C. W., University Illinois Bulletin 378 (1948).
(13) Ferguson, L., and Boulton, G. M., American Society Testing Materials—Am. Inst. Mining Eng. Symposium on Stress Cracking of Metals, p. 470 (1944).
(14) Hopkin, L. M. T., and Thwaites, C. J., J. Inst. Metals, 82, 181 (1953-54).
(15) Brock, P., and Weldon, B. A., British Non-Ferrous Metals Research Association, Research Report R.R.A. 1090, July 1955.
(16) Lead Industries Asso. "Lead in Modern Industry", p. 192 (1952).
(17) Wyld, W., Manufacture of Sulphuric Acid (Chamber Process) Vol. 2. Manufacture of Acids and Alkalis. Lunge and Cumming Series, Published Gurney and Jackson, London, 1924.

NOTE—Figures 2, 3, 4, 5, 6, 8, 9 and 10 are reproduced here by permission of *Chemical Engineering*, where these drawings were published in March, April and May 1956.

★ ★ ★

The Pyrolysis of a Heavy Crude Oil in a Fluidized Bed[1]

G. G. MADGWICK[2], C. H. AMBERG[3] and W. S. PETERSON[3]

The pyrolysis of a heavy high sulphur crude oil in an inert fluidized bed at temperatures between 550 and 800°C. has resulted in the production of an olefin rich gas and a liquid product containing increasing amounts of aromatic material with increasing temperature.

Analysis of the process gas has shown that for average reactor residence times of more than one second, equilibrium is approximated for the system ethane-ethylene-hydrogen. There is considerable scatter in the data for the analogous system propane-propylene-hydrogen but for most conditions a significant deviation from equilibrium exists.

The sulphur compounds in the light oil were of thiophenic character. The ratio of 2- to 3-methylthiophene in the toluene fractions was examined.

In this work a typical high sulphur heavy Canadian crude oil from the Lloydminster field was chosen as a feed material, and a detailed study was made of the gaseous and liquid products of pyrolysis from an inert fluidized solids system. The effect of reactor temperature and residence time on the composition of these phases was of particular interest.

The commercial significance of this study lies in the production, from a low cost raw material, of a gas rich in unsaturated hydrocarbons and a liquid product containing large proportions of aromatic compounds.

Previous studies by Peterson et al [1] have shown that substantial upgrading of similar heavy crudes may be obtained by thermal cracking under mild conditions (500-550°C.) in a fluid-solids reactor. Conventional cracking catalyst gives better results under such conditions but suffers from heavy coke deposition and metal deactivation. High temperature pyrolysis of a variety of oil fractions has also been investigated by Reid et al [2] using a fluid bed, satisfactory yields of natural gas substitute were obtained by this means. The large scale application of the fluid bed technique for cracking heavy feeds has been confined to the widely described fluid coking process [3, 4, 5, 6, 7, 8].

Gaseous product distribution resulting from the pyrolysis of various hydrocarbon feeds has been studied recently by Linden and Peck [9] who used an empty tubular reactor for their investigation. While such a reactor permits establishment of required residence times with considerably accuracy and between wide limits, it does not allow accurate estimation of true gas temperature, a major variable which can be measured directly in a fluid-solids system.

Gas flow rates through a fluid bed cannot be varied greatly; however, it is possible to induce a reasonable range of residence times by varying bed depth and reactant recycle ratio.

Experimental

(a) Equipment:

The continuous pilot plant used for this study has been described previously [1, 10]. In Figure 1 is a simplified flow diagram of the equipment. The preheated oil was injected directly into the bottom of the reactor vessel; the usual practice of feeding to the reactor riser was not followed because of rapid coke formation and consequent blocking of the small riser. The properties of Lloydminster crude oil are given in Table 1. The bed material used for all runs was finely divided silica sand; the screen analysis is given in Table 2.

TABLE 1

PROPERTIES OF LLOYDMINSTER CRUDE OIL

Specific Gravity	0.98
Degrees A.P.I.	12.4
Water Content % w/w	0.2
Solids Content % w/w	0.15
Total Sulphur % w/w	3.4
Conradson Carbon	8.2
Distillation: A.S.T.M. D86-56	
	°C.
I.B.P.	138
10%	282
20%	313
30%	325
50%	332

[1]*Manuscript received December 3, 1958.*
[2]*N.R.C. Postdoctorate Fellow.*
[3]*Division of Applied Chemistry, National Research Council, Ottawa, Ont. Contribution from the Division of Applied Chemistry, National Research Council, Ottawa, Ont.*

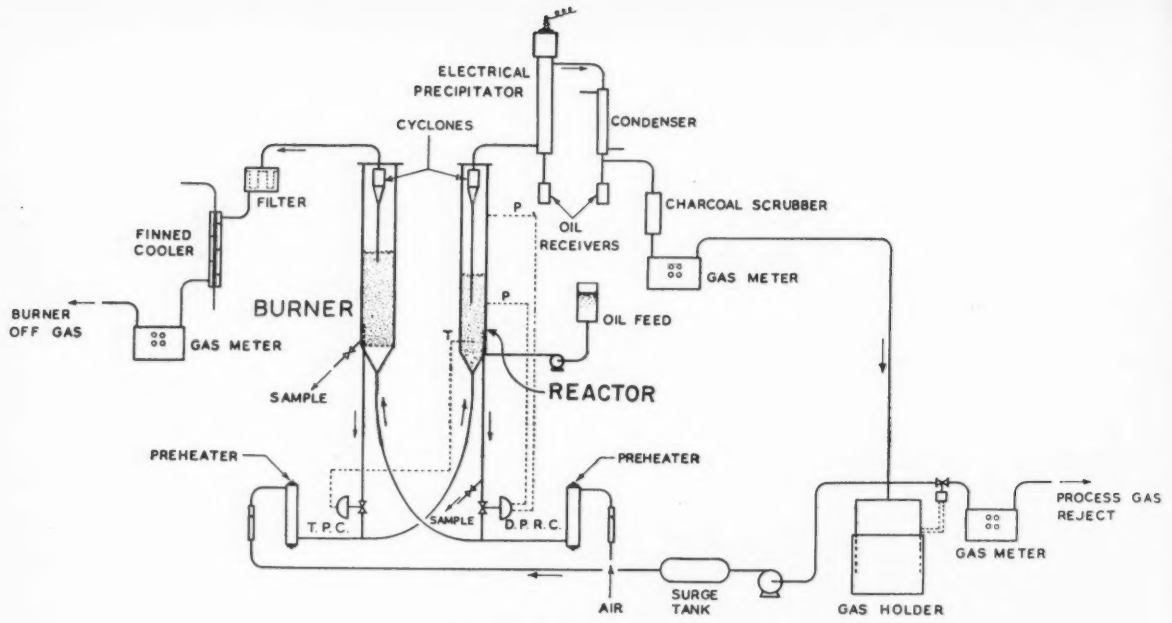

Figure 1—Pilot plant layout.

Reactor temperature was automatically maintained by supply of hot sand from the burner vessel, which was operated at a temperature 50-100°C. higher than that in the reactor. In a similar way a differential pressure recorder/controller actuating a plug valve in the reactor standpipe, controlled the level in the reactor vessel. Part of the metered reactor offgas was recycled to provide solids transfer to the reactor and to ensure smooth fluidization.

In addition to product collection from the reactor, analysis samples were withdrawn at intervals from the metered burner offgas and from the circulating burnt and coked sand stream.

Operating conditions are summarized in Table 3. Although most runs lasted ten hours no significance was attached to analysis of products collected during the first four hours. The range of useable reactor bed depths was limited by the fluidizing quality of the material; very low beds created temperature control problems and high beds caused excessive slugging with attendant coke lump formation in the reactor. The residence times given in Table 3 are average values calculated from the bed depth, bed void volume and from the mean reactor offgas flow rate at the temperature of the bed. Use of the latter parameter implies instantaneous generation of the final gas volume at the feed inlet, a valid assumption if the primary cracking reactions take place during a small fraction of the total residence time. Linden and Peck [9] have made a similar assumption. The recycling of reactor offgas increased the single-pass residence time by a factor 1/1-R where R was the fraction recycled. The walls of the reactor above the fluid bed level were kept at a temperature of 100°C. below that within the bed, to minimize additional cracking outside the reactor zone.

TABLE 2

SCREEN ANALYSIS OF BED MATERIAL

Mesh Size	Percent by Weight
On 60	4.2
Through 60 on 80	10.2
Through 80 on 100	15.0
Through 100 on 200	64.2
Through 200 on 325	6.2
Through 325	0.2

(b) **Results:**

Table 4 summarizes the overall yields of gas, oil and coke from each run. It will be noted that the weight yield of process gas reaches a maximum at a temperature of about 650°C., while volume yields rise throughout the temperature range with formation of larger proportions of hydrogen and coke.

The scatter in data does not permit any conclusions to be reached about the effect of residence time, nor does the process gas analysis, shown in Figure 2, reflect any trend in this regard. The variations in reactant partial pressure, caused by changing bleed gas (nitrogen) proportion were not large enough to effect greatly the general proportion of the components in the process gas.

The total sulphur in the light oil product decreased slightly with increase in reaction temperature, and at the same time there was a corresponding increase in the yield of heavy high sulphur residuum. The amount of sulphur detected in the process gas (as H_2S) and in the coke (as SO_2 in the burner offgas) was but a small proportion of the total yield.

Some typical A.S.T.M. distillation curves for the oil product are shown, with that of the crude, in Figure 3. While the products from runs at higher temperatures contain larger proportions of light material, reference to Table 4 will show that such gains are partly offset by lower overall yields.

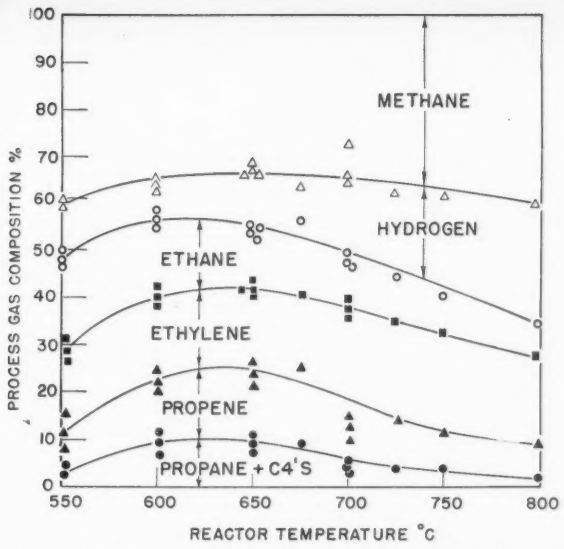

Figure 2—Process gas composition. The width of each band represents the mole percent of the constituent shown.

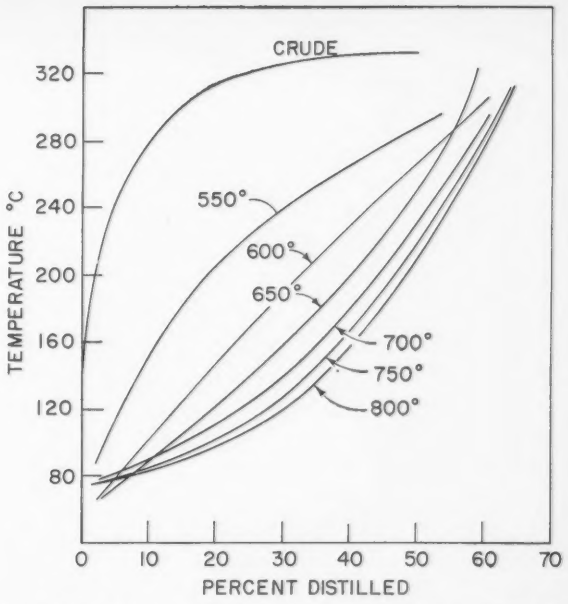

Figure 3—Representative light oil distillations (ASTM 86-56) reactor temperature in °C.

(c) **Discussion:**

(i) *Gaseous product distribution*

In their study of hydrocarbon pyrolysis Linden and Peck [9] attempted to correlate the "approach to equilibrium" of certain discreet reaction systems with residence times in an empty tubular reactor; marked similarity was found amongst the gas analyses obtained from a wide variety of feed materials. It was of interest to see whether similar results were obtained in the pyrolysis of whole crude oil in a fluidized bed.

Distribution of reactants in the following system was considered:

$$C_2H_6 \rightleftarrows C_2H_4 + H_2 \quad \text{(I)}$$

$$C_3H_8 \rightleftarrows C_3H_6 + H_2 \quad \text{(II)}$$

$$2CH_4 \rightleftarrows C_2H_6 + H_2 \quad \text{(III)}$$

Figures 4 and 5 show reactant ratios for Systems (I) and (II) as a function of temperature; on the same diagrams the corresponding K values for thermodynamic equilibrium are plotted. The latter were calculated from published free energies of formation [10]. It is apparent from Figure 4 that within the accuracy of the data, equilibrium was approximated by System (I) in all situations studied. The reaction times involved appear to have been sufficiently long to prevent any conclusions being reached about the effect of this variable on distribution of the components in this system, and in this respect, the large positive deviations of f_1 from K_1 found by Linden

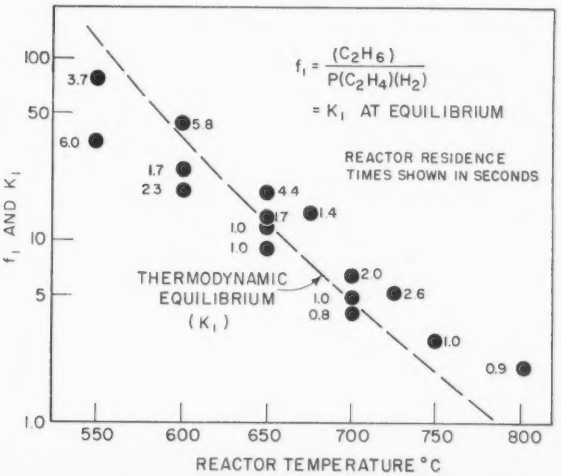

Figure 4—Distribution in the reaction system ethane-ethylene hydrogen.

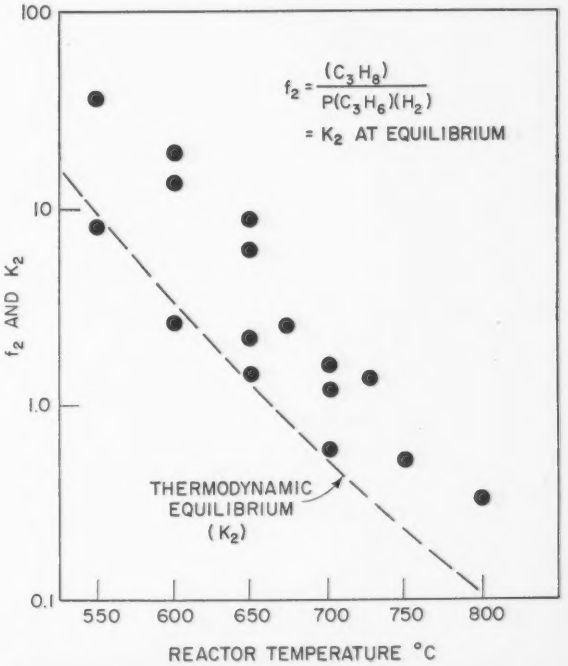

Figure 5—Distribution in the reaction system propane-propylene hydrogen.

TABLE 3

OPERATING CONDITIONS

Run No.	Duration Hours	Feed Rate lb./hr.	Reactor						Burner				
			Temp. °C.	Bed Depth (inch)	Resid. Time (sec.)	Recycle Gas s.c.f.m.	Bleed Gas s.c.f.m.	Offgas s.c.f.m.	Temp. °C.	Bed Depth (inch)	Air Rate s.c.f.m.	Bleed Rate s.c.f.m.	Offgas s.c.f.m.
1	10	8.0	550	34	3.7	0.321	0.404	0.841	640	17	2.20	0.30	2.62
2	10	5.0	550	49	6.1	0.376	0.350	0.920	630	18	2.45	0.47	2.92
3	9	7.3	600	24	1.8	0.456	0.374	1.180	675	20	2.36	0.37	2.82
4	10	6.9	600	36	2.3	0.332	0.391	0.714	670	20	2.07	0.41	2.44
5	10	4.6	600	49	5.8	0.332	0.338	0.820	675	20	2.42	0.37	2.77
6	10	7.8	650	21	1.0	0.470	0.362	1.543	715	16	2.44	0.37	2.83
7	7	6.1	650	31	1.1	0.497	0.713	1.840	750	20	2.28	0.51	2.81
8	10	8.1	650	36	1.8	0.491	0.408	1.591	720	16	2.25	0.37	2.69
9	10	4.2	650	47	4.4	0.324	0.395	1.021	710	19	2.42	0.38	2.85
10	10	8.1	675	32	1.4	0.474	0.404	1.602	730	21	2.16	0.36	2.46
11	10	7.6	700	23	0.8	0.458	0.430	1.725	740	20	2.20	0.34	2.57
12	10	7.3	700	35	1.0	0.327	0.506	1.968	810	18	2.00	0.34	2.29
13	10	6.3	700	46	2.0	0.388	0.422	1.520	750	18	2.22	0.35	2.78
14	10	5.3	725	48	2.6	0.354	0.372	1.256	770	18	2.41	0.37	2.82
15	10	7.2	750	28	1.1	0.420	0.406	1.727	820	24	2.56	0.50	3.00
16	10	6.8	800	37	1.0	0.322	0.566	1.973	850	25	2.32	0.52	2.84

and Peck [9] with residence times below about 1.5 seconds have not been duplicated. Some unpublished data obtained by W. S. Peterson, during pyrolysis studies of a heavy South American (Bachaquero) crude in a fluidized coke bed, fit remarkably well on Figure 4 and thus tend to confirm that the behavior of this system is substantially independent of feed material and of the nature of the inert bed used.

The increased scatter of data for System II, (Figure 5) is largely due to the inaccuracy of chromatographic estimation of the small quantities of propane in the gas mixture. In most cases there is significant positive deviation of f_2 from K_2; it is not apparent that increased residence time would reduce this deviation, but since some of the f_2 values depart by almost an order of magnitude from a median condition little quantitative information may be obtained from Figure 5.

System III (methane-ethane-hydrogen) has been considered by other workers [9, 11] as a stationary state or perhaps as a very slow reaction. The results obtained in this study confirm this; System III was in all conditions very far from equilibrium.

(ii) *Liquid product composition*

The light oil products from several representative runs were closely fractionated to an end point of 200°C. in a 3 ft. x 25 mm. Podbielniak column at atmospheric pressure. The overhead fractions were analysed for hydrocarbon types by the F.I.A. method (A.S.T.M. D1319); the data are summarized in Figures 6, 7, 8, and 9.

The steady increase in aromatic content of the gasoline fractions with increasing reactor temperature is quite marked, reappearance of a small amount of olefins at 800°C. has not been satisfactorily explained. Two other runs at 650°C. were also fractionated and analysed to see whether any marked differences resulted from variations in reactor residence time; no change in type distribution was apparent and therefore the data are not shown.

The light oil contained moderately large amounts (of the order 1%) of thiophenic sulphur, the discreet fractions of aromatic type were accompanied by the thiophene isomer of corresponding structure. The sulphur content of each fraction in representative runs was determined; the results are shown in Figure 10. Since

TABLE 4

PRODUCT ANALYSIS

Run No.	Temp. °C.	Calc. Resid. Time (sec.)	Process Gas To C4's Yield		Coke % w/w	Liquid % w/w	Total Sulphur	
			% w/w	Ft.³/Bbl.			Product To 320°C. Endpoint % w/w	Residuum % w/w
1	550	3.7	3.5	—	8.0	87.6	2.76	
2	550	6.05	8.0	520	6.9	85.2	2.88	
3	600	1.77	18.6	760	9.0	69.4	2.86	
4	600	2.30	23.5	880	8.8	66.0	2.04	
5	600	5.82	17.0	820	9.7	68.2	2.79	
6	650	1.01	38.3	1760	9.8	51.9	2.20	5.40
7	650	1.06	39.1	1710	9.2	52.5	2.51	
8	650	1.77	39.2	1820	8.4	50.4	1.88	
9	650	4.40	39.8	1750	10.6	46.8	1.97	
10	675	1.41	37.4	1640	13.2	48.4	1.84	
11	700	0.82	36.9	1890	13.1	50.0	1.90	4.50
12	700	1.04	34.2	1900	17.2	47.7	1.97	
13	700	2.00	35.8	1720	12.6	48.9	1.56	4.50
14	725	2.62	37.4	2200	15.5	46.8	1.67	4.70
15	750	1.07	34.2	1990	18.2	46.4	1.57	4.55
16	800	0.98	30.5	2000	25.3	44.2	1.95	

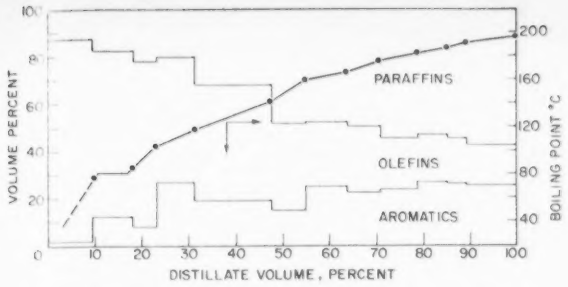

Figure 6—Distillation of light oil fraction run No. 1.

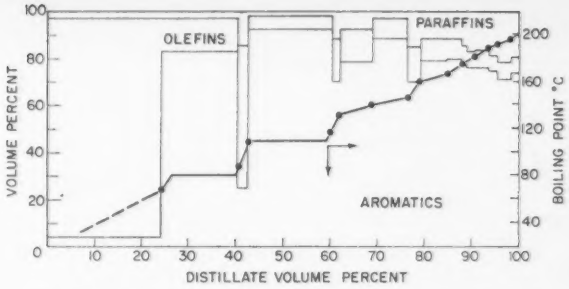

Figure 7—Distillation of light oil fraction run No. 4.

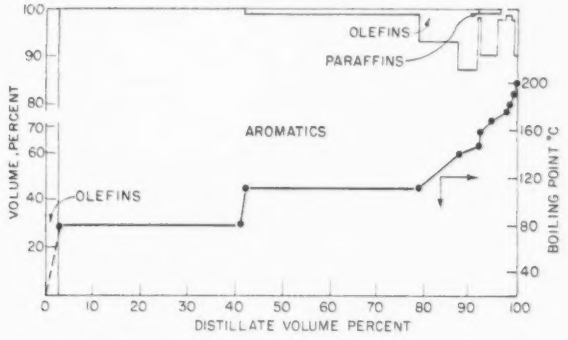

Figure 8—Distillation of light oil fraction run No. 12.

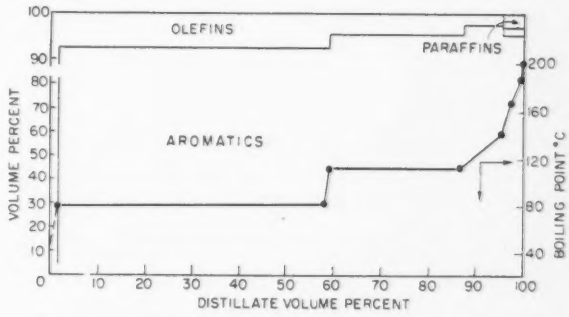

Figure 9—Distillation of light oil fraction run No. 16.

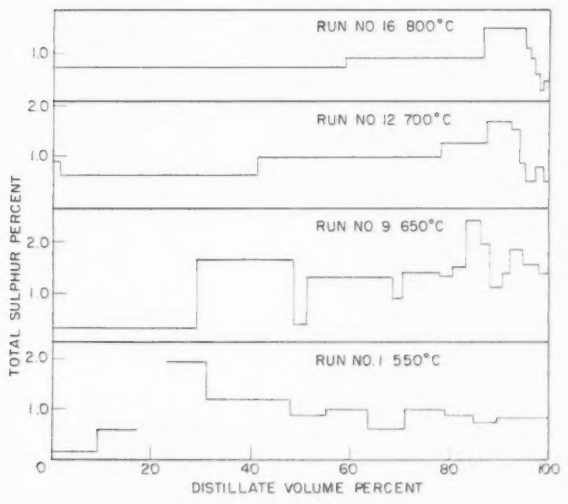

Figure 10—Total sulphur in light oil fractions.

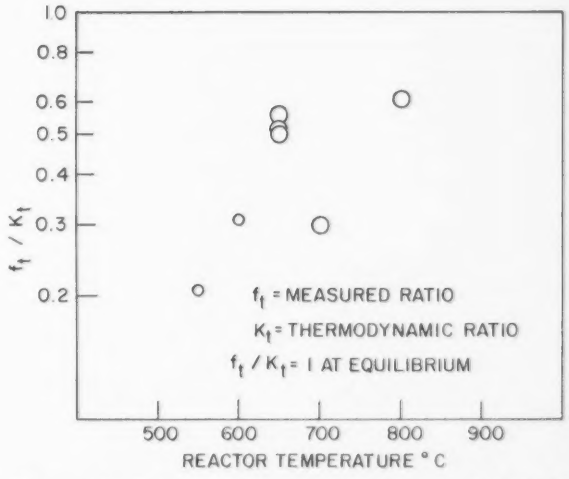

Figure 11—Toluene fractions — comparison of 2 to 3 methylthiophene ratio with thermodynamic equilibrium values.

certain gaseous systems (viz. I and II) can serve as "tags" to indicate pyrolysis severity, it was thought that some analogous system in the liquid phase might serve a similar purpose. Accordingly, the proportions of the two isomers, 2-and 3-methylthiophene were determined by analysis of the toluene cut from each fractionation using gas-liquid partition chromatography [13], and the ratio of these isomers, denoted f_t, compared with the ratio expected at thermodynamic equilibrium (K_t) [14, 15].

Figure 11 shows that in all samples tested there appears to be a general trend for the ratio f_t/K_t to approach unity with increasing cracking temperature. This is further supported by the increase in the ratios at 650°C. with longer residence times. However, an apparent change in reaction pattern has occurred in the region near 700°C., and thus more detailed interpretations are hardly warranted.

Nomenclature

P = absolute pressure, atmospheres.
T = reaction temperature ° centigrade.
f_1 = partial pressure product $C_2H_6/P(C_2H_4)(H_2)$.
f_2 = partial pressure product $C_3H_8/P(C_3H_6)(H_2)$.
f_t = mole fraction product, 2-methylthiophene/3-methylthiophene.
K_1 = f_1 at equilibrium.
K_2 = f_2 at equilibrium.
K_t = f_t at equilibrium.
% w/w = percent by weight.
s.c.f.m. = standard cubic feet per minute.

References

(1) Peterson, W. S., Keller, H., and Gishler, P. E., Can. J. Tech. 34, 104 (1956).
(2) Reid, J. M., et al., Inst. Gas. Tech. Res. Bull. No. 16, November 1953.
(3) Thornton, D. J., Pet. Processing, p. 840, June 1955.
(4) Barr, F. T., and Jahnig, C. E., Chem. Eng. Prog. 51, 167 (1955).
(5) Voorhees, A., and Martin, H. Z., Am. Pet. Inst. Proc. 33, Refining Section (1953).
(6) Maass, R. H., and Newchurch, E. J., Pet. Engr. 28, C36 (April 1956).
(7) Martin, H. Z., Barr, F. T., and Krebs, R. W., Oil & Gas J., p. 169, May 10, 1954.
(8) Johnson, F. B., and Wood, R. E., Pet. Refiner 33, No. 11, 157 (1954).
(9) Linden, H. R., and Peck, R. E., Ind. Eng. Chem. 47, 2470 (1955).
(10) Rossini, F. D., et. al., "Selected Values Properties of Hydrocarbons", Nat. Bureau Standards 464 (1948).
(11) Linden, H. R., Pet. Processing 6, 1389 (1951).
(12) Hague, E. N., and Wheeler, R. V., J. Chem. Soc. 132, 378 (1929).
(13) Amberg, C. H., Can. J. Chem. 36, 590 (1958).
(14) McCullough, J. P., et al., J. Am. Chem. Soc. 75, 5073 (1953).
(15) Pennington, R. E., et al., J. Am. Chem. Soc. 78, 2055 (1956).

Acknowledgements

Acknowledgement is made to A. Baxter, T. W. Boyd, L. Pageau and A. E. McIlhinney for assistance in operating the pilot plant. Acknowledgement is also made to D. Kulawic for precise fractionation and type analysis of the light oil, and to W. T. Houghton for analysis of sulphur in the individual fractions. J. A. H. Desaulniers and M. E. Bednas carried out detailed analysis of a large number of gas, oil and solids samples.

★ ★ ★

Empirical Correlation of Azeotrope Data

An Extension of the Meissner-Greenfield Correlation[1]

A. I. JOHNSON[2] and J. A. MADONIS[3]

The Meissner-Greenfield correlations of azeotrope composition and boiling point have been checked with new data with satisfactory results except in the cases of hydrocarbons—acids and halogen hydrocarbons—acids.

A modification of these correlations for azeotrope composition has been extended to other combinations of organic liquids where the deviations from Raoult's law can be predicted from the hydrogen bonding characteristics of the components.

A simple empirical linear equation for azeotrope boiling point has been applied to most of the cases included in the above correlation.

MANY attempts have been made to correlate azeotropy with the thermodynamic properties of solutions. In general the more successful correlations are very empirical in nature.

Hildebrand [1] has given as general rules, that a minimum boiling azeotrope is possible when the two components have nearly equal vapor pressures and also when the two components differ considerably in polarity even if the boiling points are appreciably different and that a maximum boiling azeotrope is possible when there are negative deviations from Raoult's law and a small difference in boiling points. Kireev [2] has pointed out that the smaller difference between the vapor pressures of the two components at a given temperature in the boiling range the more likely is the existence of a constant boiling mixture.

Lecat [3], Rossini et al [4] and Skolnik [5] have presented correlating equations and graphical methods for correlating azeotrope data where one component forms azeotropes with homologous series of other components. These methods are quite accurate but are sometimes restricted.

Meissner and Greenfield [6] have proposed empirical correlations for azeotrope composition and temperature which are not dependent on homologous series. Their correlation is applicable to systems where one component is a hydrocarbon or a halogenated hydrocarbon and the other is an alcohol, and aldehyde, a ketone, a carboxylic acid or a phenol. Their method has been extended in this paper.

[1] *Manuscript received October 30, 1958.*
[2] *Associate Professor, Department of Chemical Engineering, University of Toronto, Toronto, Ont.*
[3] *Present address: Canadian Petrofina Limited, Montreal, Que.*
Contribution from the Department of Chemical Engineering, University of Toronto, Toronto, Ont.

Classification of solutions according to hydrogen bonding

Hydrogen bonding refers to the coordination of hydrogen already bonded to carbon or other elements with donor atoms such as oxygen, nitrogen or fluorine. Deviations of solutions from ideality and hence azeotrope formation has been attributed to a large extent to hydrogen bonding. Ewell et al [7] have classified liquids and solutions formed by mixing these liquids in the manner summarized in Table 1. This table indicates the classifications of solutions covered by Meissner and Greenfield in their correlation and those which have been included in this study.

In this paper the main source of azeotropic data was the compilation of Horsley [8].

Test of the Meissner-Greenfield correlation

Meissner and Greenfield proposed their correlation to include solutions of class IV-II, V-II and V-III of Table 1. Figures 1 to 3 indicate a comparison of their correlations for azeotrope data compiled by Horsley for the period 1947-52. Table 2 lists the compounds included in Figures 1 to 3.

In these figures X is the azeotrope composition, as mole fraction hydrocarbon and

$$y = (T_A - T_B)\, T_B^2 \times 10^{-5} \quad \ldots\ldots\ldots\ldots\ldots\ldots (1)$$

where T_A = Boiling point of hydrocarbon, °K

T_B = Boiling point of solvent, °K

In Figure 1 line A was recommended by Meissner for hydrocarbons and halogenated hydrocarbons with alcohols only while line B applied to hydrocarbons with aldehydes, hydrocarbons with phenols, cresols, ketones and hologenated hydrocarbons with phenols and cresols.

In Figure 2 are shown Meissner's two curves for correlating experimental data of hydrocarbons and halogenated hydrocarbons with acids.

For predicting azeotropic boiling point Meissner recommended the correlation of the group

$$X = 56\,\frac{(340)^2}{T_B} - (T_H - T_L) + K \quad \ldots\ldots\ldots\ldots (2)$$

with the difference in boiling point between the high boiler T_H and the low boiler T_L in the azeotrope combination. Here T_B is the boiling point of the azeotrope. The value of K depended on the system; typical values were tabulated by Meissner. Figure 3 shows the application of their correlating line with new data.

TABLE 1

CLASSIFICATION OF ORGANIC LIQUIDS ACCORDING TO HYDROGEN BONDING POTENTIALITY AND DEVIATION FROM RAOULT'S LAW

Class	Characteristics	Examples	Class				
			I	II	III	IV	V
I	Three dimensional network of strong H bonds	Water, glycol, glycerol, amino-alcohols, etc.	P–N	P–N	P–N	(1) P LS	(1) P
II	Both donor atoms and active H atoms in the same molecule	Alcohols, acids, phenols, primary and secondary amines, nitro-compounds with active H atom, etc.		P–N	P–N LS	(2) P LS	(2) P
III	Only donor atoms	Ethers, ketones, aldehydes, esters, nitro-compounds without active H-atoms, tertiary amines etc.			(1) P	(1) N	(2) P
IV	Only active H atoms	Halogenated hydrocarbons like $CHCl_3$, CH_2Cl_2, CH_3CHCl_2, etc.				(1) P	(1) P
V	No H bond forming capabilities	Hydrocarbons, sulphides, mercaptans, halogenated hydrocarbons not in class IV					(1) P

LEGEND

N negative deviations. P positive deviations. LS limited solubility.

(1) solutions covered by modified Meissner correlation extended in this study.

(2) solutions covered by Meissner and Greenfield.

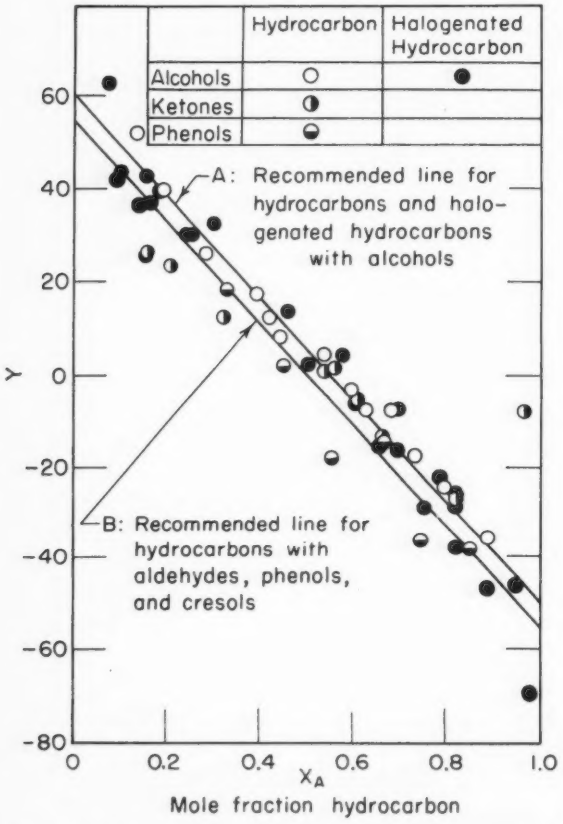

Figure 1—Test of Meissner's correlation for hydrocarbons and halogenated hydrocarbons with alcohols and for hydrocarbons with aldehydes, phenols, and cresols with more recent data. Here $y = (T_A - T_B)T_B^2 \times 10^{-5}$ where T_A = boiling point of hydrocarbon, °K and T_B = boiling point of other solvent, °K.

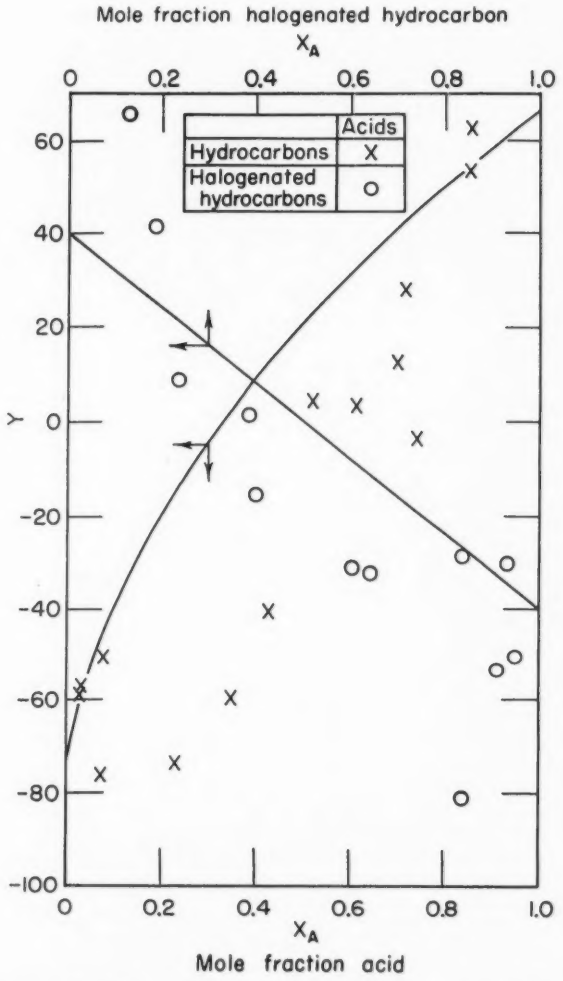

Figure 2—Test of Meissner's correlation for hydrocarbons and halogenated hydrocarbons with organic acids with more recent data. Here $y = (T_A - T_B)T_B^2 \times 10^{-5}$ where T_A = boiling point of hydrocarbon, °K and T_B = boiling point of other solvent, °K.

Table 2

HYDROCARBONS	HALOG: HYDROCARBONS
PARAFFINS	Dichloromethane
n. Hexane	Carbon tetrachloride
2,3 Dimethyl butane	Bromo methane
n. Heptane	Di bromo methane
n. Octane	Bromoform
2,5 Dimethyl-hexane	Iodomethane
1,2,4 Trimethyl pentane	Trichloroethylene
Tridecane	Tetrachloroethylene
	Tetrachloroethane
UNSATURATED	Pentachloroethane
2,3 Dimethyl 1,3 butadiene	Cis 1 bromo 1,2 dichloroethylene
1 Heptyne	Trans 1 bromo 2,2 dichloroethylene
	3-Chloropropene
ALICYCLICS	1,2 Dichloro-1-propene
Cyclopentane	2 Bromopropane
Methyl cyclopentane	1-Iodopropane
Cyclohexane	2-Iodopropane
Methyl cyclohexane	1-Chlorobutane
1,3 Dimethyl cyclohexane	2-Chlorobutane
	1-Bromobutane
UNSATURATED ALICYCLICS	2-Bromobutane
Methyl cyclopentene	1-Iodobutane
1,3 Cyclohexadiene	1-Chloro-3-methylbutane
1,4 Cyclohexadiene	1-Iodo-3-methylbutane
AROMATICS	ALCOHOLS
Benzene	Methanol
Toluene	Ethanol
Butyl benzene	Propyl alcohol
Mesitylene	Allyl alcohol
Styrene	Butyl alcohol
o-oxylene	t. butyl alcohol
m-xylene	Isobutyl alcohol
	Sec. butyl alcohol
TERPENES	Amyl alcohol
α-Terpinene	t. amyl alcohol
Terpinolene	Iso amyl alcohol
	2-Pentanol
PHENOS-CRESOLS	ACIDS
Phenol	Formic
o-cresol	Acetic
3,4 xylenol	Propionic
	Butyric
KETONES	Valeric
2-Butanone	Isovaleric
3-Pentanone	
4-Methyl-2-pentanone	

Extension of Meissner-Greenfield correlation to other H-bonding classes of organic liquids

For the combinations of Table 1 other than those treated by Meissner and Greenfield, the Meissner-Greenfield correlation was first attempted. In some cases slight modifications of the y term were used. These modified forms are denoted as y_1, y_2, y_3, and y_4. The proposed equations were obtained by the method of least squares.

In Figure 4 an attempt has been made to show the correlations obtained for systems in which one component is from class IV, halogenated hydrocarbon.

On curve A data for halogenated hydrocarbons with hydrocarbons were best correlated with Meissner's

$$y = (T_A - T_B)\,T_B^2 \times 10^{-5} \quad \ldots\ldots(3)$$

with the proposed correlating equation as

$$100\,x_A = 23 - 1.87y \quad \ldots\ldots(4)$$

On curve B data for halogenated hydrocarbons with halogenated hydrocarbons were correlated using

$$y_2 = (T_A - T_B)/T_B^3 \times 10^{-7} \quad \ldots\ldots(5)$$

to obtain the correlating equation

$$100\,x_A = 50 - 1.25y_2 \quad \ldots\ldots(6)$$

Curve C shows a limited amount of data for halogenated hydrocarbons with water correlated using Meissner's y as

$$100\,x_A = 56 - 0.56y \quad \ldots\ldots(7)$$

and curve D shows a small amount of data with glycol correlated as

$$100\,x_A = 35 - 0.438y \quad \ldots\ldots(8)$$

Curve E shows a large number of points correlated using

$$y_3 = (T_A - T_B)\,(T_A + T_B)/T_B \times 10^{-5} \quad \ldots\ldots(9)$$

by the correlating equation

$$100\,x_A = 52.1 + 1.18y_3 \quad \ldots\ldots(10)$$

These points are for halogenated hydrocarbons with esters, ketones and so on.

In Figure 5 an attempt has been made to correlate data for class III-III-systems involving ketones and esters of monocarboxylic acids. In general

$$y_1 = (T_A - T_B)\,(T_A + T_B)T_B^2 \times 10^{-7} \quad \ldots\ldots(11)$$

K VALUES	Alcohols: Primary	Alcohols: Iso- & Sec-	Alcohols: Tert-	Acids: Straight chain	Acids: Aromatic	Phenols	Cresols	Ketones	Aldehydes
Hydrocarbons	○	○	○	+	+	△	▲	●	
Paraffins	0	-3	-10	+5	—	+16	—	-20	+15
Cyclic Nonaro	-2	-5	-12	+3	—	+14	+5	-22	+13
Monoolefins	-5	-8	-15	—	—	—	—	—	—
Diolefins	-7	-10	-17	—	—	—	—	-27	—
Aromatics	-10	-13	-20	-5	+15	+6	-3	—	+5
Halogenated	-10	-10	-10	+6	+6	—	—	—	—

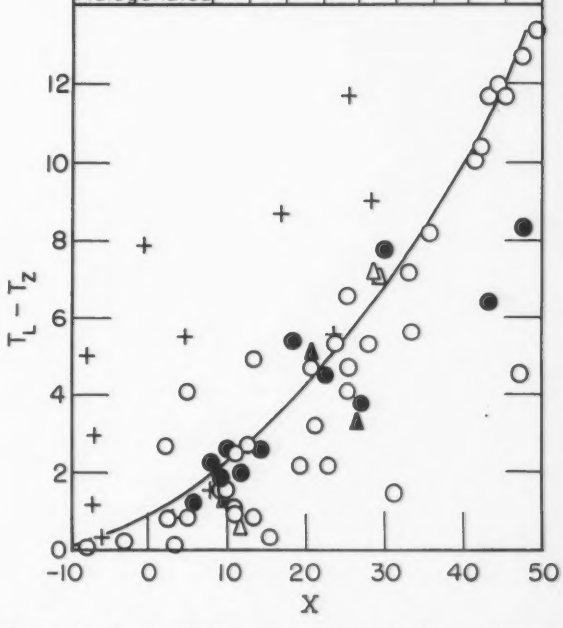

Figure 3—Test of Meissner's azeotrope boiling point correlation with more recent data. Here $X = 56\left(\frac{340^3}{T_Z}\right) - (T_H - T_L) + K$ **and T_L, T_H and T_Z are the boiling points of the low and high boiling pure components and of the azeotrope, in °K.**

If $(T_A - T_B) > 1$ and $(T_A + T_B) > 1000$, then the following simple expression can be used.

$$y_2 = (T_A - T_B)T_B^3 \times 10^{-7} \quad \ldots\ldots(12)$$

The proposed correlating equation is

$$100\, x_A = 49.7 - 1.18 y_1 \quad \ldots\ldots(13)$$

Figure 6 shows data for class V-V-hydrocarbons and hydrocarbons. Using the y_1 defined by Equation (11), the data were correlated using

$$100\, x_A = 50 - 0.5 y_1 \quad \ldots\ldots(14)$$

Finally Figure 7 shows data for class V-I. When the second component was water or 2-aminoethanol the Meissner y was used. With glycol and glycerol the following was used

$$y_4 = T_A - T_B \quad \ldots\ldots(15)$$

The correlating equation is

$$100\, x_A = 50 - 0.50 y \quad \ldots\ldots(16)$$

Table 3 lists the compounds included in Figures 3-7.

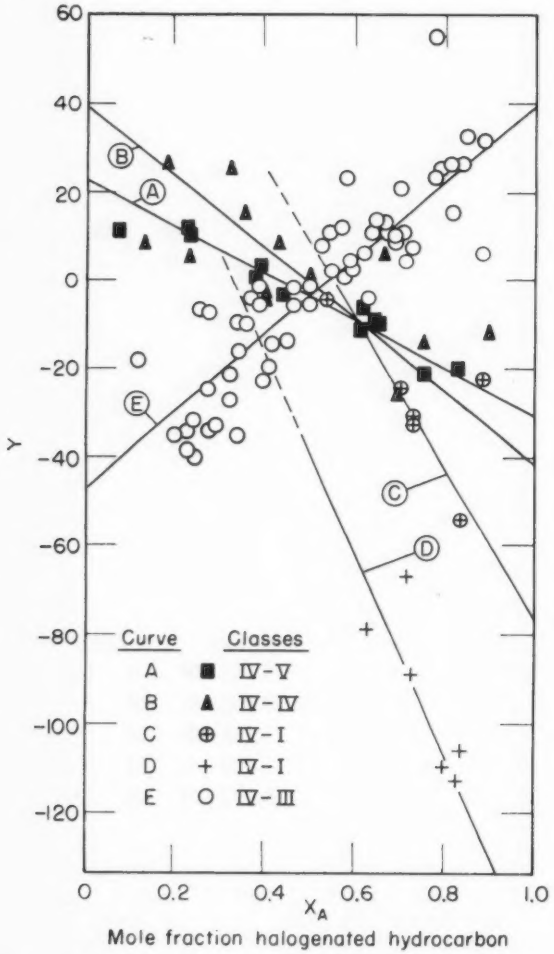

Figure 4—Azeotrope composition correlations for systems in which one component is halogenated hydrocarbon.
For curves A, C, and D $y = (T_A - T_B)T_B^2 \times 10^{-5}$
curve B $y = (T_A - T_B)T_B^3 \times 10^{-7}$
curve E $y = (T_A - T_B)(T_A + T_B)T_B \times 10^{-5}$
where T_A and T_B are the normal boiling points of the pure components, °K.

Correlation for predicting azeotropic boiling point

The following simple linear equation was found to fit azeotropic boiling point data for both Meissner's systems and most of the other hydrogen bonding classes to which the azeotropic composition correlation was extended:

$$D = A - Bz \quad \ldots\ldots(17)$$

where $D = T_A - T_B$
$z = T_L - T_z$ for a minimum boiling azeotrope
$z = T_z - T_H$ for a maximum boiling azeotrope
A and B are constants which have been determined for each combination empirically and their values are given in Table 4. The best straight lines obtained by least squares from literature data are shown in Figure 8.

Discussion

The Meissner-Greenfield equations were checked using new data compiled by Horsley and were found to give good agreement except for solutions of hydrocarbons and hologenated hydrocarbons and acids.

These correlations were extended, sometimes in a slightly modified form. The new correlations gave best results in cases such as halogenated hydrocarbons-donor atom liquids ketones-esters (although only a few azeotropes reported), hydrocarbons-hydrocarbons, and hydrocarbons-associated liquids of the first class. The average deviation in comparing actual azeotrope composition at atmospheric pressure with the correlating equations is ± 8% (mole). New correlations have been indicated for other classes but the results were not as good as in the above four classes.

Data for systems not included in Table 1 showed no tendency to correlate in the Meissner-Greenfield manner.

An azeotrope boiling point correlation has been proposed which is simpler and applicable to a wider range of compounds than Meissner's. However it is not quite as accurate as Meissner's method.

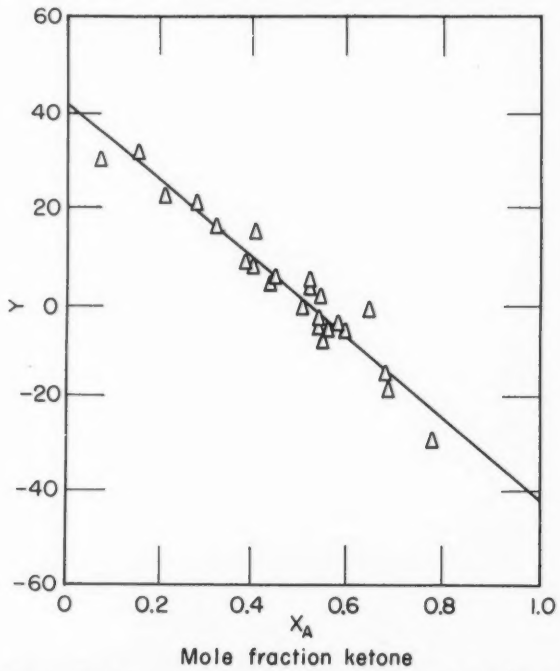

Figure 5—Azeotrope composition correlation for systems involving ketones and esters of monocarboxylic acids. Here $y = (T_A - T_B)(T_A + T_B)T_B^2 \times 10^{-7}$ where T_A and T_B are the boiling points of the pure components, °K.

While the graphs and equations presented permit the satisfactory correlation of a large amount of azeotrope data they do not predict the formation of an azeotrope; many non azeotropes are reported by Horsley for which azeotropes would be predicted by Meissner and by the extension in this paper.

Table 3

CLASS I

Water
2-Aminoethanol
Glycol
Glycerol

CLASS III

KETONES

Acetone
2-Butanone
2-Pentanone
3-Pentanone
3-Methyl-2-butanone
2,4 Pentanedione
2-Hexanone
3-Hexanone
4-Methyl-2 pentanone
Cyclohexanone
4-Heptanone
5-Methyl-2 hexanone
Acetophenone
2,6 Dimethyl-4 heptanone
p. Methyl-acetophenone
Propiophenone
Carvone
Pulegone

ETHERS

Ethyl ether
Propyl ether
Isopropyl ether
Ethyl propyl ether
Butyl ether
Benzyl methyl ether

ESTERS

Ethyl formate
Propyl formate
Iso-propyl formate
Iso-butyl formate
Iso-amyl formate
Methyl acetate
Ethyl acetate
2-Methoxy ethyl acetate
2-Ethoxy ethyl acetate
Propyl acetate
Isopropyl acetate
Butyl acetate
Amyl acetate
Bornyl acetate
Methyl propionate
Ethyl propionate
Butyl propionate
Isobutyl propionate
Methyl butyrate
Methyl isobutyrate
Isobutyl isobutyrate
Methyl isovalerate
Propyl isovalerate
Methyl caproate
Ethyl caproate
Isoamyl lactate
Propyl benzoate
Ethyl a-toluate

ALDEHYDES

2-Furaldehyde

ACETALS

Methylal
Acetal
Acetaldehyde dimethyl acetal

OXIDES

Propylene oxide
Mesityl oxide

CLASS IV

HALOGENATED HYDROCARBONS

Iodomethane
Dichloromethane
Bromo-dichloro-methane
1,2 Dibromomethane
Chloroform
Bromoform
Carbon tetrachloride
1, Bromoethane
1,1 Dichloroethane
1,2 Dichloroethane
Trichloroethylene
1,1,2,2 Tetrachloroethane
Pentachloroethane
1-Chloropropane
2-Chloropropane
2-Bromopropane
2-Iodopropane
1,2-Dichloropropane
1,2,3-Trichloropropane
1,3 Dibromopropane
1, Chlorobutane
2, Bromobutane
1-Bromo-2 methyl propane
2 Iodobutane
1 Iodo-3-methyl butane

CLASS V

PARAFFINS

Hexane
2-Methyl butane
2-3 Dimethyl butane
n-Heptane
2-2-Dimethyl pentane
2-3 Dimethyl pentane
2-4 Dimethyl pentane
2,2,3 Trimethyl butane
2,2,4 Trimethyl pentane
2,3,4 Trimethyl pentane
2,5 Dimethyl hexane
2 Methyl heptane
Nonane
Decane
2,7 Dimethyl octane

CYCLO PARAFFINS

Cyclopentane
Cyclohexane
Methyl cyclopentane
Ethyl cyclopentane
Cis 1,1,3 trimethyl cyclopentane
Trans " " "
Cis 1,3 Dimethyl cyclohexane

OLEFINS

2,3,4 trimethyl 2-pentene

CYCLO OLEFINS

Cyclohexane

AROMATICS

Benzene
Toluene
Cumene
Mesitylene
Propyl benzene
Cymene
Pseudocumene
Butyl benzene
Styrene
Ethyl benzene
p-xylene
Naphthalene
1-Methyl naphthalene
Diphenyl methane
Acenaphthene
1,2 Diphenyl ethane

TERPENES

a-Pinene
a-Terpinene
nopinene
Camphene
Terpinolene
Dipentene
2-Limonene

HALOGENATED AROMATICS

Bromobenzene
p-Dibromobenzene
o-Dichlorobenzene
p-Iodotoluene
m-Bromotoluene
1-Bromo naphthalene
1-Chloro-naphthalene

SULPHIDES-MERCAPTANS

Carbon disulphide
Ethane thiol
Allyl sulphide
Propyl sulphide
Butyl sulphide
Isobutyl sulphide

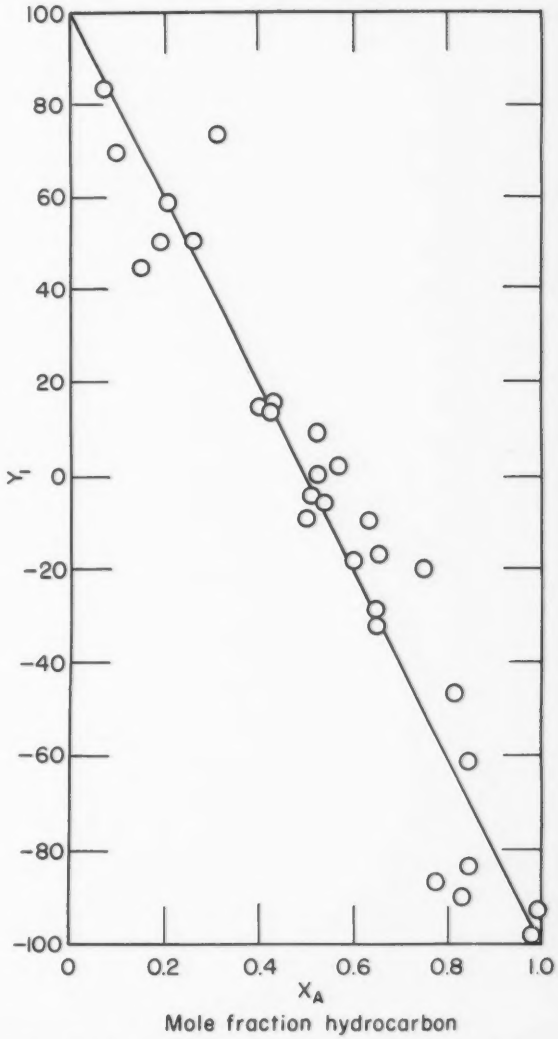

Figure 6—Azeotrope composition correlation for solutions of hydrocarbons and hydrocarbons. Here $y = (T_A - T_B)(T_A + T_B)T_B^2 \times 10^{-7}$ where T_A and T_B are the boiling points of the pure components, °K.

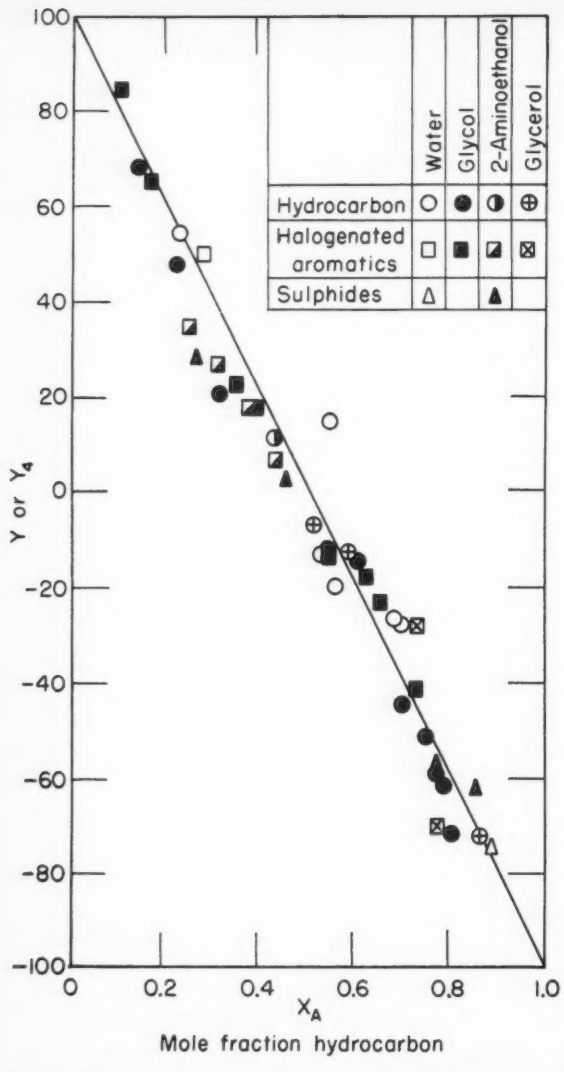

Figure 7—Azeotrope composition correlation for solutions of hydrocarbons with Type I solvents. Here $y = (T_A - T_B)T_B^2 \times 10^{-5}$ except for glycol and glycerol systems where $y = T_A - T_B$. T_A and T_B are the boiling points of the pure components, °K.

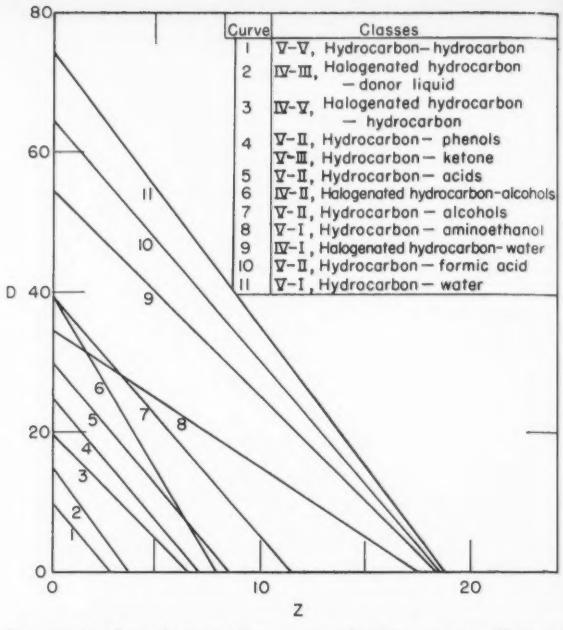

Figure 8—Correlation of azeotrope boiling points. Here D is the difference between the boiling points of the pure components and Z is defined as

$Z = T_L - T_Z$ for a minimum boiling azeotrope and $Z = T_Z - T_H$ for a maximum boiling azeotrope.

TABLE 4

Systems	Classes	A	B
Hydrocarbons – alcohols	V–II	40	3.5
Hydrocarbons – acids	V–II	30	3.5
Hydrocarbons – formic acid	V–II	65	3.5
Hydrocarbons – phenols	V–II	25	3.5
Hydrocarbons – ketones	V–III	25	3.5
Halogenated hydrocarbons – alcohols	IV–II	40	5.0
Hydrocarbons – hydrocarbons	V–V	10	3.5
Hydrocarbons – strongly associated liquids	V–I	75	4.0
Hydrocarbons – amino alcohol	V–I	35	2.0
Halogenated hydrocarbons – donor liquids	IV–III	15	4.0
Halogenated hydrocarbons – hydrocarbons, sulphides	IV–V	20	3.0
Halogenated hydrocarbons – strongly assoc. liquids	IV–I	55	3.0

Nomenclature

A = Intercept of azeotropic boiling point correlation lines.
D = Difference in boiling point of two components.
K = Meissner's equation constant (Graph 3).
T = Boiling point, degrees Kelvin.
X = Meissner's term for correlating azeotropic boiling point.
x = Mole fraction.
y = Meissner's term for correlating azeotropic composition.
z = Difference of boiling points of high or low boiler from azeotropic boiling point.

Subscripts

A,B = Components A,B
H = High boiler
L = Low boiler
Z = Azeotrope
1,2,3,4 = Modifications of Meissner's y term.

References

(1) Hildebrand, J. H., and Scott, R. L., "The Solubility of Nonelectrolytes", 3rd Ed., 1950, Reinhold Publishing Corp., New York.
(2) Kireev, B. A., Zhur, Phys., Khim 14, 1469 (1940).
(3) Lecat, M., "L'Azeotropisme", Brussels (1918); Ann, Soc. Sci. Brux. Vol. 45, 47B, 48B, 50B, 55B, 56B (1926-37).
(4) Moir, B. J., Glascow, A. R., and Rossini, F. D., J. Research Natl., Bur. Standards 27, 39 (1941).
(5) Skolnik, H., Ind. Eng. Chem. 40, 442 (1948).
(6) Meissner, H. P., and Greenfield, S. H., Ind. Eng. Chem. 40, 438
(7) Ewell, R. H., Harrison, J. M., and Berg., L., Ind. Eng. Chem. 36, 871 (1944).
(8) Horsley, L. H., and coworkers (Azeotropic Data) 1st Ed. Advances in Chemistry Series, A.C.S. (1952).

★ ★ ★

Solar Energy

Economics and Engineering Research at the University of Wisconsin[1]

J. A. DUFFIE[2] *and G. O. G. LÖF*[3]

The use of solar energy, in most applications, is dependent primarily on economic considerations; solar energy can become an important energy source when the costs of its use become competitive with the costs of energy from other sources. The basic and usually most costly item of equipment for solar energy utilization is the collector, or solar heat exchanger, and the amortization of the first cost of this and associated equipment is the major cost of solar energy. In this paper, the probable economic feasibility of several solar applications is assessed by using the costs of energy from present sources as a basis for estimating upper limits on the first cost of solar heat exchangers and their associated equipment. For example, for space heating in temperate climates, heat exchanger costs would have to be in the range of $1-6 for solar heating to be competitive; this appears to be within an attainable range. Economic considerations have helped shape the development of the Wisconsin solar energy program, and studies of solar heat exchangers and their application to heating, cooling and power generation are briefly described.

Solar radiation reaching the earth constitutes an enormous energy resource. It is a continuing energy supply which will be available after the supplies of readily available fossil fuels have become expensive or insufficient for our needs. The solar energy supply is several orders of magnitude larger than the world's total energy demands. The challenge of solar energy research is to make the use of this resource technically and economically feasible.

The amount of solar radiation incident on the earth is great, but the energy flux received at the earth's surface is both low and variable with time and location. The intensity of radiation varies from zero to a maximum of about 1¼ hp./sq. yd. and in sunny, temperate climates, the annual average radiation on a horizontal surface is in the range of 1500 to 2000 B.t.u./sq. ft./d. Table 1 shows average daily June, December, and annual radiation for several locations. The collection and utilization of this energy for most purposes are not now economically attractive, as any solar-operated device or system which requires much energy must depend on large areas of energy collecting surfaces which are at present expensive to construct. The major problems in solar energy utilization can be considered to be of technical and economic nature, although sociological or other considerations may be equally or more important in some applications. Discussions of these problems are given in the proceedings of several recent symposia [1, 2, 3, 4].

TABLE 1

AVERAGE DAILY HORIZONTAL RADIATION FOR SEVERAL LOCATIONS, B.t.u./ft.²

	December	June	Annual
San Juan, P. R. (18° N. Lat.)	1540	2000	1940
El Paso, Tex. (32° N. Lat.)	1210	2730	2040
Fresno, Calif. (37° N. Lat.)	610	2620	1660
Denver, Colo. (40° N. Lat.)	670	2180	1550
Madison, Wis. (43° N. Lat.)	450	1990	1220

The sun radiates at an effective temperature of about 6000°C.; the radiation reaching the earth's surface (after scattering and absorption of some wave lengths by atmospheric components) is divided about 45% in the visible range, 51% in the near infra-red, and 4% in the ultra-violet range [5]. The radiation reaching the earth consists of diffuse (scattered) and direct (beam) components; on cloudy days all of the incident radiation may be diffuse, and on very clear days up to 90% of the total incident radiation may be direct. The orientation of a solar absorbing surface has substantial effect on the amount of radiation it intercepts, with a surface continuously oriented toward the sun receiving the maximum radiation. In temperate climates, the optimum orientation of a *fixed* receiver for winter-time use is south facing, with a tilt equal to the latitude plus 10 to 15 degrees; for summer use the optimum tilt is less by 20 to 30 degrees.

[1] *Manuscript received October 23, 1958.*
[2] *Director, Solar Energy Laboratory, University of Wisconsin, Madison, Wis.*
[3] *University of Wisconsin and Chemical Engineering Consultant, Denver, Col.*
Based on a paper presented at the Joint A.I.Ch.E.-C.I.C. Chemical Engineering Conference, Montreal, Que., April 20-23, 1958.

The most important part of the solar energy utilization system is the solar heat exchanger, or "collector". These are of two types, as shown schematically in Figure 1. The flat-plate type uses a solar energy absorbing surface equal in area to the total area of the collector, is now apparently the less expensive to build and can absorb both direct and diffuse radiation. The focusing type uses an optical system, usually a reflector, to concentrate the direct component of the radiation onto a heat exchanger smaller than the projected area of the collector, thus achieving higher energy flux at the exchanger and reduced area for thermal energy loss. The flat-plate heat exchanger should have its most practical applications in low temperature operations whereas the focusing collector should best be applied where higher temperatures are required.

In principle, any process which utilizes heat could have this energy supplied from solar energy. However, the intermittent and diffuse nature of solar energy make its utilization for some purposes more promising than for others. Included among those processes which appear to have potential economic interest are comfort heating and air conditioning, power for special applications such as pumping irrigation water, and evaporation or distillation of saline waters to recover potable water. In these applications, methods are available for handling the fluctuations in the energy supply. The intermittency of solar energy supply can be "smoothed out" by adding thermal inertia or storage to the comfort heating process, and good correlation between energy supply and cooling demand minimizes the storage requirements for space cooling. In applications such as pumping irrigation water or solar distillation, the equipment can be sized to produce the desired total output during periods of operation, and inertia then has the form of product storage. Other applications of potential interest are solar cooking and food refrigeration.

Two other types of processes of interest are photoelectric and photochemical processes. The photoelectric processes permit direct conversion of radiation to electrical energy by semiconductor cells, as described by Pearson [3]. Photochemical processes which utilize energy of the solar spectrum in endothermic reactions that can be subsequently reversed to recover the energy are of interest in the collection and storage of solar energy.

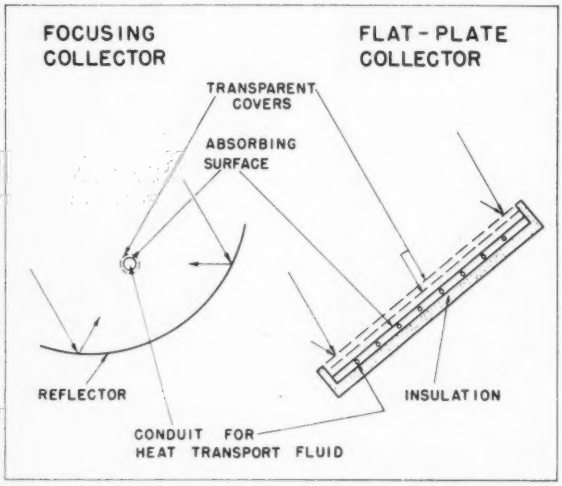

Figure 1—Schematic sections of focusing and flat-plate solar collectors. The focusing collector operates only in direct, or beam, radiation. The flat plate collector operates on direct and diffuse radiation, and does not have to be moveable.

Examples of this type of reaction, although still in the research stage, are the photochemical decomposition of water in the presence of cerium or iron salts to obtain hydrogen and oxygen, as studied by Heidt [2], and photochemical decomposition of nitrosyl chloride, studied by Niewirth and Daniels [6].

ECONOMICS OF SOLAR ENERGY UTILIZATION

Solar energy in most applications is not now competitive with energy from other sources, and until it is, widespread use can not be expected. The costs of collecting and using solar energy include the major items of amortization of first cost, direct operating costs, and realistic maintenance costs. There have been little quantitative data available on these costs for most of the promising applications. Economic studies can serve to indicate the more promising applications, where research and development studies may be fruitful.

The first cost of a system for utilizing solar energy, for any of the purposes indicated, includes (a) the collector system with its pumps, ducts, piping, etc., (b) the storage system, if required, (c) the "energy-utilizing" unit and (d) the necessary auxiliaries such as control systems and instruments. These first costs should be amortized over periods which realistically represent the expected life of the equipment. Direct operating costs should include power costs for such purposes as pumping heat transport fluids and labor for operation. Maintenance expense includes costs of cleaning and repair of collector systems, glass or reflector cleaning and replacement, servicing of plumbing or duct-work, and maintenance of storage units, engines, coolers, and auxiliaries.

Where continuous output or continuous availability of output of a process is required, in most temperate climatic zones it appears to be economically impractical to provide sufficient collector area and storage capacity to operate processes exclusively on solar energy. Auxiliary energy sources must be provided to carry the load during prolonged non-sunny periods. As with most processes, the major economic consideration is the minimization of the total cost of the product of the process. Thus, if fuel is the major cost factor in a conventional system and if the costs of the product of the solar-operated system are lower than the corresponding fuel costs on the conventional system, total costs can be reduced by use of the solar-operated system. For example, in a house heating system in areas where central heating is required, a conventional furnace is needed; if the total cost of heat delivered from a solar heating system is lower than the fuel saved by it, the overall cost of heating can be reduced by use of the solar heating system.

Costs of energy for several applications

The availability and costs of energy from various sources over the world are widely variable, and the possibilities for economic utilization of solar energy are correspondingly variable. The competitive position of solar radiation as an energy resource for many applications may be expected to improve with time, as advances in the new fields of solar technology make its use less expensive and as the costs of energy from other sources rise. The economics of solar energy utilization are also dependent on the development of local resources. The competitive position of solar energy thus varies with location, nature of the application, and time, and generalizations on the relative costs of energy from solar radiation and other sources are difficult to make. In this discussion, the probable economic feasibility of several solar applications is assessed by using the range of costs

TABLE 2

ESTIMATED COSTS OF ENERGY FOR SEVERAL APPLICATIONS AT SELECTED LOCATIONS

Location	Type and Capacity	Cost	Notes and References
SPACE HEATING			
1. Central U.S.	10^5B.t.u./hr. oil burner	\$1.50/10^6B.t.u.	Fuel oil at 15¢/gal., fuel cost only.
2. Western U.S.	10^5B.t.u./hr. LPG system	\$2.00/10^6B.t.u.	Propane at 17¢/gal., fuel cost only.
3. Denver	Natural gas	\$0.75/10^6B.t.u.	Fuel cost only.
SPACE COOLING			
1. South U.S.	2–5 tons compression	5–8¢/ton–hr.	Electric power at 2–4¢/k.w.h, C.O.P. = 2.5, 20% load factor, equipment cost included at 10%/yr.
2. South U.S.	2–5 tons absorption	2.5–6¢/ton–hr. 5.5–9¢/ton–hr.	Fuel cost only, at \$0.75 to \$2.00/10^6B.t.u. Same, with equipment cost included as in No. 1.
3. Cairo, Egypt	2–5 tons compression	12¢/ton–hr.	Electric power at 7.5¢/k.w.h. fixed cost. 40% load factor.
4. Dakar, West Africa	2–5 tons compression	25¢/ton–hr.	Electric Power at 17¢/k.w.h. 10%/yr. fixed cost, 40% load factor.
POWER			
1. U.S.A.	Industrial large capacity	1¢/k.w.h.	Power generated at large central thermal power stations or hydroelectric stations.
2. U.S.A.	Small central power plant	3¢/k.w.h.	Power from a 10,000 k.w. central power station.
3. Rural U.S.	Auxiliary generator	4–8¢/k.w.h.	Power from small gasoline generator plants of 2–3 k.w. capacity.
4. Cairo, Egypt		7.5¢/k.w.h.	Residential lighting rate [7].
5. Dakar, West Africa		17¢/k.w.h.	Residential rate [3].
6. Rural India	Animal power	15–30¢/k.w.h.	Power for lifting irrigation water [8], estimated in terms of electrical equivalent.

of energy from present sources as a basis for estimating upper limits on the first costs of the solar operated systems.

Table 2 shows the range of costs of energy for three applications which are of potential interest as solar processes.

Solar and conventional processes are compared by estimating the maximum cost chargeable to a solar-operated process in order for it to compete with conventional energy sources. The comparison is simplified by two assumptions. First, even though solar intensity is widely variable over the earth's surface, the climates where solar energy is most likely to be widely used do not have greatly differing annual solar energy reception. Second, although various designs and applications involve solar collection efficiencies which vary considerably, research on materials and thermal properties of collectors should lead to improvements in design and selection of systems which permit average efficiencies of conversion of solar radiation to sensible or latent heat in a working fluid to reach about 60%. This figure is used in the following analysis, except where another choice is dictated by the special nature of the application. Attainment of this efficiency is contingent on further engineering advances in collector design and operation.

In solar energy applications discussed here, only the fixed costs, including amortization of the solar equipment, are considered. Since there is no information available in the literature on maintenance or operating costs for any solar operated systems, they have not been included. Ultimately these costs must be minimized by satisfactory design.

Some of the assumptions made in estimating the allowable costs of solar units are in part arbitrary, and the estimates are considerably affected thereby; this is particularly true of the assumptions of useful life of the equipment. Where there is reasonable indication of the useful service life of a solar unit, this has been taken as the basis for amortization cost, or the amortization rate has been taken equal to a typical rate for the energy source replaced. No account is taken of the availability of capital for investment in the solar operated systems.

In contrast to many items of process equipment, the cost per unit of capacity for a system of flat plate solar heat exchangers, if made up of a number of factory-produced units, would be nearly independent of the capacity of the system. Thus, in the estimates following, the costs are considered on the basis of a square foot of collector without regard to the total capacity of the system. The assumption that cost is independent of capacity for a focusing collector is less valid because of variability of requirements for moving and positioning the reflector, wind loading, and other factors.

Space heating

Space heating is an application of solar energy which is of interest because (a) the temperatures required are low enough (100° to 150°F.) to permit the use of flat-plate collectors, (b) the solar energy incident on a dwelling during the winter in most temperate climates is more than the energy needed for comfort heating, (c) there is no requirement for conversion of thermal to other forms of energy, and (d) comfort heating is a major user of conventional fuels.

Space heating costs in the United States are to a large extent dependent on the proximity of the user to fuel supplies. In Table 2 the approximate costs of one million B.t.u. net heat delivery to a residence from inexpensive natural gas (based on rates in Denver, Colo.), propane "bottled gas" (typical western U.S. price) and fuel oil (typical national price) are listed. In estimating space heating costs, a combustion efficiency of 80% has been assumed, and only fuel costs have been considered as the fixed costs of the conventional (auxiliary) equipment are not reduced by the solar heat supply. In the United States, typical costs of fuel for residential space heating generally range from 75¢ to $2.00 per million B.t.u. delivered. In other areas, costs may be several times as great.

With heat collection by one square foot of a flat-plate solar heat exchanger at a rate of 150,000-300,000 B.t.u. per annual heating season (variable with the length of the heating season), the value of the output per square foot of exchanger would range from 11-60¢, based on a value of delivered heat of $0.75-$2.00 per million B.t.u. At a fixed cost of 10%/yr., an expenditure of $1.10-6.00/sq. ft. could be justified for the collector and associated equipment. The flat-plate heat exchangers suitable for house heating applications can be fabricated from materials such as glass, sheet metal, and insulation; costs of these materials in most proposed designs total less than $1.00/sq. ft. of collector. However, the labor costs for fabrication of the solar collectors for the few solar houses built to date have been many times the material costs.

For a practical solar heating system, heat storage must also be provided. This may be in the form of a liquid (hot water), solid (crushed rock), or a change-of-state material. With a heat storage capacity equivalent to a day's solar collector delivery capacity, the cost of heat storage equipment should be much less than that of the solar collector. Auxiliary equipment such as fans, ducts, piping, and control instruments, where required in addition to the conventional system will add further investment to the system. However, it appears that collectors and associated equipment can be built, in quantity, for costs within the range of $1.00-$6.00/sq. ft., and development of solar space heating systems appears attractive.

Space cooling

Research on solar space cooling is suggested by the generally good correlation between energy supply and cooling demand, as areas of high solar incidence usually have uncomfortable summer temperatures. Technical feasibility is assured by the fact that heat-operated absorption refrigeration units require temperatures well within the range of working temperatures of solar heat exchangers. Comfort cooling by solar energy can be associated with a solar heating system, and if used for both purposes, the allowable cost of the solar heat exchanger would be greater than for either of the separate purposes because of its useful energy collection over a greater part of the year.

In evaluating the potential economics of solar cooling, costs of energy for conventional refrigeration systems have been presented in Table 2 as ¢/t.hr. of refrigeration, (i.e., cost/12,000 B.t.u. of cooling). The compression system has been evaluated in terms of total fixed and operating cost with a use factor of 20%. For absorption systems, in which heat could be supplied to the refrigerant generator either by solar or conventional means, it is of interest to make two comparisons: the fuel cost only can be compared with the cost of heat from a solar collector, or the total costs of both fuel and equipment can be compared. Operating costs for air conditioning vary greatly with location as shown in the examples selected, which were chosen primarily for their comparatively high solar availability, and also their wide energy cost range.

Table 2 shows typical Unites States costs in the range of 5-9¢/t.hr. of refrigeration, applicable to small compression or absorption units of two to five tons refrigeration capacity. In a heat-operated system the cost of fuel would usually lie in the range of 3-6¢/t.hr. equivalent to $36 to $72 worth of fuel per year of 1200 operating hours. If solar heat is substituted for fuel in an absorption system about 150 sq. ft. of solar collector would be necessary to provide sufficent heat for replacing each ton of cooling capacity. Considering use of solar energy only for cooling, at 10% annual fixed cost, $2.50 to $5.00 could be paid per square foot of solar collector and the necessary storage facilities. These costs are in an approachable range. Substitution of solar energy for the usual heat source in a conventional cooler will require some modification in cooler design, particularly if flat-plate collectors are used, because of the variable nature of the solar energy supply.

Replacement of an entire compression cooling system by a solar operated absorption type cooler requires consideration of air conditioner costs as well as solar heat exchanger costs. At total conventional costs of 5-8¢/t.hr. of refrigeration, there would be an investment of approximately $4.00-$7.00 allowable per square foot of solar collector and associated air conditioning equipment. If the costs of an air conditioning unit operable with solar heat are reducible to those of a conventional unit, $100-$200/t. of refrigerated capacity, the allowable cost of the solar collector would be reduced to the range of $3.00-$6.00/sq. ft.

Two other factors improve the prospects of solar cooling. In many installations, particularly in temperate climates, space heating will also be accomplished by use of the solar collector; this increases by a substantial amount the allowable investment in the solar collector, storage unit, and other common facilities. Secondly, in other parts of the world where energy is more expensive than in the United States, the economic situation is more attractive for the solar operated cooling system. In Dakar, for example, the cost of electricity for air conditioner operation is ten times as great as in the United States. This permits a substantial increase in allowable investment in solar cooling facilities. In many such areas space cooling is now used to a very limited extent. As the purchasing power of the peoples in these countries rises, however, and the modern conveniences enjoyed in industrialized countries come into increasing demand, solar air conditioning should achieve substantial application.

Solar power

Generation of power from solar energy, in the form of mechanical work, has been accomplished on a limited scale by the production of steam or other vapor in a boiler heated by a solar collector and the expansion of this fluid in a reciprocating engine. Electricity has been generated by coupling a generator to this type of engine, or by converting sunlight directly to electrical energy in a silicon semi-conductor cell or "solar battery". These applications have been either experimental or specialized, and not based on the economics of substantial energy supply.

Costs of power from several selected types of power installations shown in Table 2 range from 1-30¢/k.w.h. Most residential consumers of electricity in the United States and Canada pay 2-3¢/k.w.h. for power from central plants. Power from some small central installations is more expensive, ranging up to 3.5¢/k.w.h., and that from

gasoline or diesel-powered generator sets used on non-electrified farms for pumping irrigation water, etc., costs in the range of 4-8¢/k.w.h. In some foreign locations much higher costs prevail, even in central stations. In estimating these costs, it was necessary in some cases to assume load factors and fuel costs; the best available data and reasonable assumptions of load factors and useful life of equipment were employed. In most of the small installations fuel is the major item of cost.

For a solar power plant consisting of a focusing collector or a flat-plate solar exchanger producing steam for use in an expansion engine, the maximum plausible efficiency from steam (100 p.s.i.) to electricity in small units appears to be about 15%. With a focusing collector having a 60% solar collection efficiency, about 15 sq. ft. of solar collection surface would be required for the daily generation of one k.w.h. Over the total cost range of electric power shown in Table 2, from 1-30¢, and at a total annual fixed cost of 15% of the original investment, the allowable expenditure for solar collector, power plant equipment, and all auxiliary facilities would range from \$24 to \$720 for the 15 sq. ft. of collector and associated equipment necessary to develop one k.w.h./d. Per square foot of solar receiving surface, these figures become \$1.60 and \$48, respectively; or for an average delivery of one kilowatt for 10 hours daily, \$240 to \$7200 are the maximum allowable costs for the 150 sq. ft. collector and associated power plant.

Small steam engines, if manufactured in quantity, should be obtainable for less than \$50/k.w. capacity, and electric generators should be in the \$50 range. At \$100 for these items, the allowable investment in solar heat exchange units would be \$140 to \$7100. Thus, in areas of high power costs (e.g., rural India and parts of North Africa), the allowable investment in a solar boiler and associated equipment is high enough to make solar power of potential economic interest. With these high allowable investments per square foot of solar reflector or flat-plate exchanger, the prospects appear promising; however, there are no small prime movers presently available that will operate at an efficiency near 15% on 100 p.s.i. steam, nor are there focusing collectors of reasonable cost which will produce this steam at 60% efficiency. A further deterrent in these areas may be lack of capital to make the initial investments required for the solar power systems.

Since solar power is not continuous and electrical storage appears to be prohibitively costly, auxiliary energy supply would have to be provided where continuous power is essential. The load factor on the auxiliary facilities would be reduced by the solar power plant, and in effect, only a portion of the fuel cost reduction in the competing (standby) electric power station should be credited to the solar power plant. In some applications, such as pumping irrigation water, auxiliary energy would not be required and the economic comparison involves the total alternative original investments and operating costs.

For large central power plants, Hottel [2] has made economic studies of the use of flat-plate collectors and low pressure turbines and has concluded that the costs are potentially in the range of two to three times the current costs of power from conventional fuels in the United States.

Other processes

There are several additional uses of solar energy which merit consideration. Among these are applications in non-industrialized areas where sociological considerations may be as important as the economic factors; solar cookers and food coolers are examples. If solar cookers can be made cheaply enough and if the requirements for their operation can be made consistent with the eating and living habits of the users, they could be used by millions of people who are now using wood or other primitive fuels. In northern Mexico, for example, fuel for cooking is a major item of expenditure for many low-income families, and reduction in the use of wood could improve their economic situation as well as decrease the rate of deforestation. Small, inexpensive refrigerators, operated by solar energy or other heat sources, could provide facilities for food preservation not now existent in many of these areas.

Salt water demineralization by solar distillation could provide potable water in arid regions where solar radiation is high. At a distilled water cost of \$2.00/1000 gals. (based on costs in several large fuel-operated evaporation plants) and at a typical daily productivity of one-tenth gallon of potable water per square foot of solar distillation plant [9], about 75 cents is the maximum allowance for investment in each square foot of solar distiller and accompanying auxiliary equipment if annual fixed and operating costs are 10%. With the lower cost of capital used for public works, annual fixed costs could be somewhat lower and the total allowable investment might be increased to \$1.00-\$1.25/sq. ft. Large scale construction methods and the use of cheap materials such as bituminous coatings, glass, and some plastic films may permit construction in this cost range. The problem is difficult, however, and exceptional economies in design, construction, and operation must be developed if solar distillation is to compete with fuel-operated demineralizers.

In comparison with the usual costs of natural fresh water, the projected prices for solar-distilled water are very high. However, the need for demineralized saline water is expanding, and in favorable locations, solar distillation of saline water has the potential of becoming economically attractive where potable water must be available for human consumption.

Summary

The foregoing appraisal of several solar energy applications from the standpoint of their competitive position with respect to conventional sources of energy shows the possibilities and limitations of these applications. In each case chosen, solar energy appears to have promise in some areas and some scales of use. Other applications may be similarly considered.

THE WISCONSIN PROGRAM

The Engineering Experiment Station of the University of Wisconsin, in cooperation with the chemical, mechanical, civil engineering, Chemistry and meteorology departments, is studying some of the problems of the engineering applications of solar energy. This program includes studies of flat-plate solar heat exchangers and focusing collectors, intermittent and semi-continuous absorption cooling systems, focusing collectors for small power units and food cookers, photochemical processes, and solar radiation measurements and correlation.

The Wisconsin program was initiated in 1953, when a conference of persons who had been active in research in this field was held at Madison. This conference was supported by the National Science Foundation and the University. From this meeting, and as a result of the interest of Professor Farrington Daniels of the Chemistry Department, a program of research in the field was initiated. With support from the John Simon Guggenheim Foundation, the National Science Foundation, the Wisconsin Alumni Research Foundation, and the Uni-

versity, and more recently with grants from the Rockefeller Foundation, several principal investigations, and a number of related researches in engineering, chemistry and meteorology have been undertaken.

Collector research

Basic to all of the thermal applications discussed is the solar heat exchange unit, of either the flat-plate or focusing type. The economic studies outlined indicate that the major item of cost in space heating and cooling and in small power systems is the collector. Performance of this unit is described by a heat balance for the solar energy absorbing surface, which can be expressed as:

$$HR\frac{A_a}{A_x}r\tau\alpha = q_u + q_{th} + q_{hc}$$

where

- H = the solar radiation rate on a horizontal surface (total radiation for a flat plate heat exchanger, direct radiation only for a focusing collector).
- R = the ratio of radiation on a tilted surface to that on a horizontal surface.
- A_a = projected area of the collector.
- A_x = the solar energy absorbing surface area of the solar heat exchanger (= A_a for a flat-plate exchanger).
- r = effective specular reflectivity of the reflector of a focusing collector. (This factor does not enter for a flat-plate exchanger).
- τ = the transmissivity for solar radiation of any system of transparent covers over the absorbing surface.
- α = absorptivity of the blackened surface for solar radiation.
- q_u = the useful energy transferred to the heat transport fluid of the collector, per unit area of absorber, per unit time.
- q_{th} = the sum of all losses from the absorber, including losses by convection and radiation through the transparent covers, and downward losses by conduction, and shading, per unit area of absorber, per unit time.
- q_{hc} = heat capacity effect of the heat exchanger, per unit area of absorber, per unit time, if it is not operating at constant temperature.

The left side of the equation represents the absorbed radiation, while the terms on the right show the distribution of the absorbed radiation. This heat balance has been extensively studied for a flat-plate heat exchanger by Hottel and Woertz [10]. For either type of collector, performance is improved by minimizing the optical losses (i.e. the departure of the product $r\tau\alpha$ from unity) and the thermal losses, the most important of which are usually the losses from the absorber by convection and radiation.

The objective of collector studies is to minimize the cost of collected energy, by achieving higher collector efficiency and/or by use of more economical materials and designs. The Wisconsin flat-plate heat exchanger studies are presently oriented toward the reduction of the optical ($\tau\alpha$) losses, which limit the absorption of solar energy, and the reduction of upward radiation losses from the absorber by the use of semi-transparent coatings to make surfaces having selective radiation characteristics. Progress has been made in the latter area, and surfaces of metal oxides on metals, having absorptivities for solar radiation above 0.9 and emissivities for long wave radiation less than 0.4, are now being used in studies of experimental solar heat exchangers. The recent availability of plastic materials with desirable characteristics for flat-plate exchanger covers or for fabrication of collector parts has permitted study of their performance and utility. The concept of a unitized solar heat exchanger design, suitable for factory assembly and easy installation, is being explored as a means of reducing costs.

Focusing collector studies have included consideration of the use of plastics and plastic forming techniques for solar reflectors [11] and studies of the performance of radiation receivers. Research on surfaces with semi-transparent coatings is applicable to focusing collector receivers also, as they are designed to operate in a temperature range above 250°F. where radiation losses may become a large fraction of the thermal losses. Several geometric arrangements of reflector and receiver are being studied, as are the precision of fabrication and orientation of the reflectors (which limit the ratio of areas of reflector to receiver). The overall objective is to minimize the cost of collected energy at the temperature levels required for promising applications.

Figure 2 shows an experimental flat-plate exchanger under construction, and Figure 3 shows an experimental focusing collector with a flat-plate receiver. The performance of both types has been discussed in a recent publication [12].

Solar cooling

The Wisconsin program of solar cooling development includes consideration of continuous absorption cycles for air conditioners and intermittent cycles for food coolers. Intermittent units, designed for use as food refrigerators in non-industrialized countries, have been described by Williams, et al [13]. The continuous systems under study are absorption coolers with heat supplied to the generator of the cooling units from flat-plate solar heat exchangers. A schematic diagram is shown in Figure 4. A storage unit is shown between the collector and the generator; an alternative is the location of storage facilities between the evaporator and the cooled space.

Figure 2—Experimental flat plate heat exchanger during assembly, prior to blackening of the copper absorber surface. Provision is made for mounting three glass covers over the absorber.

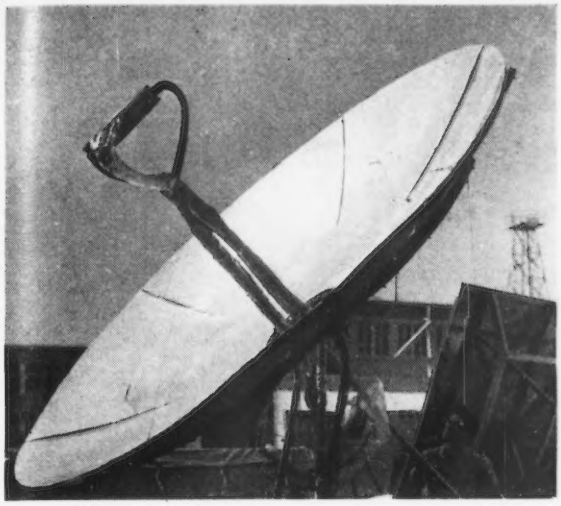

Figure 3—Experimental focusing collector, 12′ diameter, with polystyrene-aluminum reflector and a flat plate heat exchanger.

Ambient temperature, horizontal radiation, and radiation incident on a south-facing tilted collector during a typical hot summer day in Madison show in Figure 5 the variability of radiation on a fixed flat-plate solar heat exchanger and an approximation of the changing cooling loads. A study of the relationships between cooling load and energy supply on collectors of various orientations indicates that hot days in Madison are usually accompanied by high radiation.

The challenges in this program lie in the development of techniques to meet the limitations and variability of the solar energy supply by suitable design of the combined solar exchanger-cooler system. The immediate objectives are to investigate some of the many possible design combinations of solar heat exchangers, short-term storage systems, and cooling units, by analytical studies and by operation of an experimental cooler. It is also of considerable importance to optimize collector design for combined summer cooling and winter heating use.

Solar power

The development of small (1 to 10 h.p.) solar power units using steam engines or other prime movers is being studied. The problems are divided into separate investigations of the solar exchangers and prime movers, with subsequent combination of the two elements to obtain optimum systems. The solar heat exchanger studies outlined above contribute to the solar power investigations, and parallel with them have been studies of several conventional and specialized types of prime movers which might be combined with a solar collector. Most of these efforts on engines have been concerned with low pressure steam, 35 to 40 p.s.i., and higher pressure ranges are now being investigated. The experimental results with low pressure engines indicate that with presently available equipment of this capacity, engine efficiencies are less than 4%; 15% will be very difficult to achieve unless substantially higher steam pressures (and correpsondingly better solar heat exchangers) are employed. For solar power units in underdeveloped areas, ease of maintenance and operation by unskilled personnel is also being considered in the development and design of equipment.

Another approach to the problem of solar power generation lies in the use of solar "batteries" of light-sensitive silicon cells. The present cost of these units is prohibitive, but if the temperature of the cells can be controlled, there is the possibility of increasing the energy flux on them by use of a focusing reflector. With the increased electrical output per cell, the number of cells required and the total investment may be reduced. Studies of these factors are in progress.

Other applications

For potential applications of solar energy in underdeveloped areas the economic factors may be no more important than sociological considerations. This point may be illustrated by reference to a recently developed reflective type solar cooker comprising a conveniently supported plastic parabolic reflector large enough to deliver heat to a grill at a rate of 600 to 800 watts. Some of these units have been distributed to low-income families in northern Mexico with the objective of assessing their effectiveness in replacing part of the wood or other cooking fuels used in that area.

In connection with problems of obtaining solar radiation data in the desired form, i.e., as the total radiant energy over hourly periods, an integrator-recorder has been developed. This instrument shows hourly values of integrated radiation rather than the record of radiation vs time usually obtained with recording potentiometers.

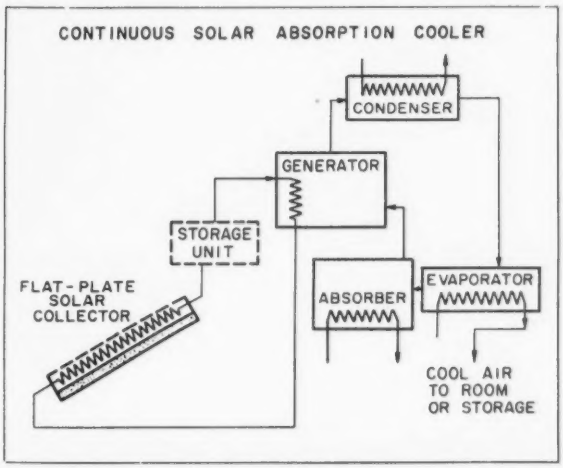

Figure 4—Schematic diagram of continuous solar absorption cooler.

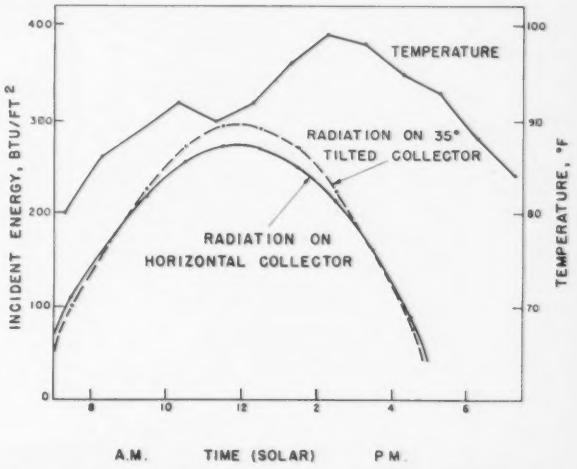

Figure 5—Ambient temperature, radiation on horizontal collector, and radiation on a collector tilted 35° to the south, for a hot summer day at Madison, Wis.

Conclusion

The challenges in solar energy research are great, and the potential fruits of engineering research and development studies in this field are substantial, if they can achieve the major objective of making solar processes economically competitive with processes using other energy resources. Solar energy is a tremendous, virtually untapped resource which should be available as long as men are on earth to use it. The Wisconsin program seeks to contribute to the solution of the problems which must be met before this energy resource can be a significant factor in our economy.

References

(1) Hamilton, R. W., ed., "Space Heating with Solar Energy", Massachusetts Institute of Technology (1954).

(2) Daniels, F., and Duffie, J. A., eds., "Solar Energy Research", University of Wisconsin Press, Madison (1955).

(3) Proceedings, World Symposium on Applied Solar Energy", Stanford Research Institute, Menlo Park (1956).

(4) Carpenter, E. F., Kassander, A. R., and Bliss, M. D., eds., "Transactions of the Conference on the Use of Solar Energy—The Scientific Basis", The University of Arizona Press, Tucson (1958).

(5) Moon, P., J. Franklin Institute, 230, 583 (1940).

(6) Niewirth, O., and Daniels, F., Paper presented at Symposium on Photochemistry of Solids and Liquids, Boston, Massachusetts (1957).

(7) Salam, E. M. A., Private Communication to the Authors (1958).

(8) Daniels, F., Private Communication to the Authors (1956).

(9) Annual Report of the Office of Saline Water, U.S. Department of the Interior, Washington (1958).

(10) Hottel, H. C., and Woertz, B. B., Trans. Am. Soc. Mech. Engrs., 64, 91 (1942).

(11) Duffie, J. A., Lappala, R. P., and Löf, G. O. G., J. Solar Energy Sci. Engr. 1, 9 (October 1957).

(12) Duffie, J. A., Löf, G. O. G., and Salam, E. M. A., paper on "Developments in Solar Energy Collectors" presented at Salt Lake City meeting, A.I.Ch.E., September (1958).

(13) Williams, D. A., Chung, R., Löf, G. O. G., Fester, D. A., and Duffie, J. A., Refr. Engr., 66, 33 November (1958).

★ ★ ★

The Effects of Shape and Reynolds Number on Drag in the Motion of a Freely Oriented Body in an Infinite Fluid[1]

H. A. BECKER[2]

The drag on freely oriented bodies in motion relative to an infinite fluid is related to the Reynolds number, Re_S, by the formula

$$K = 24Re_S + C_I Re_S^2$$

where $Re_S = D_S u_o \rho/\mu$ is formed from the diameter, D_S, of a sphere with the same surface area as the body, and $K = 8\rho F_D/\pi\mu^2$ is defined as the drag number. The inertial drag coefficient, C_I, is related to shape, orientation, and the Reynolds number. At Reynolds numbers above 2000 the relation is expressed by the formula,

$$C_I = 2.53 - 0.283e^{2\psi}$$

where ψ, the surface sphericity, is the ratio of the surface area of a sphere with the same volume to the surface area of the body. Correlations are also developed for predicting C_I at Reynolds numbers below 2000.

THE problem of predicting the drag on a body in motion relative to an infinitely extending fluid has been solved analytically in only a few special cases. Dimensional analysis was therefore used by Rayleigh to obtain the well known drag formula,

$$F_D = \tfrac{1}{2}\rho u_o^2 A.f(Re) \quad \ldots\ldots(1)$$

The unique relation between the drag coefficient, f(Re), and the Reynolds number, Re, predicted by this formula for geometrically similar bodies similarly oriented with respect to the motion has been investigated for a wide variety of bodies. However, few attempts have been made to correlate the effects of shape and orientation as they affect chemical engineering operations. Since this is a problem of importance in operations such as sedimentation and elutriation and in techniques such as sedimentation analysis, it was decided to subject it to a general study.

[1]*Manuscript received November 30, 1958.*
[2]*Prairie Regional Laboratory, Saskatoon, Sask.*
Contribution from the Prairie Regional Laboratory, National Research Council of Canada, Saskatoon, Saskatchewan. Issued as N.R.C. No. 5138.

Theory

The Rayleigh drag formula, Equation (1), states the general predictions of dimensional analysis concerning the solution of the drag problem. It does not, however, incorporate explicitly any expectation as to the form of the relation between the drag coefficient and the Reynolds number. Since such an expectation exists, (as shown in the following), it is evident that this general statement of the drag law is capable of some refinement.

The Navier-Stokes equations—the general differential equations of motion of a viscous fluid—contain viscous and inertia terms to describe the features of a real fluid in motion, and it is to be expected that the solutions of these equations are also composed of additive viscous and inertia terms. This is shown, for example, by Oseen's approximation [1] to their solution for a sphere, in which an inertia term is added to Stokes' familiar solution for the viscous drag. The additivity of viscous and inertia drags is also suggested in principle by the Rayleigh drag formula itself, for in a region where the inertia forces are unimportant the drag must be proportional to the viscous forces, while in a region where the inertia forces dominate the reverse is approximately true. It may therefore be supposed that the drag on a body in motion through an infinite fluid is composed of a viscous drag and an inertial drag:

$$F_D = F_V + F_I \quad \ldots\ldots(2)$$

The proportionality between the viscous drag and the viscous forces is formally stated by the Stokes' law-type expression

$$F_V = \frac{\pi}{8} C_V \mu u_o D \quad \ldots\ldots(3)$$

in which C_V is defined as the *viscous drag coefficent*, (the coefficient of the viscous drag force), and $\pi/8$ is arbitrary. Similarly, proportionality between the inertial drag and the inertia forces gives Newton's formula

$$F_I = \tfrac{1}{2} C_I \rho u_o^2 A \quad \ldots\ldots(4)$$

where C_I is the *inertial drag coefficent*. On inserting these values of the component drags in Equation (2) and multiplying through by $8\rho/\pi\mu^2$, there is obtained the quadratic drag formula

$$K = C_V Re + C_I Re^2 \quad \ldots\ldots(5)$$

in which K is defined as the *drag number*. It may be noted that if Rayleigh's total drag coefficient, (f(Re) in Equation(1)), and the Reynolds number Re are based on the *same* characteristic diameter D, then $A = \pi D^2/4$ and $K = f(Re).Re^2$. It is also to be noted that the viscous drag coefficient is *by definition* independent of the Reynolds number, since any drag in excess of that predicted by Equation (3) is directly ascribable to the action of the inertia forces. The viscous and inertial drag coefficients are coefficients of terms in a drag equation, but should not be confused with Rayleigh's total drag coefficient as defined by Equation (1). The only case in which equality exists is at high Reynolds numbers, when the inertial drag coefficient C_I becomes formally equal to Rayleigh's drag coefficient *if* the characteristic dimension D is expressed in consistent terms.

It may be seen that the above quadratic formulation of the drag law has the following advantages over Equation (1):

1. The coefficient C_V is a constant for a given shape and orientation, and the coefficient C_I should be only weakly dependent on the Reynolds number. By contrast, the total drag coefficient f(Re) is a strong function of the Reynolds number.

2. The equation gives a quantitative picture of the viscous and inertial aspects of drag. This is likely to be of first importance in the transition zone, and may facilitate a rational investigation of the effects of shape and orientation in this region.

3. The drag F_D and the fluid velocity u_o do not appear together in any term, whereas the conventional drag coefficient involves F_D/u_o^2. Moreover, the dimensions of the body appear only in the Reynolds number, and not in terms involving the drag force.

4. Different definitions of the charcteristic dimension D, appropriate to the nature of the drag, can be used in the Reynolds numbers, (right side of Equation (5)). Similarly, the coefficients C_V and C_I can be related to different parameters describing shape and orientation. This advantage will be most apparent in the transition zone.

The remaining problem, before applying the quadratic formula to the analysis of experimental data is to decide on suitable parameters for describing the size and shape of solid bodies in motion through a fluid. It is evident that, in order to have practical merit, these parameters should be both simple and universal. This criterion is met reasonably well by parameters constructed from the volume V, the surface area S, and the area A_P projected in the direction of the motion. There are thus obtained (i) the *surface sphericity*

$$\psi = \pi D_v^2/S \qquad (6)$$

and (ii) the *form sphericity*

$$\phi = D_v^2/4A_P \qquad (7)$$

where $V = \pi D_V^3/6$. For prolate bodies there may also be added the *slimness ratio*, (the length to diameter ratio). Previous investigators [2, 3, 4] have attempted to relate the total drag coefficient of Equation 1 to one or another of these parameters. There do not appear to be any other criteria which are worthy of practical consideration when dealing with freely oriented bodies.

It may be observed, in conclusion of this section, that in general the inertial drag, (Equation (4)), can be resolved into a component resulting from tangential forces,

$$F_{IT} = \tfrac{1}{2}C_{IT}\,\rho u_o^2 A_S \qquad (8)$$

and a component resulting from normal forces,

$$F_{IN} = \tfrac{1}{2}C_{IN}\,\rho u_o^2 A_P \qquad (9)$$

where $F_I = F_{IT} + F_{IN}$. For bluff shaped bodies tangential (friction) drag is generally small compared with the normal (form) drag, while for streamlined bodies the opposite is true. Most chemical engineering problems treat with bluff shaped bodies, and hence this distinction is not of present interest.

The viscous drag coefficient

Stokes, by neglecting the inertia terms in the equations of motion of a viscous fluid, derived theoretically the law, verified by numerous experimental measurements [1, 2, 3], for the viscous drag on a sphere:

$$F_V = 3\pi\mu u_o D \qquad (10)$$

The value, (in Equation (3)), of the viscous drag coefficient for a sphere is, thus, $C_V = 24$.

In the general case, in which analytical solution of the equations of motion is not practicable, the viscous drag on a body of arbitrary shape can be expected to be proportional to the intensity of shear at the surface and to the surface area. If, then, the diameter of the body is taken as the diameter, D_S, of a sphere with the same surface area, the variation of the viscous drag coefficient with shape and orientation should be small and should be directly related to the attitudes of the surface to the motion. It will therefore be assumed that

$$C_V = 24\, f(\phi) \qquad (11)$$

where the function (ϕ) is equal to unity for spheres.

Figure 1 shows $f(\phi)$ for oblate and prolate bodies, evaluated from the data of Heiss and Coull [2], and for isometric bodies, evaluated from the data of Pettyjohn and Christiansen [3]. The oblate and prolate bodies were oriented, respectively, with their flat sides or long axes either parallel or perpendicular to the motion. The isometric bodies showed no effect of orientation on their terminal velocities in a still fluid [3], and give values of $f(\phi)$ of 0.968 to unity. Figure 1 suggests that if the orientation is unknown or random a value of $f(\phi)$ of unity can be assumed, whence

$$F_V = 3\pi\mu u_o D_S \qquad (12)$$

A practically interesting consequence of this result is that if the volume and density of a small particle and its terminal velocity in a gravitational field are known, Equation (12) can be used to estimate its surface area.

The inertial drag coefficient

The inertia drag on a sphere at very low Reynolds numbers has been approximated theoretically by Oseen [1, 2], who obtained for the inertial drag coefficient the value $C_I = 4.5$.

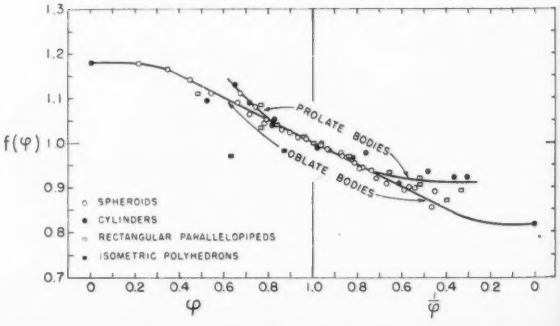

Figure 1—The shape function $f(\phi)$ for oblate, prolate and isometric bodies.

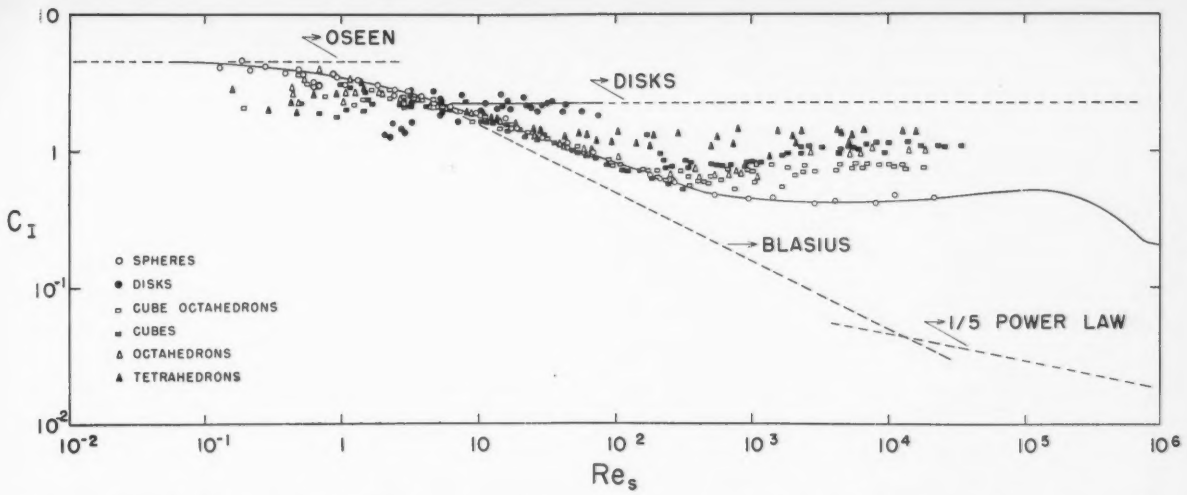

Figure 2—Inertial drag coefficients of freely oriented isometric bodies and disks as a function of the Reynolds number.

At high Reynolds numbers, the inertia forces predominate over the viscous forces everywhere except in the shallow boundary layer and in the wake. Here Prandtl's boundary layer theory has been used to estimate the tangential drag on a variety of bodies, chiefly of streamline shape [5]. However, this theory has little utility in treating the bluff, freely oriented bodies of present interest: the flow around a bluff body normally separates, and the greater part of the drag is due to the normal stresses produced by this separation.

The inertial drag on a sharp-edged, bluff body in a separating flow can be expected to be roughly proportional to the area projected in the direction of the motion. However, in chemical engineering operations an additional complexity is introduced by the absence of orientational restraint, which allows the superposition of rotational and other motions on the general translation of the body relative to the fluid. The projected area to which the inertial drag on a freely rotating body should be roughly proportional is not clearly defined, but it appears reasonable to choose the projected area, A_S, of a sphere of equal surface area; this area is roughly intermediate between that of a sphere of equivalent volume and that of the sphere swept out by free rotation of the body. On inserting this value of the projected area in the expression for the inertial drag, Equation (4)), and noting that the viscous drag is best expressed by putting $D = D_S$ in Equation (3), the exact formulation (for the present purposes) of the quadratic drag law, Equation (5), becomes

$$K = C_V Re_S + C_I Re_S^2 \quad \ldots\ldots\ldots\ldots\ldots\ldots (13)$$

Figure 2 shows inertial drag coefficients for isometric bodies, calculated by Equation (13) from the data of Pettyjohn and Christiansen [3], and for disks, calculated from the data of Squires and Squires [6], as a function of the Reynolds number. At Reynolds numbers greater than five the inertial drag coefficients of these bodies fall between the solution of Blasius [7] for a flat plate oriented parallel to the motion and the experimental value for a disk oriented perpendicular to the motion. At Reynolds numbers smaller than five the coefficient for spheres approaches Oseen's solution, but the coefficients of nonspherical bodies appear to approach considerably smaller limiting values. The experimental evidence indicates that freely oriented bodies show three distinct types of behavior, each of which is characteristic of a well defined range of Reynolds numbers:

(1)($Re_S < 2 - 10$. At Reynolds numbers smaller than $2 - 10$ the flow is wholly laminar, and it has been shown that bodies possessing three perpendicular axes of symmetry are equally stable in all orientations [3]. The trend in the behavior of the inertial drag coefficient appears to be directly opposite to that found in all subsequent regimes; Figure 2 indicates that the coefficient decreases in value with increasing bluffness and angularity.

(2) $2 - 10 < Re_S < 100 - 400$. Entry into this region is marked by the manifestation of specific orientational stability in the position of maximum drag. Thus, isometric bodies and disks orient themselves with a flat side forward, perpendicular to the motion [3, 6]. It has been shown [5] that at a Reynolds number of about five the streamlines behind a disk broaden out, and a stationary region at its rear is separated from the main flow by a vortex sheet. In this region of retarded fluid there is a permanent circulation corresponding to a vortex ring. Hence, the appearance of specific orientational stability of bluff bodies is coincident with the development of vorticity in the wake, and is directly associated with the stability of the vortex ring. The dimensions of the ring increase with increasing Reynolds number until a critical Reynolds number is reached at which the stability of the ring and orientational stability of the body are lost together. For disks, a critical Reynolds number of 195 has been found [5]. The orientational stabilities observed by Pettyjohn and Christiansen [3], indicate that the critical value may be as high as 400 and as low as 100, but is generally in the neighborhood of 200.

Figure 3 indicates that the relation between the inertial drag coefficient and the Reynolds number in this region is accurately described by the power formula

$$C_I = C_O . Re_S^{-r} \quad \ldots\ldots\ldots\ldots\ldots\ldots (14)$$

The coefficients in Figures 2 and 3 have a common value $C_I = 2.25$ at $Re_S = 5.5$, suggesting that

$$C_O = 2.25\,(5.5)^r \quad \ldots\ldots\ldots\ldots\ldots\ldots (15)$$

Table 1 gives the experimental values of the exponent r. It appears that the exponent lies between a minimum value of zero and a maximum value of 0.5, and is predicted with reasonable accuracy by the formula

$$r = 0.34\sqrt{\phi} \quad \ldots\ldots\ldots\ldots\ldots\ldots (16)$$

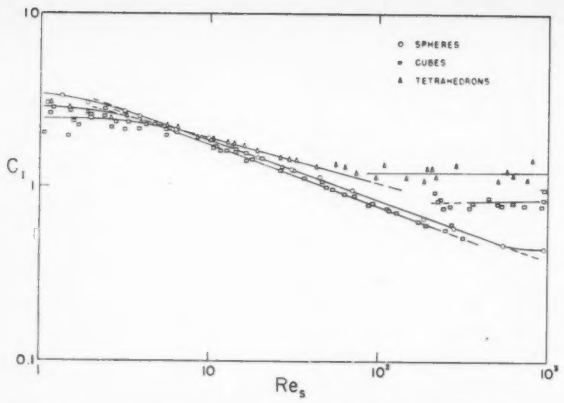

Figure 3—Inertial drag coefficients of freely oriented isometric bodies as a function of the Reynolds number, showing the linearity of the logarithmic relation in the region where the orientation is stable in the position of maximum drag.

(3) $Re_s > 100 - 400$. It has been shown [5] that when the Reynolds number exceeds the critical value, approximately 200, a disturbance of the vortex ring becomes visible, and successive portions of its substance are discharged downstream at regular intervals of time. Freely oriented isometric bodies simultaneously develop a rotational motion [3], and Waddel [4] notes that disks develop a wobbling or teetering motion. The discharge of vorticity increases in rate and irregularity with increasing Reynolds number, and eventually the wake becomes a completely turbulent mass of eddies and vortices. Figure 2 indicates that the discharge of vorticity is generally accompanied by an increase in the inertial drag coefficient which continues until the wake becomes completely turbulent at a Reynolds number near 2000. From this point onward the inertial drag coefficients of sharp-edged bluff bodies are substantially independent of the Reynolds number. The final portion of the curve for spheres, Figure 2, is based on the results of Bacon and Reid [8], and shows the decrease in the coefficient as the Reynolds number increases above about 2 x 10^5. This decrease is typical of round-edged bodies, and is due to the retardation of separation induced by the growth of turbulence in the boundary layer [5].

Experimental

Pettyjohn and Christiansen [3] defined the total drag coefficient of Equation (1) by

$$C_R = f(Re) = 8F_D/\pi\rho_o^2 D_v^2 \quad \ldots\ldots\ldots\ldots (17)$$

i.e., $A = \pi D_v^2/4$, and found that at Reynolds numbers $D_v u_o \rho_o/\mu$ greater than 2000 the total drag coefficients of freely oriented isometric bodies are related to the surface sphericity ψ by the formula

$$C_R = 5.31 - 4.88\psi \quad \ldots\ldots\ldots\ldots (18)$$

Since, by equation (13), $C_I = K/Re_S^2 = 8F_D / \pi\rho u_o^2 D_S^2$ when the viscous drag is negligible, it is evident that in a purely inertial regime of flow $C_I = C_R\psi$. Also, it appears from Equation (18) that

$$C_I = 5.31\psi - 4.88\psi^2 \quad \ldots\ldots\ldots\ldots (19)$$

However, examination of Equation (17) indicates that Equation (18) can only be valid for high surface sphericities ψ; *e.g.* Equation (18) predicts a maximum value of C_R of 5.31, whereas for flat, platy particles of negligible thickness the factor D_v^2 in the denominator of C_R can become so small that C_R approaches infinity, as it indeed does at $\psi = 0$. Similarly, Equation (19) predicts a value of C_I of zero at $\psi = 0$, when it should predict a finite value. It is evident, therefore, that Pettyjohn and Christiansen's formula cannot be extrapolated beyond their data to values of ψ smaller than those covered by isometric bodies, ($\psi = 0.67$ to 1.00).

A study of the inertial drag coefficients C_I of non-isometric bodies was therefore undertaken to test the generality of Pettyjohn and Christiansen's formula at high surface sphericities ψ, and to investigate the relation between C_I and ψ at low values of ψ.

Shapes studied. Solid prisms and cylinders were cut from cork and cardboard. Table 2 summarizes the properties of typical specimens.

Method. The time of fall in stagnant air was determined from heights of 840 and 1250 cm.

TABLE 1

VALUES OF THE EXPONENT r FOR FREELY ORIENTED BODIES

	ψ	ϕ	r	$0.34\sqrt{\phi}$
Spheres	1.000	1.000	0.340	0.340
Cube octahedrons	0.906	1.07	0.340	0.352
Octahedrons	0.846	0.732	0.325	0.306
Cubes	0.806	1.210	0.353	0.373
Tetrahedrons	0.670	0.670	0.253	0.297
Disks	0.000	0.000	0.000	0.000

TABLE 2

DRAG COEFFICIENTS OF NON-ISOMETRIC BODIES FOR REYNOLDS NUMBERS $Re_S > 2000$

m gm.	Dimensions* cm.			ψ	$\frac{\bar{u}}{\bar{u}_t}$	C_I
	Cylinders					
	D	h				
0.615	1.52	2.20		0.86	0.81	0.99
0.231	2.39	0.35		0.57	0.94	1.82
	Rectangular Prisms					
	w	h	l			
0.140	1.20	0.45	1.71	0.68	0.92	1.30
0.180	1.13	1.00	1.27	0.80	0.89	1.34
0.60	3.85	0.63	3.85	0.146	0.98	2.20
	Right Triangular Prisms					
	b	h	l			
0.149	1.00	1.31	1.57	0.65	0.91	1.18
0.137	1.30	1.49	0.92	0.71	0.89	1.36
0.41	2.50	7.6	0.063	0.172	0.95	1.82

*D denotes diameter; w, width; h, height; l, length; and b, base.

Orientational behavior. The flat-shaped disks and prisms, when so dropped, were oriented perpendicular to the translation, and showed a regular fluttering motion about the axis of least inertia. The stability of this orientation was easily destroyed by atmospheric disturbances. The stable motion for all bodies consisted of spiral translation accompanied by rotation about the axis of least inertia, this axis being oriented perpendicular to the translation. This motion could be imparted at the beginning of fall by manual rotation of the body. The time of fall of flat shaped bodies with rotational motion was 5-10% greater than for oriented fall in the position of maximum drag.

Calculation of drag coefficients. The force balance for a body falling from rest is

$$ma = mg\left(1 - \frac{\rho}{\rho_s}\right) - F_D \quad \ldots\ldots(20)$$

When the Reynolds number is large, the drag can be expressed as

$$F_D = \frac{1}{8} C_I \rho u_o^2 S \quad \ldots\ldots(21)$$

The differential equation of the motion is, therefore,

$$\frac{du_o}{dt} + \frac{1}{8} C_I \frac{\rho S}{m} u_o^2 = g\left(1 - \frac{\rho}{\rho_s}\right) \quad \ldots\ldots(22)$$

Solution of the differential equation, subject to the initial condition $u_o = 0$ when $t = 0$, gives for the velocity of the motion

$$u_o = \frac{\alpha}{\beta} \frac{e^{2\alpha\beta t} - 1}{e^{2\alpha\beta t} + 1} \quad \ldots\ldots(23)$$

where

$$\alpha^2 = g\left(1 - \frac{\rho}{\rho_s}\right) \text{ and } \beta^2 = \frac{C_I \rho S}{8m}$$

The equation for the time of fall is

$$x = \int_o^t u_o \, dt \quad \ldots\ldots(24)$$

whence, on substituting Equation (23) for u_o,

$$X = \int_o^t \frac{e^t - 1}{e^t + 1} dT \quad \ldots\ldots(25)$$

where $T = 2\alpha\beta t$ and $X = 2\beta^2 x$. Semi-graphical evaluation of the integral on the right of this equation then yields the approximation

$$X = T - 1.374 \quad \ldots\ldots(26)$$

for values of T greater than five, ($u_o = 0.985\ u_t$ at $T = 5$). We thus obtain for the drag coefficient

$$C_I = \frac{4gm}{\rho u_o^2 S}\left[1 - 1.374 \frac{\bar{u}_o^2}{gx} + \sqrt{1 - 2.748 \frac{\bar{u}_o^2}{gx}}\right] \quad \ldots\ldots(27)$$

where $T > 5$; $\rho/\rho_s \ll 1$; and $\bar{u}_o = x/t$.

The significance of the drag coefficient calculated from the above equation is as follows. Until T approaches a value of about 0.6, Equation (25) reduces to

$$X = \tfrac{1}{2}T^2 \quad \ldots\ldots(28)$$

At $T = 0.6$, $u_o = 0.3\ u_t$. Hence, if the terminal Reynolds number is sufficiently large, it can be assumed that the Reynolds number will be large when the point is reached when the drag appreciably reduces the acceleration, and the velocity at this point will be of the same order as the terminal velocity. The drag coefficient calculated from Equation (27) should, therefore, closely approximate the inertial drag coefficient for steady motion if the time parameter T and the terminal Reynolds number are both large. In the present experiments T was in all cases larger than five, and the terminal Reynolds number was above 2000.

Table 2 gives experimental values of the inertial drag coefficient for a number of representative bodies. Figure 4 shows the coefficient as a function of the surface sphericity for all the bodies investigated. It is seen that the data for high sphericities are fairly closely distributed about Pettyjohn and Christiansen's data [3] on isometric bodies. No significance can be attached to the unevenness of the distribution, since it is not improbable that it simply reflects the average nature of nonisometricity among the shapes studied rather than a general trend. The deviations from a curve through the data on isometric bodies are endurable from a practical point of view, and hence there is no justification for attempting to recognize the effects of nonisometricity quantitatively. Nor is there usually any convenient basis for making such recognition. It may be concluded, therefore, that the present data are best represented by a curve which (1) begins at the point $C_I = 0.42$ to 0.44, $\psi = 1.00$ for the sphere, the point on which all data must converge as the surface sphericity approaches unity; (2) passes through the data on isometric bodies; and (3) satisfactorily represents the data on nonisometric bodies in the range $\psi < 0.67$ which lies below that ($\psi > 0.67$) spanned by isometric bodies. The simplest relationship which satisfies these conditions is

$$C_I = 2.25 + 0.283\,(1 - e^{2\psi}) \quad \ldots\ldots(29)$$

The present data indicate that the above relationship is good for all freely oriented, bluff shaped bodies of uniform density, with the exception of pronouncedly prolate bodies; *i.e.*, bodies with slimness (length to diameter) ratios higher than about three. A body with a slimness ratio of four was included in the present studies, and gave a value of C_I nearly 50% greater than predicted by the equation.

Flat plates and disks ($\psi = 0$) held perpendicular to the direction of fluid motion [5] have inertial drag coefficients which are practically identical with those of freely oriented bodies as given by Equation (29); *e.g.*, for a square plate $C_I = 2.32$, while for a disk $C_I = 2.24$,

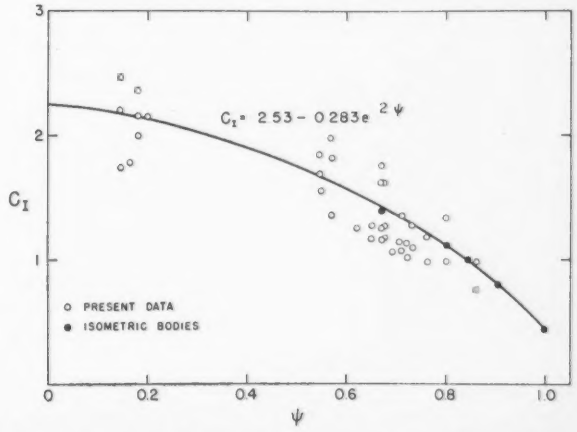

Figure 4—Inertial drag coefficients of isometric and nonisometric bodies as a function of the surface sphericity at Reynolds numbers greater than 2000.

TABLE 3

INERTIAL DRAG CHARACTERISTICS OF FREELY ORIENTED BLUFF BODIES

Re_s	Flow regime	Wake	Free orientation	Inertial drag coefficient
0.1	Viscous	Irrotational	All orientations are stable when there are three or more perpendicular axes of symmetry	Inertial drag is negligible
0.1 – 5.5	Transition I			For angular bodies assume $C_I = 2.25$. For spheres and rounded bodies see Figure 5
5.5 – 200	Transition II	Fixed vortices	Stable in position of maximum drag	$C_I = 2.25\left(\frac{5.5}{Re_s}\right)^{0.34\sqrt{\phi}}$ For non-stagnant fluid assume $C_I = 2.53 - 0.283e^{2.3\psi}$ when this gives the greater value of C_I
200 – 500	Transition III	Periodic discharge of vorticity	Unpredictable. Disks and plates tend to wobble, while fuller bluff bodies tend to rotate	$C_I = 2.53 - 0.283e^{2.3\psi}$ for $\psi < 0.8$ If $\psi > 0.8$, see Figure 5
500 – 3000	Transition IV	Increasing disorder	Rotation about axis of least inertia, frequently coupled with spiral translation	See Figure 5
3 – 200 x 10^3	Inertial I	Fully turbulent		$C_I = 2.53 - 0.283e^{2\psi}$
2 x 10^5	Inertial II	Boundary layer becomes turbulent. Wakes of rounded bodies narrow		Coefficients of rounded bodies decrease as the wake narrows

compared with the value $C_I = 2.25$ predicted by the equation. The slimness (length to width) ratio of rectangular plates has little effect until it exceeds a value of ten. The inertial drag coefficient then climbs to a limiting value of 3.9 at a slimness ratio of infinity. These figures give some indication of the behavior to be expected of prolate bodies in free orientation.

It may be remarked that the total drag coefficients of plates held perpendicular to the fluid motion are conventionally based on the projected area A_P; $f(Re) = F_D/\frac{1}{2}\rho u_o^2 A_P$. At a surface sphericity of zero, $S = 2A_P$, and when the viscous forces are negligible, $C_I = 4F_D/\frac{1}{2}\rho u_o^2 S$. Thus f(Re) so defined equals one half C_I; *i.e.* $C_I = 2f(Re)$ in a purely inertial regime and at a surface sphericity of zero.

Summary of correlations

1. The present paper relates the drag on a freely oriented body (or particle) in motion through an infinite fluid to the relative fluid velocity and to the properties of the fluid and the body by the relation

$$K = 8\rho F_D/\pi\mu^2 = C_V.Re_S + C_I.Re_S^2$$

where $Re_S = D_S u_o \rho/\mu$. (It may be noted that the commonest value of the drag force is that obtaining when the body is at a terminal velocity in a uniform gravitational field; $F_D = Vg(\rho_S - \rho)$).

2. The best experimental value of the viscous drag coefficient C_V for randomly oriented bodies (excepting prolate bodies with slimness ratios larger than 5) is $C_V = 24$. This value should be accurate within ±18% for individual bodies, and within a few percent as an average for statistical populations. If a particular orientation of an individual body is being considered an accurate value is obtained by using the relation $C_V = 24.f(\phi)$ in conjunction with Figure 1.

3. Table 3 gives a summary of formulae relating the inertial drag coefficients of freely oriented bluff bodies to shape and Reynolds number. The behavior of the coefficients is also shown graphically in Figure 5. The transition regime has been divided into four subregimes and the inertial regime into two subregimes. There is a

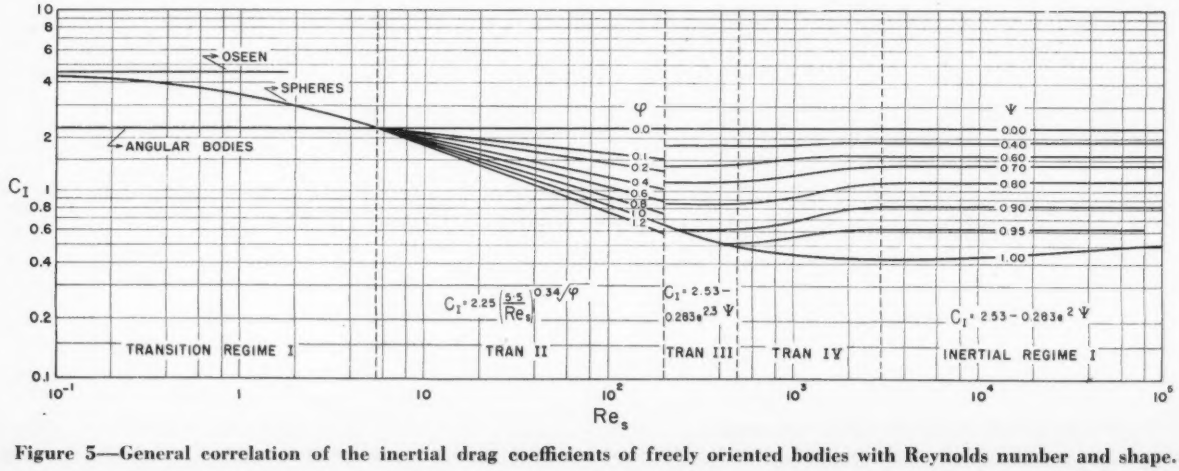

Figure 5—General correlation of the inertial drag coefficients of freely oriented bodies with Reynolds number and shape.

discontinuity in passing from transition subregime II to subregime III. Goldstein [5] notes that entry into the transition subregime III is considerably advanced by the presence of turbulence in the fluid, and for this reason it is recommended in Table 3 that in problems on non-stagnant fluids the correlation for the subregime III should be extended to subregime II when this gives the higher value of the coefficient. The correlations for the inertial drag coefficient do not appear to be reliable for prolate bodies with slimness ratios greater than three. Other than this, they can be applied to all freely oriented bluff bodies. They should usually be accurate within ±20%, regions of abrupt transition excepted (such as that at $100 < Re_S < 400$).

4. The correlations in this paper apply to motion in an infinite fluid. To apply them to motion in cylindrical vessels it may be assumed that the correlations of Francis [9] and Monroe [10] for viscous and turbulent flow respectively are applicable to bluff shaped bodies in general:

$$C_V = (C_V)_{\theta=0}/(1-\theta)^{2.25}$$

and

$$C_I = (C_I)_{\theta=0}/(1-\theta^{1.5})$$

where $\theta = D_S/D_C$ is the ratio of the diameter of the body to the diameter of the column.

5. The correlations in this paper apply to the motion of isolated bodies. The quadratic drag formula, Equations (2-5), was first used by the author in a Master's thesis presented to the University of Saskatchewan in the Department of chemistry and chemical engineering, and entitled "Flow of fluids through beds of particles in the fixed and fluidized states", (May, 1955). The thesis (p. 112) gives a general correlation of the relative terminal velocity or settling ratio u/u_t with the fraction void and the drag number for dispersions of uniform particles in motion relative to a liquid. The correlation facilitates extension of the present results to fractions void between 0.45 to 0.55 and unity in a full spectrum of Reynolds numbers.

Conclusion

The present work shows that the quadratic formulation of the drag law facilitates a precise, theoretically significant analysis of experimental data on freely oriented, bluff shaped bodies. Application of the formula demonstrates the role of the inertial forces at low Reynolds numbers, and shows that data on spheres do indeed extrapolate exactly to Oseen's theoretical solution. It is interesting to note that the coefficient of the inertial drag, C_I, decreases with increasing Reynolds number through the transition zone. This decrease is connected with the growth of the fixed vortices which attach themselves to any bluff body in this region.

It does not appear that the scheme of correlation adopted in the present study can be simplified or altered with any significant advantage; *i.e.* the coefficients of the drag equation, as presently defined, show minimum dependence on shape and Reynolds number. The correlations extend over a full spectrum of shapes, orientations, and Reynolds numbers for freely oriented bluff shaped bodies, and thus provide practical information on regions previously neglected, especially in the transition zone. The weak dependence of the coefficients C_V and C_I on shape and Reynolds number, in contrast to previously proposed total drag coefficients, increases the reliability of the present correlations and simplifies interpolation.

The chief need for new or supplementary data appears to lie in the following two areas: (1) data on freely oriented prolate bodies in turbulent flow; and (2) data on non-isometric bodies in the transition zone region $10 < Re_S < 100$ to check Equation (16) or to replace it with a better expression for the exponent of the Reynolds number.

Nomenclature

Dimensions in absolute units:

M = mass
L = length
t = time

A	= an area representative of the size of a body	L^2
A_P	= area projected by a body in the direction of its motion	L^2
A_S	= area projected by a sphere with the same surface area as the body	L^2
D	= diameter representative of the size of the body	L
D_V	= diameter of a sphere with same volume as the body	L
D_P	= diameter of a circle of area A_P	L
D_S	= diameter of a circle of area A_S	L
F_D	= drag force on a body	ML/t^2
F_V	= viscous component of the drag force	ML/t^2
F_I	= inertial component of the drag force	ML/t^2
g	= local acceleration due to gravity	L/t^2
m	= mass of a body	M
S	= $4A_S$ = surface area of a body	L^2
u_o	= velocity of a body relative to the undisturbed fluid in motion of the body through an infinite fluid	L/t
$\bar{u}_o$	= x/t = average velocity of the body over a time t after falling from rest	L/t
u_t	= terminal (steady-state) velocity approached by the body after falling from rest	L/t
x	= distance	L
ρ	= fluid density	M/L^3
ρ_s	= density of a body	M/L^3
μ	= fluid viscosity	M/Lt

Dimensionless factors

C_V	= viscous drag coefficient
C_I	= inertial drag coefficient
K	= $8\rho F_D/\pi\mu^2$ = drag number
r	= exponent dependent on shape and orientation
Re	= $Du_o\rho/\mu$ = Reynolds number
Re_P	= $D_P u_o \rho/\mu$
Re_S	= $D_S u_o \rho/\mu$
ϕ	= $\pi D_v^2/4A_P$ = form sphericity
ψ	= $\pi D_v^2/S$ = surface sphericity

References

(1) Oseen, C. W., Ark. of Mat., Astr. Och fys. 6 (1910).
(2) Heiss, J. F., and Coull, J., Chem. Eng. Prog. 48, 133 (1952).
(3) Pettyjohn, E. S., and Christiansen, E. B., Chem. Eng. Prog. 44, 157 (1948).
(4) Waddel, H., J. Franklin Inst. 217, 459 (1930).
(5) Goldstein, S., "Modern developments in fluid mechanics", Vol. II, University Press, Oxford (1938).
(6) Squires, L., and Squires, W., Trans. Am. Inst. Chem. Engrs. 33, 1 (1937).
(7) Blasius, H., Zeitschr. J. Math. u Physik 56, 4 (1908).
(8) Bacon, D. L., and Reid, E. G., N.A.C.A. Report No. 185 (1924).
(9) Francis, A. W., Physics 4, 403 (1933).
(10) Monroe, H. S., Trans. Am. Inst. Mining Met. Engrs. 17, 637 (1888-1889).

★ ★ ★

The Canadian Journal of Chemical Engineering

formerly

Canadian Journal of Technology

INSTRUCTIONS TO AUTHORS

Manuscript Requirements

1. The manuscript should be in English or French.
2. The original and two copies of the manuscript should be supplied. These are to be on 8½ x 11 inch sheets, typewritten, and double spaced. Each page should be numbered.
3. Symbols should conform to American Standards Association. An abridged set of acceptable symbols is found in the third edition of Perry's Chemical Engineers' Handbook. Greek letters and subscripts and superscripts should be carefully made.
4. Abstracts of not more than 200 words in English indicating the scope of the work and the principal findings should accompany all technical papers.
5. References should be listed in the order in which they occur in the paper, after the text, using the form shown here: "Othmer, D. F., Jacobs, Jr., J. J., and Levy, J. F., Ind. Eng. Chem. 34, 286 (1942). Abbreviations of journal names should conform to the "List of Periodicals Abstracted by Chemical Abstracts". Abbreviations of the common journals are to be found in Perry's Handbook also. All references should be carefully checked with the original article.
6. Tables should be numbered in Arabic numerals. They should have brief descriptive titles and should be appended to the paper. Column headings should be brief. Tables should contain a minimum of descriptive material.
7. All figures should be numbered from 1 up, in Arabic numerals. Drawings should be carefully made with India ink on white drawing paper or tracing linen. All lines should be of sufficient thickness to reproduce well, especially if the figure is to be reduced. Letters and numerals should be carefully and neatly made, preferably with a stencil. Generally speaking, originals should not be more than twice the size of the desired reproduction; final engravings being 3¼ in. or 7 in. wide depending on whether one column or two is used.
8. Photographs should be made on glossy paper with strong contrasts. Photographs or groups of photographs should not be larger than three times the size of the desired reproduction.
9. All tables and figures should be referred to in the text.

Submission of Manuscripts

1. The three copies of the manuscript, including figures and tables, should be sent directly to:

   D. W. Emmerson, publishing editor,
   The Canadian Journal of Chemical Engineering,
   18 Rideau Street,
   Ottawa 2, Ont.
2. The authors addresses and titles should be submitted with the manuscript.
3. The author may suggest names of reviewers for his article, but the selection of the reviewers will be the responsibility of the editor. Each paper or article is to be reviewed by two chemical engineers familiar with the topic. Reviewers may request that they remain anonymous.
4. All correspondence regarding reviews should be directed to the publishing editor.

Reprints

1. At least 50 free "tear sheets" of each paper will be supplied.
2. Additional reprints may be purchased at cost. An estimated cost of reprints, with an attached order form, will be sent to the author with the galley proofs.
3. Orders for reprints must be made before the paper has appeared in the Journal.

* * *

7 in.
wo is

with
hoto-
size of

e text.

figures

ng,

mitted

or his
be the
e is to
with
emain

ld be

vill be

t. An
order
roofs.
er has

1959